NREL/TP-411-7695 • UC Category: 1260 • DE95004088

Comprehensive Research on the Stability and Electronic Properties of a-Si:H and a-SiGe:H Alloys and Devices

Final Subcontract Report
10 March 1991 – 30 August 1994

V. Dalal
Iowa State University
Ames, Iowa

NREL technical monitor: W. Luft

National Renewable Energy Laboratory
1617 Cole Boulevard
Golden, Colorado 80401-3393
A national laboratory of the U.S. Department of Energy
Managed by Midwest Research Institute
for the U.S. Department of Energy
under contract No. DE-AC36-83CH10093

Prepared under Subcontract No. XG-1-10063-8

April 1995

MASTER

DISTRIBUTION OF THIS DOCUMENT IS UNLIMITED

NOTICE

This report was prepared as an account of work sponsored by an agency of the United States government. Neither the United States government nor any agency thereof, nor any of their employees, makes any warranty, express or implied, or assumes any legal liability or responsibility for the accuracy, completeness, or usefulness of any information, apparatus, product, or process disclosed, or represents that its use would not infringe privately owned rights. Reference herein to any specific commercial product, process, or service by trade name, trademark, manufacturer, or otherwise does not necessarily constitute or imply its endorsement, recommendation, or favoring by the United States government or any agency thereof. The views and opinions of authors expressed herein do not necessarily state or reflect those of the United States government or any agency thereof.

Available to DOE and DOE contractors from:
Office of Scientific and Technical Information (OSTI)
P.O. Box 62
Oak Ridge, TN 37831
Prices available by calling (615) 576-8401

Available to the public from:
National Technical Information Service (NTIS)
U.S. Department of Commerce
5285 Port Royal Road
Springfield, VA 22161
(703) 487-4650


Printed on paper containing at least 50% wastepaper and 10% postconsumer waste

DISCLAIMER

Portions of this document may be illegible electronic image products. Images are produced from the best available original document.

Preface

This report describes the research performed at Iowa State University during the three years of this program, from March 1991 to May 1994, under subcontract XG-1-10063-8 to NREL.

The objectives of this program were to resolve:

1) How the performance of solar cells made with narrow bandgap state-of-the-art a-SiGe:H material can be enhanced.

2) How particular materials and device parameters determine the stabilized performance of a-Si:H and a-SiGe:H solar cells.

3) How particular device structures may enhance the performance of a-Si:H based solar cells.

The Scope of Work included performance of analytical and numerical modeling to optimize device performance; development of models for the microscopic defect sites; measurement of diode parameters to help with device analysis by providing input data to multijunction optimization; identifying which material parameters pose the most serious limitation on the device performance; evaluation of stabilized single-junction devices; and determining the effects of interfaces.

The contributors to this work, in addition to the PI, are:

Ralph Knox, Ruth Shinar, Kay Han, J. K. Lee, Mohan Bhan, Mark Leonard, Anand Garikepati, E. X. Ping, Scott DeBoer, Greg Baldwin, Sanjeev Kaushal, Sanjeev Chopra, Francisco Martin, Stacy Van Zante, Behnam Moradi, Nabeeh Kandalaft and J. Xu.

The tin oxide substrates used in this work were supplied by Solarex, and we thank Dr. Rajeev Arya of Solarex for his kindness and generosity in supplying these. We also thank Professor David Redfield of Stanford University for many fruitful discussions regarding stability.

Finally, Werner Luft and Bolko Von Roerden of NREL have been extremely helpful in stimualting many fruitful discussions, and we thank them for reviewing this manuscript critically, and significantly improving it.

Table of Contents

Listing of Tables

List of figures

Executive Summary

Objective

The objective of the program was to investigate the stability and electronic properties of a-Si:H and a-(Si,Ge):H materials and devices deposited using alternative growth techniques, and using alternative device structures.

Research on an Alternative Growth Technique for a-Si:H Material and Devices

We investigated the growth of a-Si:H using a remote plasma beam technique, using plasmas generated by electron-cyclotron-resonance (ECR) conditions. Both reactive (hydrogen) and non-reactive (helium) gases were used as the primary plasma gas. The reactants generated by the ECR plasma from these gases were allowed to flow towards the substrate, where they reacted with silane to give rise to growth of a-Si:H. In general, we use a high dilution ratio of plasma gas (H_2 or He) to silane, about 15:1 to 20:1, for growing a-Si:H. We found the following interesting results:

- The ECR plasma is quite intense, with the ion densities in the ECR zone being in the $10^{10}cm^{-3}$ range. By controlling the pressure in the reactor, a significant amount of H ions and higher excited states of H radicals are allowed to travel to the substrate, where they do etching-during-growth of the film. By controlling this etching, the structure of the film can be smoothly changed from amorphous to polycrystalline. The polycrystalline films have very good mobilities (in the range of 30 cm^2/Vs), even when deposited at low temperatures (300°-350°C).

- Very high quality a-Si:H films can be deposited using H-ECR plasma at relatively higher temperatures (325°-375°C). These films are more stable to Staebler-Wronski degradation (by a factor of 2-3) compared to glow-discharge-deposited films.

- The use of He in the discharge does not lead to any etching during growth, but does lead to significant ion bombardment. The ion energies with a He discharge are higher than with a H discharge, and can be increased by lowering the pressure. We find that by using a highly diluted He-ECR growth technique, we can reduce the Tauc bandgap of a-Si:H to 1.67 eV, which is significantly lower than the 1.75 eV obtained with H as the plasma gas. This fact may be useful for growing a 2-junction a-Si/a-Si solar cell.

- We discovered that there were two different instability mechanisms in a-Si:H, one which followed a mono-molecular type kinetics, and one which followed a bimolecular-type kinetics. The first one we attribute to a trap-to-dangling bond conversion model, and the second to a bond-breaking type model. The trap-to-dangling bond type instability can be related to the presence of impurities such as O and P in the film.

- We discovered that compensation of the material at sub parts per million (sub-ppm) levels with diborane leads to a significant decrease in both the initial and degraded state defect densities. Using compensation, we have been able to reduce the defect density after

prolonged light soaking to $2x10^{16}$ cm^{-3} level, significantly lower than the $8\text{-}10x10^{16}$ cm^{-3} levels commonly found in glow-discharge deposited material. We attribute the influence of compensation to a reduction in 3-center bonds caused by impurities in the material. We speculate that compensation leads to a stable donor-acceptor type bond formation with an attendant decrease in dangling bond defects.

- We have succeeded in making reasonable quality devices from the ECR-deposited a-Si:H materials prepared at high temperatures. The devices were deposited on tin oxide substrates. To deposit these devices, we had to overcome several difficult problems. Among these were reduction in tin oxide at high temperatures by the intense H beam, and diffusion of B across the *p-i* interface at the high temperatures. The reduction in tin oxide was avoided by using a He-diluted *p* layer deposited at lower temperatures. The diffusion of B was avoided by using an a-(Si,C):H buffer layer with a high C content between the *p* and the *i* layers. We found that the design of the buffer layer was critical in achieving good performance. Too thick a buffer layer, or too much C, led to an I(V) curve with an inflection point, which we could trace back to a band diagram where there is a hole trap being created between the *i* layer and the *p* layer. On the other hand, not having enough C in the buffer layer led to B diffusion. Too thick a buffer layer always led to an increase in voltage, but a decrease in fill factor. This fact can also be explained by drawing the band diagram, which shows that under these conditions, we effectively have two solar cells in series, one a normal *p-n* junction type, and the second created by grading in the conduction band, with the voltages due to the two cells being in the same direction. A thick buffer layer more effectively traps the holes at the *p-i* interface, thereby leading to fill factor problems. When we used the right buffer layer, we obtained a cell with about 8% efficiency, with a fill factor of 64%. All the layers in this cell were made using the ECR deposition technique.

Research on Alternative Device Structures for Improving Stability

One of the objectives of our program was to study the device design, and to see if the design can be improved to improve stability. Towards this end, we designed a new type of solar cell, where the *i* layer was graded in the middle, so as to provide a drift field for holes in addition to the drift field created by the *p-i-n* junction. The design called for a grading of about 0.15 eV in the middle, from a low of 1.65 eV to a high of 1.8 eV. The low-gap side is next to the *p* interface, immediately following the buffer layer, and the high gap side is next to the *n* layer, in the back. We made an approximation to the above structure, where the gap was graded from 1.72 eV to about 1.78 eV, simply by changing the deposition temperature during growth. This cell was made using RF triode glow-discharge deposition process. The efficiency of the cell was about 8.5%, with Al back contacts. We compared the stability of this graded gap cell with the stability of a standard glow-discharge cell, also of 8.5% efficiency which had the same fill factor (0.69) before degradation. Both the cells were exposed to identical conditions of accelerated illumination, using a xenon lamp set to give 7000 W/m^2 illumination at the cell surface. We found that the fill factor of the graded gap cell degraded to about 85% of the initial value after 40 hours of light soaking, whereas the fill factor of the normal cell degraded to 75% of its initial value over the same period. Thus, we verified that our design, which was selected to minimize the degradation of the fill factor, seems to produce more stable cells. We also verified that a reverse grading produced worse and less stable cells.

Note, that our design was only addressing the question of fill factor losses in the bulk of the

material. In addition, there is significant degradation in fill factor due to changes in recombination at the *p-i* interfaces, and we need to study how to minimize this degradation also in order to produce more stable cells.

Research on a-(Si,Ge):H Materials and Cells

During this contract, we undertook research to develop reproducible a-(Si,Ge):H materials and devices, and to determine some basic material parameters, such as Urbach energies and hole mobility-lifetime products by making measurements in *p-i-n* devices. We also undertook research to design appropriate graded bandgap cells, and to design the best interfaces for a-(Si,Ge):H cell.

Reproducible growth of high quality materials

We used a hydrogen-diluted RF triode glow discharge process to grow a-(Si,Ge):H films and devices. The properties of the material were highly reproducible, in contrast to results from some other groups.

Material properties

We found a systematic increase in Urbach energy of valence band tails states in **materials** as the Ge content increased. While the increase was small compared to some previous results, it was nevertheless systematic, especially for Ge contents greater than 20%. The Urbach energy increased from 45-46 meV for a-Si:H to about 55 meV for a-(Si,Ge):H with a 40% Ge content. Concurrently with this increase in Urbach energies, we found a systematic increase in subgap absorption coefficient α, measured at the shoulder in the absorption spectrum. It increased from about 0.3 cm^{-1} for a-Si:H, to about 2 cm^{-1} for a-(Si,Ge):H with a 40% Ge content. When we plotted the product of electron $\mu\tau$ product and α vs. Ge content, we found a relatively flat curve, independent of Ge content. This fact indicates that the mid-gap defect density is the major controlling factor behind the decrease in electron $\mu\tau$ product as Ge content increases.

Measurement of hole $\mu\tau$ product in devices

We measured hole $\mu\tau$ product in devices, by making a systematic series of **devices**, all with the same *p* and *n* layers, but with *i* layers of different Si:Ge ratios. Using quantum efficiency spectroscopy, we could deduce the hole $\mu\tau$ product as a function of Ge content. We found that the hole $\mu\tau$ product decreased with increasing Ge content, similar to the behavior of electron $\mu\tau$ product. When we plotted the product of hole $\mu\tau$ product and subgap α as a function of Ge content, we again obtained a curve that was relatively flat, independent of Ge content, implying that increasing defect density was directly reducing the hole $\mu\tau$ product. The valence band Urbach energies of the materials were also determined in devices, and had values very close to the values found in films with the same Ge content.

Design of devices

We found that the best design was again to use a graded bandgap structure, with a constant low bandgap near the *p* layer, a grading from a low gap to a higher gap in the middle of the *i* layer, and an ungraded a-Si layer next to the *n* layer. We made devices with this grading, and they had the best fill factor, whereas devices with a reverse grading had the worst fill factors.

Design of interfaces

We started some work on design of appropriate interfaces between the *p* and the *i* layers of the a-(Si,Ge):H cell. We found that it was critical to grade the bandgap of the buffer layer all the way from a high gap approximating that of the *p* layer, to the lowest gap used in the material. This grading had to be continuous in bandgap, otherwise hole trapping effects occurred, with disastrous consequences for device fill factors.

Chapter I
Research on Alternative Growth Techniques for a-Si:H Materials and Devices

1.1 Introduction

Amorphous silicon (a-Si:H) by its nature is a disordered semiconductor. Its optical properties derive directly as a consequence of its inherent disorder. It is thought that H diffuses into the material during growth and forms covalent bonds with the broken Si dangling bonds, thereby passivating the mid-gap defect states that arise as a consequence of atomic disorder. From fundamental physics argument (minimization of disorder), one would want a material which only had occasional broken bonds, and we would want these bonds to be passivated by a single H atom, i.e., we would want just Si-H type bonding. However, that is not what a-Si:H is. Rather, the material has H bonded randomly (as Si-H bonds), and in clusters [1], presumably at the surfaces of microvoids which are known to exist in this material [2]. The material has both Si-H bonds, and some polymeric Si-H_2 type bonds. The amount of polymeric bonding is a function of growth conditions. Thus, the material is anything but just randomly disordered, homogeneous material that one would want as an ideal amorphous semiconductor. It is clear that this heterogeneous structure, particularly the microvoids and associated polymeric bonds, are a prime contributor to the Staebler-Wronski instability in the material.

Therefore, to improve stability, we need to look at growth of the material, and see if we can make the material more homogeneous without hurting the electronic properties. In this chapter, we discuss one particular technique, remote reactive plasma deposition using electron-cyclotron-resonance (ECR) techniques, which seems to produce a more stable, device-quality material.

1.2 Introduction to Growth Chemistry of a-Si:H

A-Si:H is generally grown on a foreign substrate. Therefore, for the initial layers, there is no template which dictates the growth of a suitably ordered Si layer. Rather, it is likely that many islands of a-Si:H growth are started, and they may coalesce into a "homogeneous" structure after some thickness has been deposited [3]. In this sense, a-Si:H grows like any other material. In common with any heterogeneous growth, we would expect that the initial layers of a-Si:H are possibly the worst layers in terms of structure, H bonding, homogeneity, and the like. And yet, in a superstrate device made directly on a foreign (tin oxide) substrate, the most critical layer of a-Si:H, namely the *p* layer and the *p-i* interface, are the worst layers from a structural viewpoint. This fact may have something to do with the instability observed at the *p-i* interface in most a-Si:H devices.

Once the a-Si:H layer starts growing in a "homogeneous" fashion, away from the substrate, a growing surface may be represented as shown in Fig. 1.1. There, we schematically show a

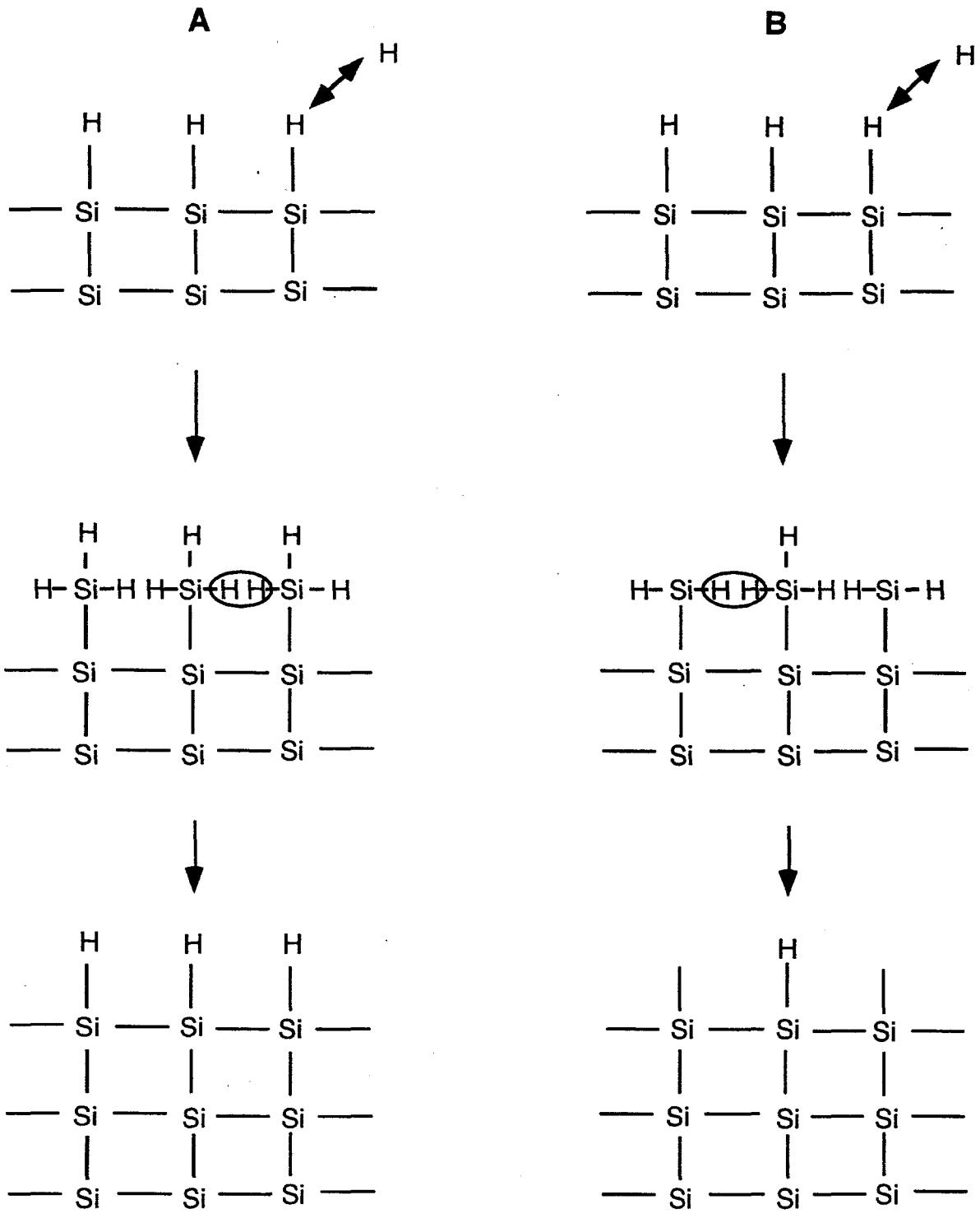

Fig 1.1 : Steps in growth of a-Si films

H-terminated a-Si:H surface, a very likely event, given the strong Si-H bond strength (300 kJ/mole). To build a layer of a-Si:H on this surface, first the H has to be eliminated, and then, a radical such as SiH_3 or SiH_2 inserted into the growing surface. Therefore, we need, preferably, an excess of atomic H to extract the H from the surface, a likely reaction given the high bond strength of H-H radicals (435 kJ/mole). And we need a radical for insertion.

This is a stage where the wrong growth technique can give a poor film. If the growth technique produces only one kind of radical, either SiH_2 or SiH_3, the surface would grow by insertion of either of the radicals into the surface bond (see Fig. 1A). However, if both types of radicals are present, then both can insert themselves, and we end up with a surface after insertion which looks as in Fig. 1B, where part of the surface is terminated with an H (insertion of SiH_3) and part is not (insertion of SiH_2). Therefore, a uniform surface has been converted into a non-uniform surface. The consequence of such a mixed mode can only be increased surface roughness, since the type A site (one without H) can immediately accept a radical, but type B needs a H elimination before accepting a radical. And, indeed, computer simulations and experiments show that having significant concentrations of SiH_2 in the plasma leads to increased roughness of the surface [4].

From this basic chemical argument, one would want excess H and only one type of radical predominating in the chemical growth technique. Fortunately, having excess H around assures that both these events take place. In a highly H-diluted plasma reaction, the likely reaction leading to fractionation of silane is: $SiH_4 + H \rightarrow SiH_3 + H_2$

Therefore, we expect that in such a system, the growth reaction will proceed via the H-elimination by the H and SiH_3 insertion mode, and the surface will be the smoothest. It is, therefore, not a surprise that H dilution is now being shown to produce better, more stable devices [5].

The next logical step in improving the material beyond H dilution is to further use hydrogen chemistry during growth. In particular, since the bond strengths of Si-Si and Si-H are so similar, one can argue that the weaker Si-Si bonds present in a highly disordered a-Si:H may be etched away by H during growth, leading to an intrinsically more stable material. For this to happen, we need high energy, high density H in the discharge. Our ECR reactor is one way we can produce such energetic, high density H. To show how energetic this H is, we show, in Fig.1.2, the etching rate for a thermally grown SiO_2 by the H discharge in the ECR reactor. Quite clearly, H is very effective at etching off even strongly bonded silicon oxides, let alone poorly bonded Si. Thus, in principle, the ECR discharge can provide H to do etching-during-growth, etching away the weakest bonds, and allowing a second chance for a more perfect bond to form.

The next logical step in improving the film would be to improve the surface mobility of radicals such as SiH_3. One way of increasing this mobility would be to increase the growth temperature, to say 350-400°C. However, at such high temperatures, the few SiH_2 bonds in the material may break, unless there was an excess of atomic H around, which would then reform the bonds.

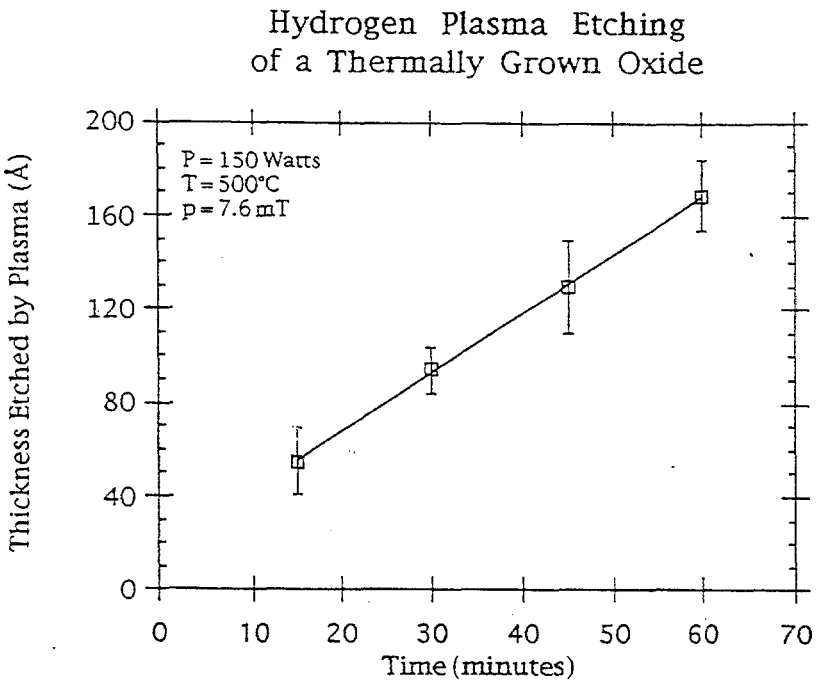

Fig.1.2 Etching rate of Thermal SiO_2 by H in ECR Plasma

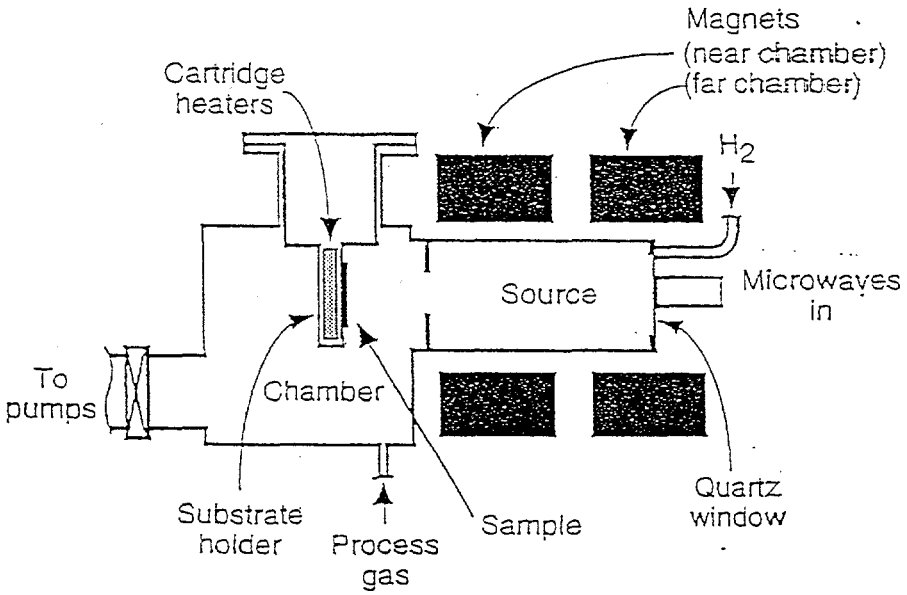

Fig.1.3 Schematic Diagram of ECR Reactor

Once again, the ECR discharge, with its high density of excited H radicals and ions coming to the surface, will help in improving the bonding at higher temperatures.

Note that if we used a highly diluted He discharge instead of H_2 discharge, there would be none of the beneficial etching effect of H, but there would be improved ion bombardment effects. A high He dilution would assure that the growth took place from SiH_3, since the most likely collision would be between SiH_4 and He*, leading to fractionation of SiH_4 into SiH_3 and H. There would be little opportunity for SiH_3-SiH_3 collisions, which can lead to formation of disilane and higher polymers. Since He does not do any chemical etching, the bandgap of a-Si:H produced from He discharge should be lower than the bandgap produced from a H discharge, since during the etching phenomenon, the weakest states, those at the top of the valence band, get etched away, and the band gets pushed down in energy [6]. Indeed, Dalal et al., many years ago, observed such an influence of etching by F on the bandgap of a-Si:H [7]. We will show in this chapter that indeed, a He discharge in an ECR reactor does produce films with much lower Tauc gap than a H_2 discharge.

1.3. Description of the ECR reactor

The reactor used in this study is shown schematically in Fig. 1.3. It consists of a microwave source which feeds power through a 3-stub tuner into a cavity. The cavity has a quartz window to let in microwave power. The axial magnetic field to create the ECR condition is produced using two coils, whose relative position and magnetic field strengths are controllable by the operator. A typical profile of the magnetic field strength is shown in Fig. 1.4. Thus, the position of the resonance plane can be changed by us, and generally, we set it so that the resonance plane is about 20-30 cm away from the substrate.

The plasma gases, hydrogen or helium, are introduced into the microwave cavity. The silane is introduced near the substrate through a separate manifold. The typical pressures used for growing a-Si:H are in the range of 10-15 mT. At these pressures, the excited H radicals have a long mean free path, and they arrive at the substrate with significant energies. A simple optical emission spectroscopy (OES) system detects the presence of these radicals by looking at emission coming from a region near the substrate. In Fig. 1.5, we show the typical OES spectrum of a hydrogen plasma. The peaks at 656 nm, and at 610 nm are noteworthy, and they represent, respectively, H_a and H_2* emission lines. The intensities, and the relative ratios of these lines, change as we change the plasma conditions, thereby providing us with some information about the nature of the chemical species arriving at the substrate as we change the plasma conditions. In Fig. 1.6, we show what happens to the ratio of 610 to 656 nm line as we decrease the pressure. Quite clearly, at lower pressures, the relative intensity of the H_a line increases, implying that more H atoms and, particularly, more of the energetic H atoms, are arriving at the substrate at these pressures. It will be seen later that under such conditions, one can actually grow a polycrystalline rather than an amorphous film, at the same growth temperatures.

Note that we call our process a remote reactive plasma beam deposition process. We use the term *remote* to emphasize the fact that the main plasma is remote from the substrate, and that

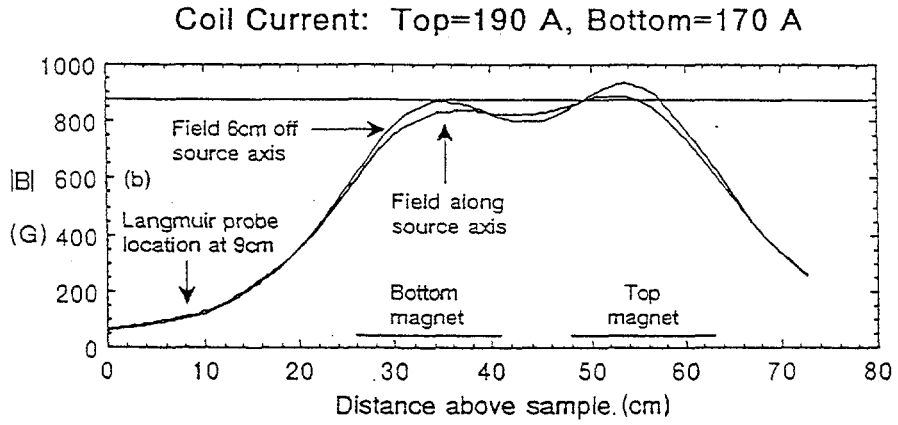

Fig. 1.4 Magnetic field profile in ECR reactor

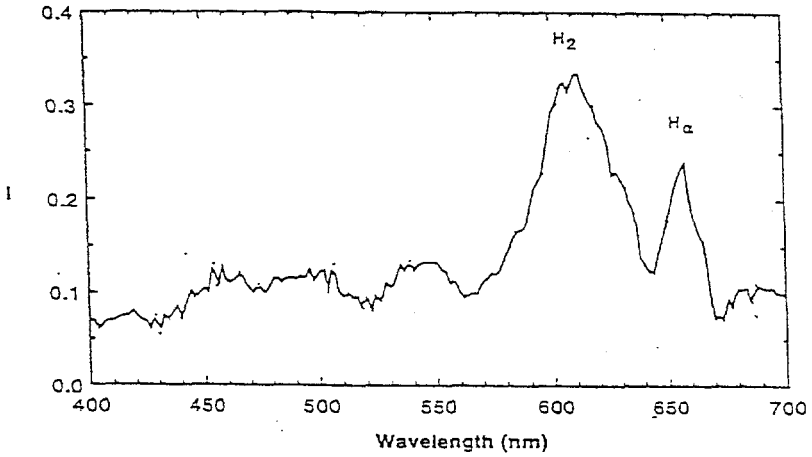

Fig. 1.5 Optical emission spectrum of H_2 plasma in ECR reactor

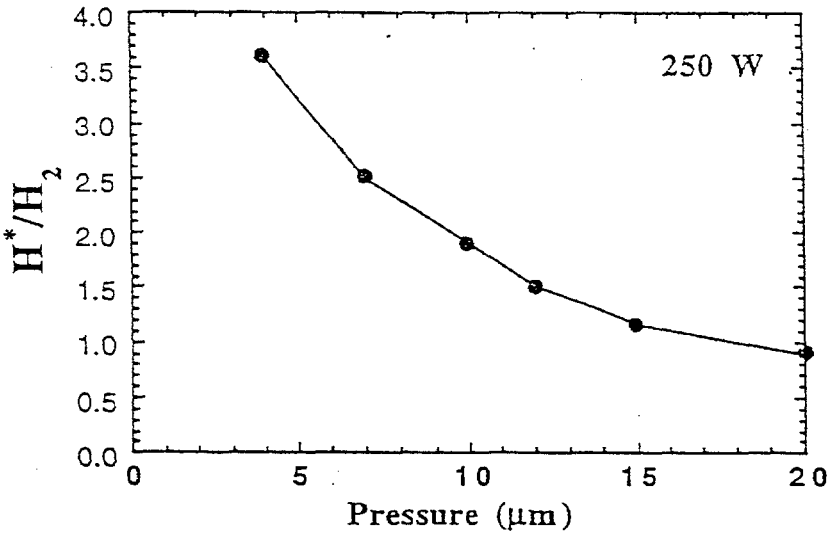

Fig. 1.6 Ratio of H/H_2 emission lines as a function of pressure in the reactor

radicals such as H and excited molecules and ions such as He* generated by the ECR plasma are playing a role in the deposition. At the low pressures, clearly, silane can and does diffuse back into the plasma zone. However, since the mean free path of silyl radicals at these pressures is low (of the order of 1 cm or less) these radicals do not play a role in growth on the substrate. Rather, the silyl radicals generated near the substrate by the fractionation of silane upon reaction with either H or excited He give rise to growth, as explained above in Sec. 1.2.

The entire ECR system is pumped by a turbo molecular pump, even during growth. The base vacuum is in the $3\text{-}5\text{x}10^{-8}$ T range. The gases for doping are introduced near the substrate through a separate manifold. This way, cross-contamination of the *i* layer by dopant gases flowing through the same manifold is avoided. Thus, we have three manifolds, one for the plasma gases, one for the *i* layer gases, and one for the dopant gases. Each manifold has a valve near the system which is cut off so that cross-contamination between manifolds is avoided. Such cross-contamination can lead to severe contamination problems at the interface between the *p* and the *i* layers.

The substrate is tightly mounted on a polished substrate holder with a thick stainless mask, and heated by heating up the substrate block from the outside using cartridge heaters. The substrate temperature is calibrated versus the heated block temperature, and generally is about 30-40°C lower than the block temperature for the typical pressure, gas flow, and plasma conditions that we use.

1.4 Diagnostics of Plasma using Langmuir Probes

An additional diagnostic tool that we have used to understand the plasma properties is a Langmuir probe analysis of the plasma. The Langmuir probe is inserted near the substrate to study the ion and electron concentrations. The typical results obtained by using the Langmuir probes are shown in Figs. 1.7-1.10. In Fig. 1.7, we show the electron temperature, in Fig. 1.8 the plasma potential, in Fig. 1.9 the ion current, and in Fig. 1.10 the plasma density, all as functions of pressure in the reactor. From these figures, we can draw the following conclusions:

- As pressure decreases, electron temperature and plasma potential increase. This implies a stronger ion bombardment of the substrate as the pressure decreases.

- As pressure decreases, the current density of ions arriving at the substrate also increases, implying a greater flux of H ions to participate in chemical reactions at the surface of the film.

- The plasma density seems to be a maximum at about 7 mT pressure. We do not quite understand why this is the case.

The Langmuir probe results are in excellent agreement with the OES results, which also showed an increase in excited H_α radical concentration at the surface as the pressure decreased. From the Langmuir probe results, we can predict that at lower pressures, there will be increased

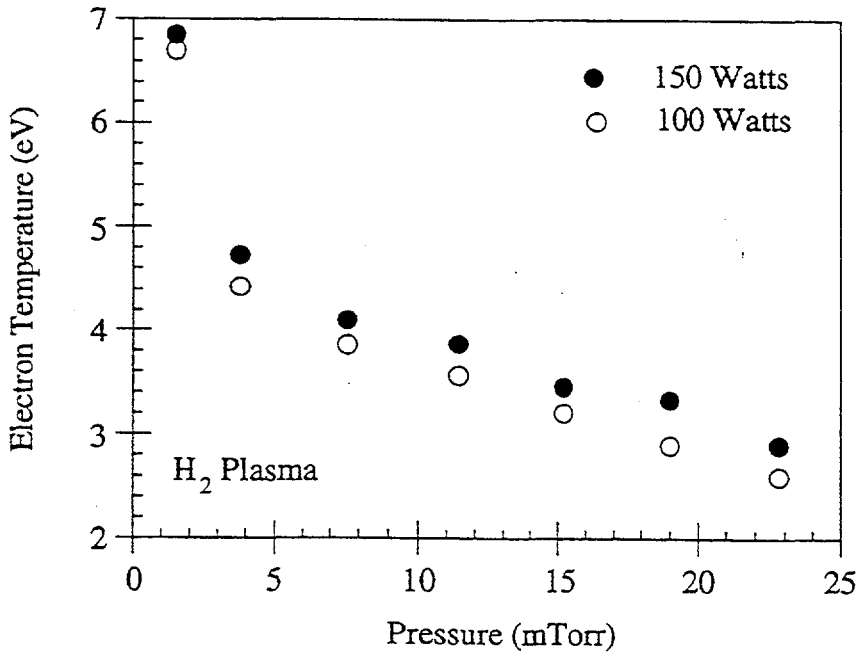

Fig. 1.7 Variation of the electron temperature with chamber pressure.

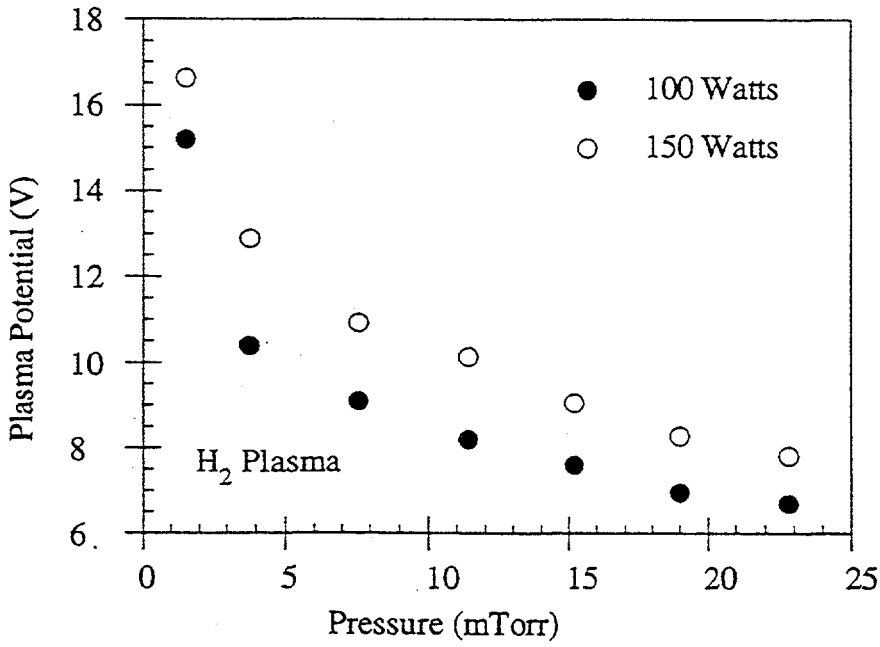

Fig. 1.8 Variation of the plasma potential with chamber pressure.

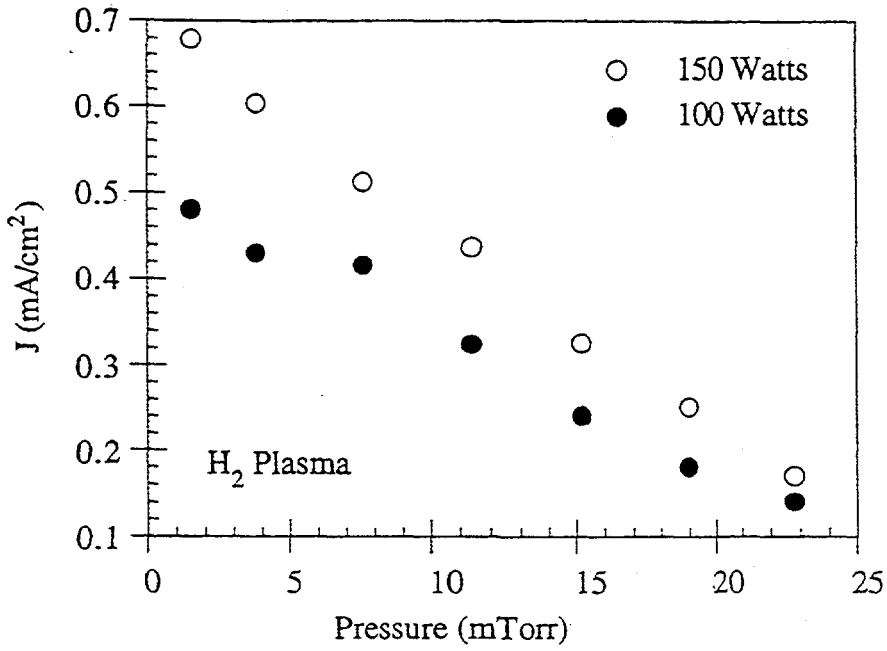

Fig. 1.9 Dependence of the ion current on pressure.

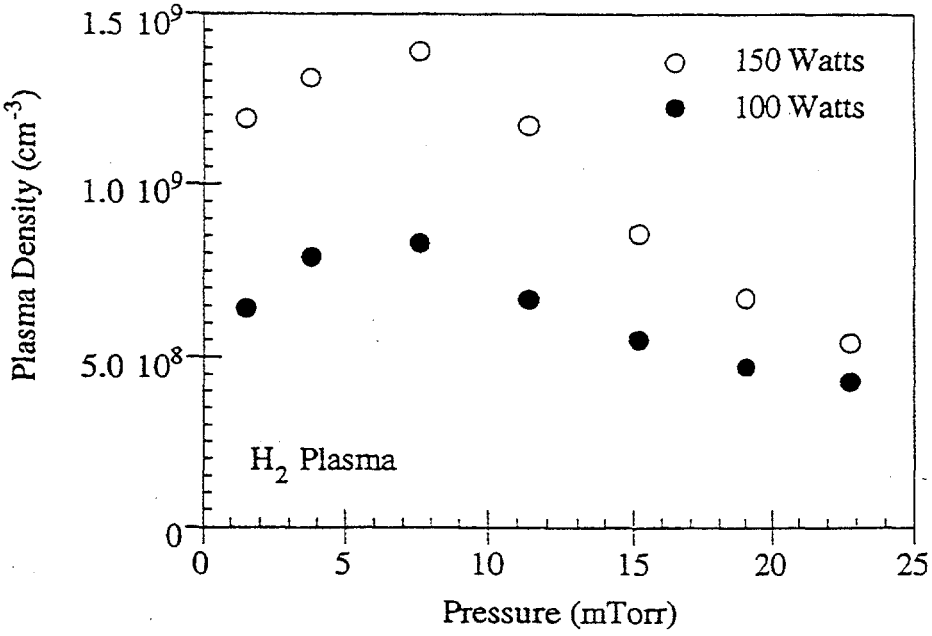

Fig. 1.10 Variation of the plasma density with chamber pressure.

etching of the film by H and increased ion bombardment by H (and He) ions.

1.5 Properties of a-Si:H Films Deposited using ECR

1.5 1 Structure

We have measured the structure of a-Si:H films using infrared Raman spectroscopy [8]. In Fig. 1.11, we show the Raman spectrum of typical a-Si:H film grown in the ECR reactor under conditions of H plasma excitation. The pressure in the reactor during this growth was 15 mT. Next, in the same figure, 1.11, we show what happens when we change the deposition pressure to 5 mT and the H dilution was increased by about 25%. The Raman spectrum is now very different, and is characteristic of a polycrystalline film. Note that both films were grown under the same power and temperature conditions. Only the etching action of H was changed by reducing the pressure. These results are in excellent agreement with the predictions made by observing the plasma characteristics. Thus, our ECR reactor offers a very powerful tool for changing the chemistry of growth, which was one of the objectives we had set for ourselves.

1.5 2. Electronic properties

1.5.B.1 Growth Conditions

The typical growth conditions for a-Si:H films are listed in Table 1.1.

Table 1.1 Typical deposition conditions for a-Si:H films

Silane flow rate: 1.5-2.0 sccm
Hydrogen flow rate: 30 sccm
Power: 120-160 W
Growth rate: 0.5-1.0 Å/s
Substrate temperatures: 300°-375°C
Pressure: 10-15 mT

The following electronic properties were measured: Dark conductivity, Photoconductivity under 1000 W/cm^2 ELH lamp, Activation energy, H content by FTIR, Optical absorption, Sub-gap absorption using a 2-beam photo-conductivity technique **[9]**, Urbach energy of valence band tails, from subgap α measurements.

The typical properties of a-Si:H films made using the deposition conditions listed in Table 1.1 are listed in Table 1.2.

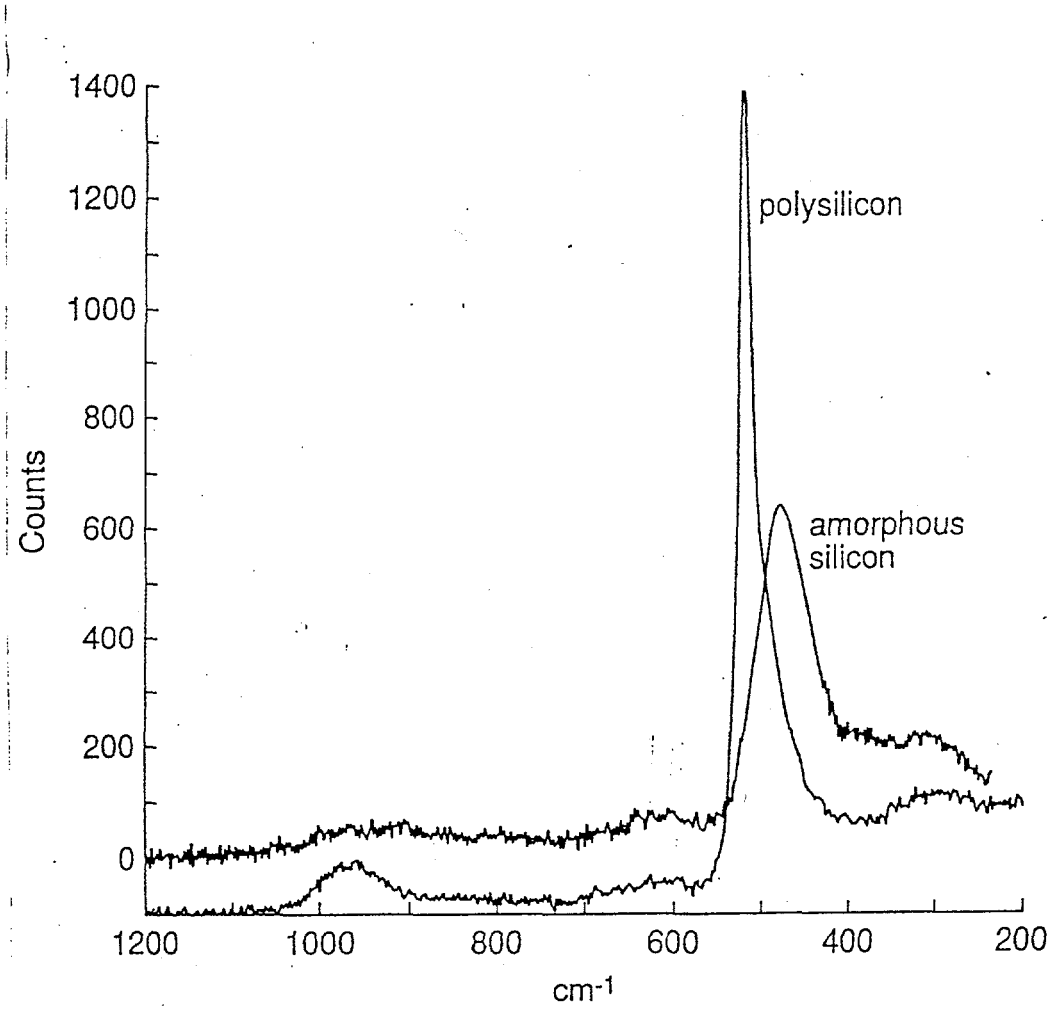

Fig. 1.11 Raman Spectra of ECR deposited amorphous and polycrystalline Si:H

Table 1.2 Electronic properties of a-Si:H films deposited using H-ECR

Tauc gap: 1.76 eV

H content: 8%

Urbach energy: 45 meV

Subgap α at 1.2 eV: 0.2 cm^{-1}

Dark conductivity: 1-2x10^{-11} S cm^{-1}

Photoconductivity (AM1.5): 2-4x10^{-5} S cm^{-1}

Activation energy: 0.85 eV

From this table, we can see that the a-Si:H films appear to be of electronic quality, even though they were grown at considerably higher temperatures (325-375°C) than typical glow-discharge deposited films.

In Fig. 1..12, we show the typical α(E) curve for an a-Si:H film made using H_2-ECR conditions. The Urbach energy for this film is of the order of 45 meV, a very low value indeed. For comparison, we show, in Fig. 1.13, the α(E) curve for a good quality glow-discharge a-Si:H film, deposited at a temperature of 250°C. Upon comparing Fig. 1.12 and 1.13, we find that the qualities of the two films (subgap α and Urbach energy) are very comparable.

Next, we made a-Si:H films using He-ECR. We obtained a much lower Tauc bandgap, 1.67 eV, compared to 1.76 eV for the H_2-ECR film. The subgap α(E) curve for the He-ECR film is shown in Fig. 1.14, and shows that the film is of good quality (subgap a less than 1 cm^{-1} at the shoulder). The lower bandgap is potentially significant for photovoltaic devices, since many device designs call for the mid-gap device to be of 1.6-1.65 eV. We have almost achieved the required bandgap without using Ge, which may be of some significance for commercialization, since germane is so much more expensive and toxic than silane.

1.5.3 Stability

1.5.3.1 Stability of ECR films

The photo-induced degradation of H-ECR deposited films was measured using high intensity light soaking, typically under 10 x sun photon intensity. To measure degradation, we measured subgap α(E) curves for each sample after periodic light soaking. In Fig. 1.15, we show the increase in subgap α, measured at 1.2 eV, as a function of light soaking time, for both a H_2-ECR film, and for a glow-discharge film. It is clear from Fig. 1.15 that the ECR deposited film is more stable than a comparable quality glow-discharge film.

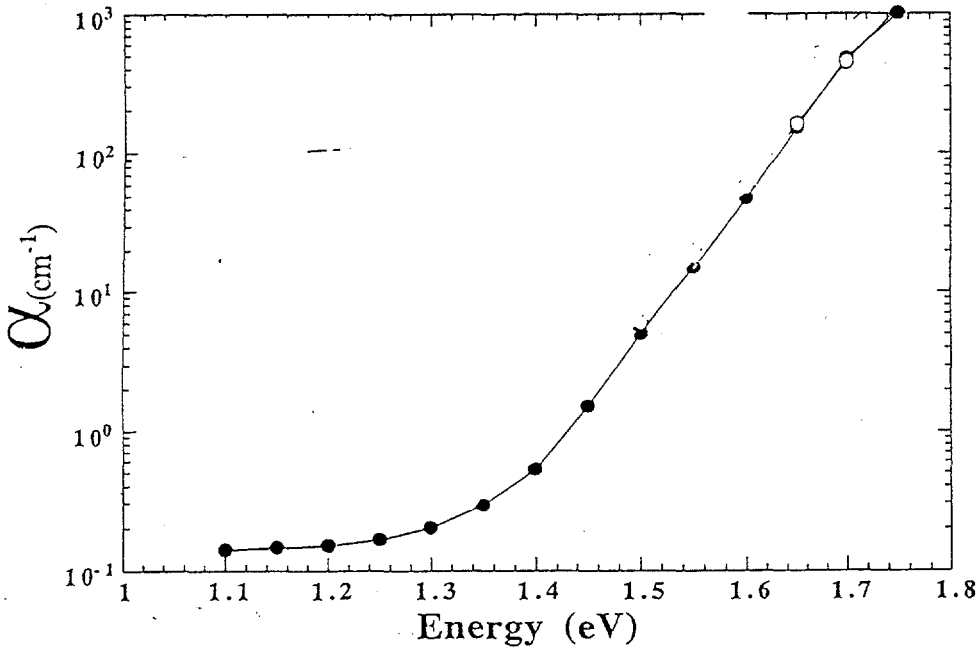

Fig.1.12 Absorption Coefficient α of ECR a-Si:H film

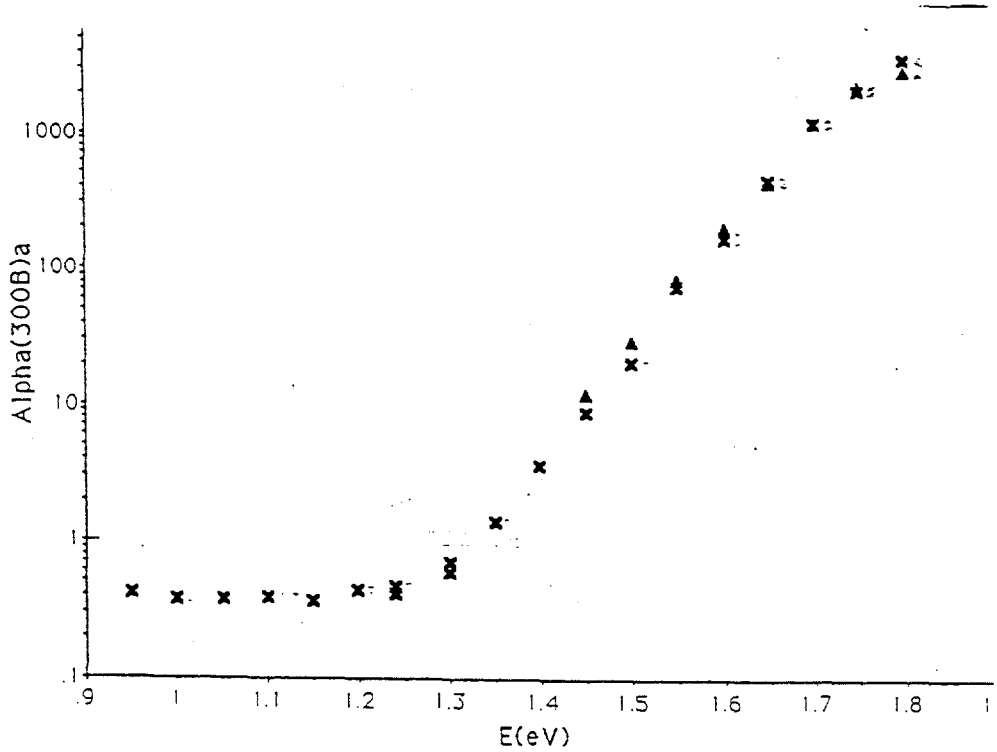

Fig. 1.13 Absorption Coefficient of Glow-discharge deposited a-Si:H [Courtesy of Prof. C. Wronski, Penn State]

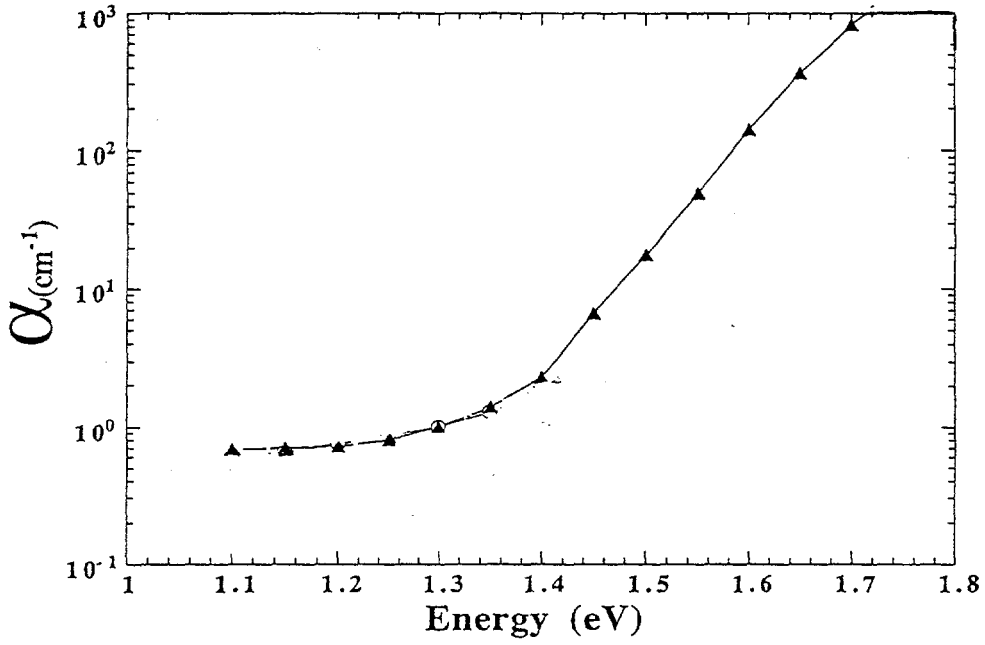

Fig. 1.14 Subgap α(E) spectrum of ECR film deposited using He

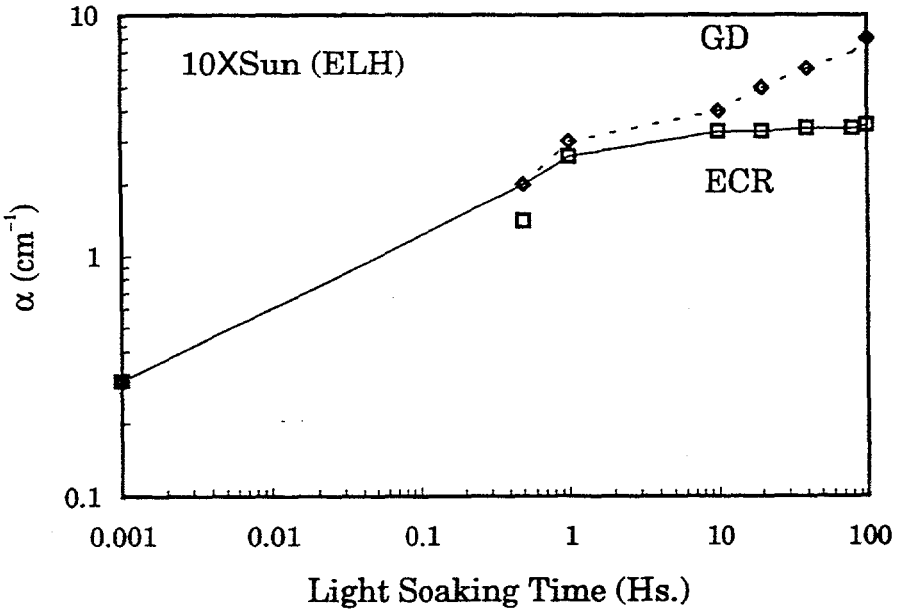

Fig. 1.15 Changes in subgap α of ECR and Glow-discharge films upon light soaking under 1000 mW/cm^2 illumination

1.5.3.2 Trap to dangling bond conversion.

In the past, we had observed that impurities plays a major role in degradation of the material [8, 9]. In particular, we had found that adding sub-ppm amounts of phosphine, or increasing the oxygen content of the material by deliberately contaminating the system with moisture during growth, increased light-induced degradation. We had also found that there were two distinctly different kinetics of degradation. The first was an initial, rapid decay of photoconductivity (over the first few ten to hundred seconds), which could be explained by invoking Adler's trap-to-dangling bond conversion model [6]. In this model, Adler suggested that impurities such as donors create a negatively charged trap, which absorbs a photo-generated hole and changes its local structural order, and becomes a neutral dangling bond with a higher cross-section for electron capture. Since the hole capture is a mono-molecular process, the kinetics of this recombination should essentially be of exponential type, with a lifetime which is inversely proportional to the intensity of light, something which we had previously verified experimentally [10].

The second, independent mechanism for degradation is the creation of additional defect states by bond-breaking, as postulated by Stutzmann et al. [11], and quantified by Redfield in his equilibration models [12]. In this mechanism, the weak bonds actually break due to energetic excitation created by electron-hole recombination, and the kinetics of this process, over some range in intensities, can be quantified by an $(\text{intensity})^2$ relationship. In time, this is a much slower process than the first process of trap-to-dangling bond conversion. In our materials, we do observe such relationships, but at later times, over the period of hours at normal 1-sun intensity.

During the course of this work, we decided to study the behavior of sub-gap a during the first few minutes of degradation, when the trap-to-dangling bond conversion model applies. In this model, a negatively charged trap absorbs a hole, and is converted into a neutral, singly-occupied dangling bond. The energetic positions of the two states are essentially the same, for small correlation energies. Therefore, since a doubly-occupied state is being converted into a singly-occupied state, the net optical absorption after this degradation should be less than that caused by an electron excitation from a singly occupied state. Therefore, the optical absorption should decrease after light soaking. This is totally contrary to all previous experimental data, and we wanted to see if such a phenomenon actually happened. The answer was yes, and the details of the experiment and the associated results are shown in Appendix A.

Therefore, based on the kinetics of the degradation process, and the decrease in optical absorption that accompanies this initial kinetics, we conclude that indeed, there are negatively charged traps in the material,and that they are converting into dangling bonds, and that this type of process does play a role in the degradation of the material.

1.5.3.3 Influence of compensation.

It occurred to us that since all a-Si:H material has donors, due to the presence of materials like oxygen, perhaps it might be useful to compensate this material and see what the influence is on

stability[13]. To do this, we prepared a series of films in the ECR reactor under carefully controlled and reproducible conditions, at temperatures ranging from 300-375°C. All the films were nominally undoped, but were partially compensated with controlled amounts of diborane. The results of the experiment are detailed in Appendix B. We found that when exact compensation is achieved, the films are the best (lowest defect density), both in the initial state and after light soaking. We postulate that this behavior is a result of compensation reducing the amount of 3-center bonds created by donors in the material. Too much compensation leads to defective bonding created by excess of B. This model was suggested to us by Professor Redfield of Stanford University , and we are grateful to him for pointing out his work to us.

1.6 Device Fabrication

Many groups have reported more stable materials in recent years [14-16]. Many of these more stable materials were made at higher deposition temperatures, such as 350-450°C. Fabricating devices at such temperatures creates unusual problems. Among these are:

- Reduction of tin oxide or zinc oxide by H plasma.
- Diffusion of B from the *p* layer into the *i* layer

These problems are particularly severe for the superstrate design, because in a superstrate, the device is made on tin oxide, and since *p* layer is the first layer made, there is significant time during the fabrication of the remaining layers for B to diffuse into the *i* layer.

We decided to systematically try to solve these problems.

1.6.1 Reduction of Tin Oxide at Higher Temperatures

To overcome this problem, we started the growth of the *p* layer at lower temperatures, e.g., 175-190°C, and then ramped the temperature up to the *i* layer temperature. Also, to minimize interaction between hydrogen and tin oxide, we used a He-diluted *p* layer, rather than H-diluted. The *p* layers were a-(Si,C):H, grown using mixtures of silane, methane, diborane, and helium. Typical dilution ratio by He was 10:1 during the *p* layer growth. The growth rate of the *p* layer was about 0.5 Å/s. The typical conductivity vs. bandgap curve for the ECR deposited *p* layers is shown in Fig. 1.16.

1.6.2 Preventing B Diffusion into the *i* Layer

B is known to diffuse rapidly into a-Si:H . When significant amount of B goes into the *i* layer, severe recombination problems can arise for the electrons generated in the i layer. To see this, consider two band diagrams as shown in Fig. 1.17. The solid curve shows what the band profile will look like when no B is present in the *i* layer, and the broken curve shows the band profile when B has diffused into the *i* layer. Therefore, when significant B is present in the *i* layer, the electric field in the *p-i* interface region will be less, leading to a reduction in the drift velocity of electrons away from the interface, and increasing recombination. In addition, the presence

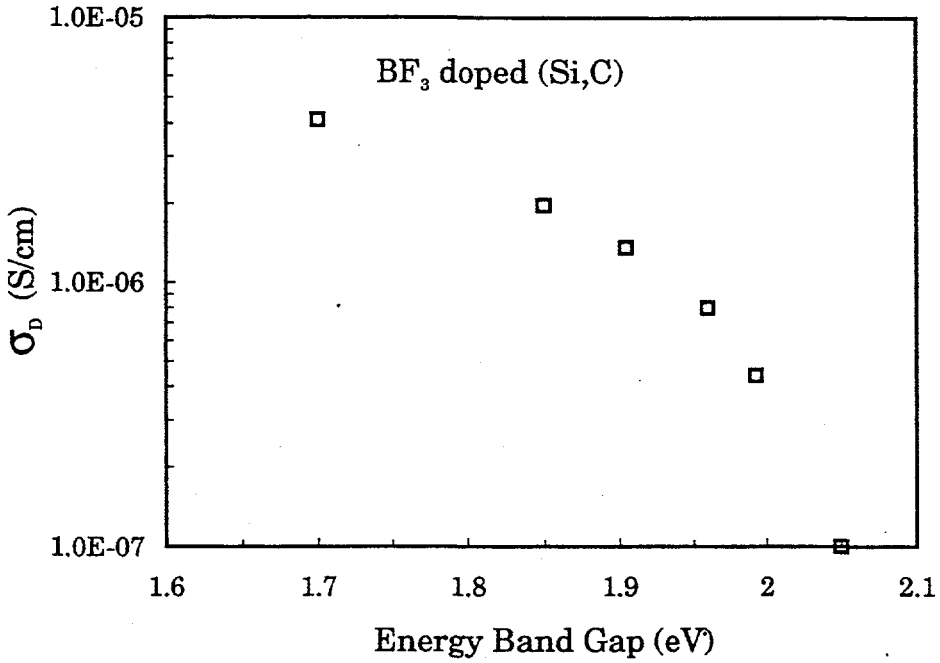

Fig.1.16 Conductivity of B-doped ECR deposited a-(Si,C):H Film

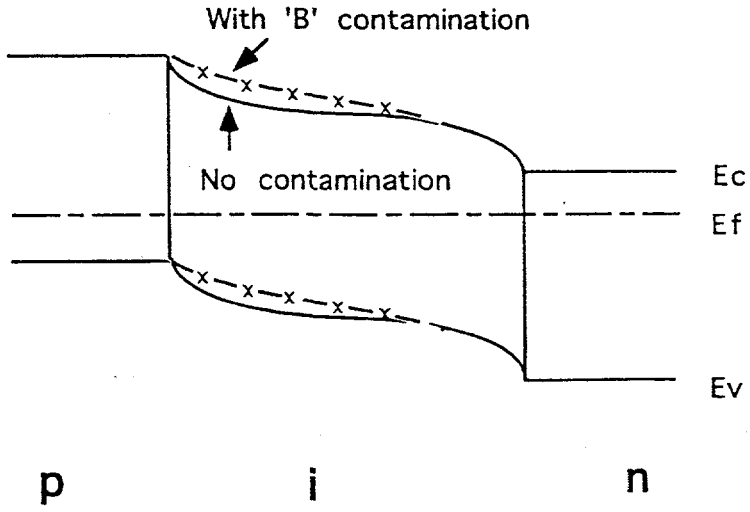

Fig. 1.17 Band bending near p-i interface with and without B contamination

of B will lead to the creation of positively charged centers in the *i* layer near the *p-i* interface region, and these centers will likely have a higher capture cross-section for electrons, and therefore, also lead to increased recombination of electrons in this region. So, for both these reasons, it is not useful to have B in this region.

These considerations are easily borne out by measuring quantum efficiency of devices [17], particularly under different bias conditions. One typically finds increased ratio of QE under reverse to zero bias in this region when significant contamination exists [17]. An example of such a QE ratio curve is shown in Fig. 1.18, and the corresponding I(V) curve is shown in Fig. 1.19. To reduce the B diffusion into the *i* layer from the *p* layer, we used a strategy of using a high C content (Si,C) buffer layer. We found that the diffusion of B is substantially suppressed in a-(Si,C):H compared to the diffusion in a-Si:H. The device structure we use is shown in Fig. 1.20. The a-(Si,C):H buffer layer is graded between the bandgap of *p* a-(Si,C):H and *i* a-Si:H.

The design of the buffer layer is critical, in that too little C or too thin a layer lead to diffusion of B, but too much C or too thick a buffer layer lead to inflection points in the I(V) curve, as shown in Fig. 1.21. To understand this curve, we measured quantum efficiency ratio under zero and forward bias for such a device. Under forward bias, the electric field is reduced significantly in the device, and any recombination problems should be immediately evident. In Fig. 1.22, we show the QE and the QE ratio for this device. It is apparent from the curves that a reduction in field causes a reduction in carrier collection over almost the entire wavelength range of interest, except for the very short wavelength photons. These short wavelength photons are strongly absorbed in the first few ten nm of the *i* layer, whereas photons of longer wavelength are absorbed over longer distances. From this observation, then, we can conclude that there appears to be a problem in collecting carriers generated by photons which are absorbed beyond a few ten nanometers into the *i* layer.

This fact is very suggestive of a hole trapping phenomenon, as shown in Fig. 1.23. When the band gap of the buffer layer is too high, there may be a notch developing in the valence band between the buffer layer and the *i* layer, leading to a trapping of holes. Under reverse bias, the fields are high enough for holes to tunnel through the buffer layer, but under forward bias, the decrease in field may lead to hole trapping. Under still stronger forward bias, holes are being injected from the *p* into the *i* layer, and the notch plays no part in the current. Therefore, we get an inflection point in the I(V) curve. A thicker buffer layer makes the problem worse, by reducing the tunneling of holes across the barrier created by the notch.

Thus, one has to be very careful when making devices with buffer layers, particularly at higher temperatures. The two conflicting requirements of preventing B diffusion, and allowing good hole transport, are not always met. However, when the buffer layer is done right, a normal I(V) curve as shown in Fig. 1.24 results. The corresponding QE and QE ratio curves are shown in Fig. 1.25. Please note that the QE ratio curve for this device shows a normal behavior for good devices, with only small changes upon application of bias, and almost independent of wavelength [17]. Note that the *i* layers in both the device curves, Fig. 1.21 and 1.24, were identical.

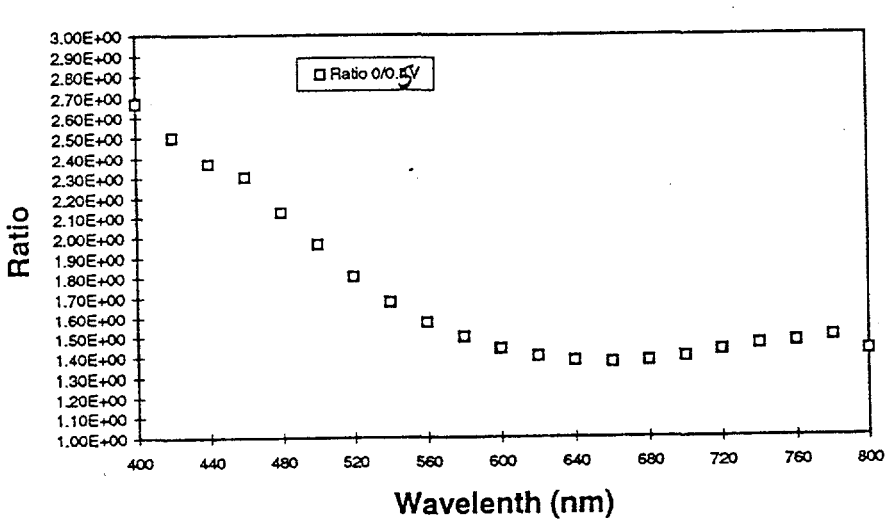

Fig. 1.18 Ratio of Quantum Efficiencies at 0V to +0.5V for a sample which had suffered B diffusion because of inadequate buffer layer

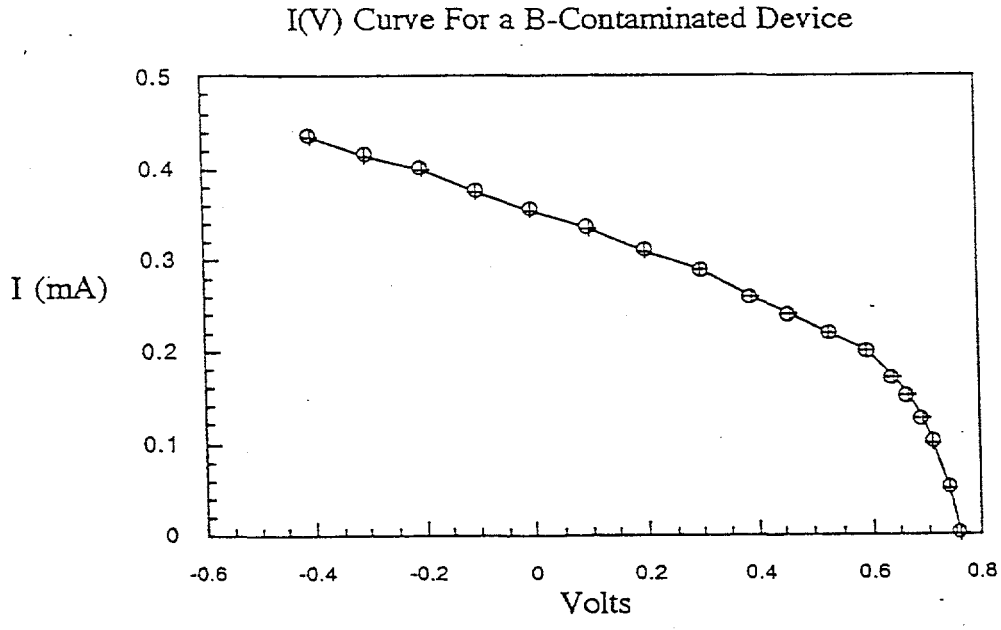

Fig. 1.19 I(V) curve of a device with excessive B diffusion

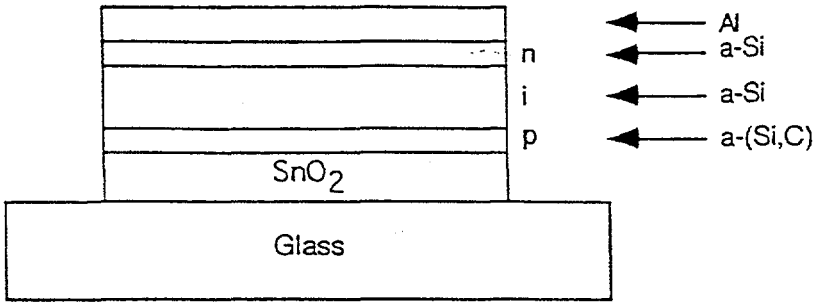

Fig. 1.20 Device Structure Used In This Work

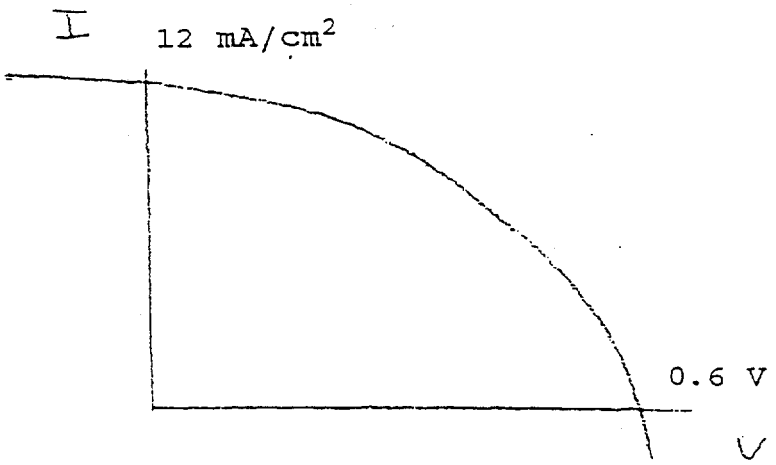

Fig. 1.21 I(V) Curve of a device with an inflexion point

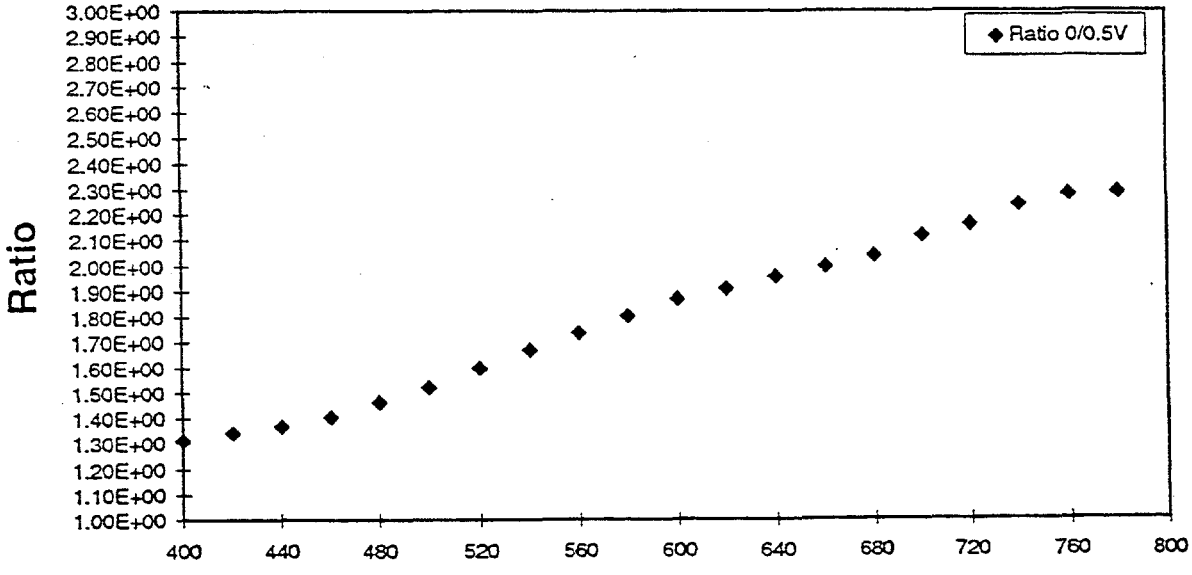

Fig. 1.22 QE Ratio (0V/+0.4V) for device of Fig. 1.20, showing problems with carrier collection.

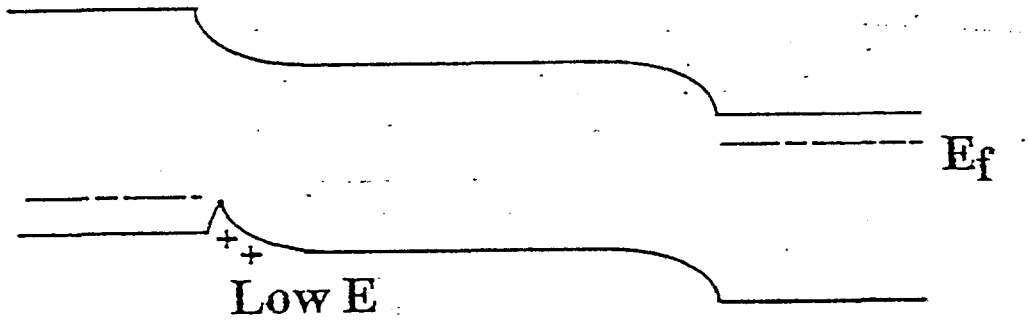

Fig. 1.23 Explanation of I(V) Curve of Fig. 1.21, and QE curve of Fig. 1.22, by postulating a notch in the valence band at which holes can get trapped under forward bias.

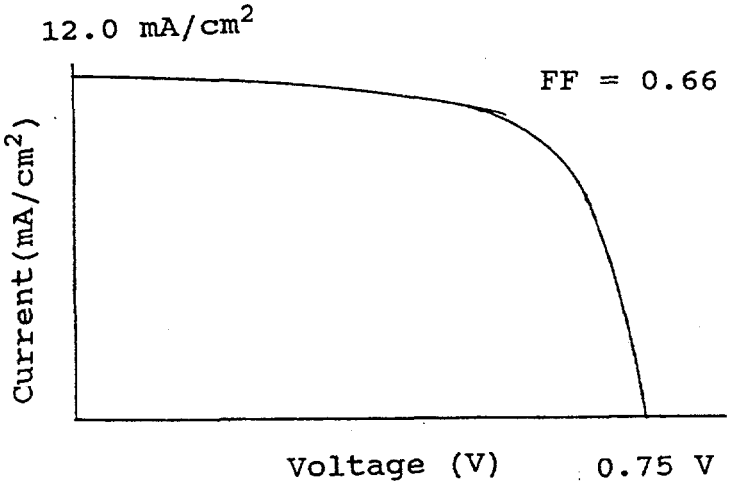

Fig. 1.24 Normal I(V) curve for a device

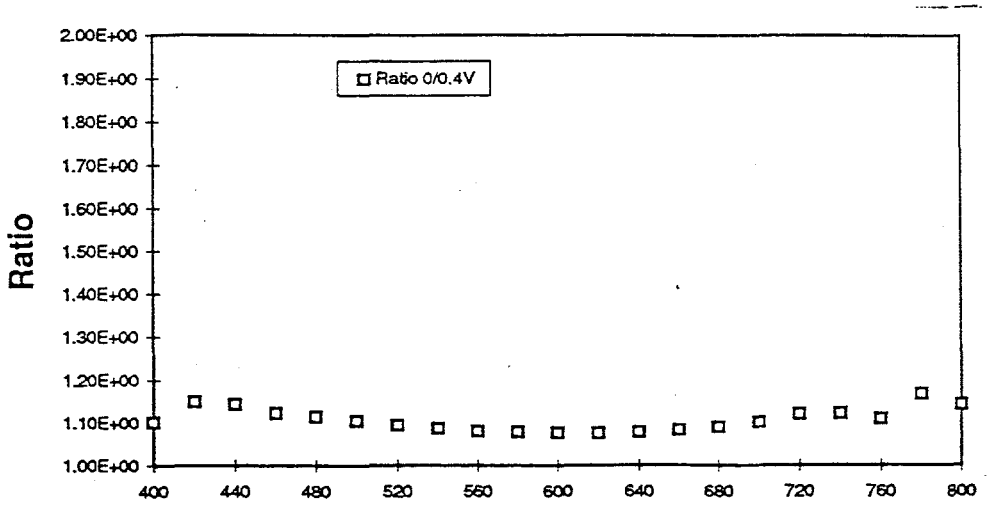

Fig. 1.25 QE Ratio curve for a normal device

The best device we have made is approximately 8% efficient before light-induced degradation. Its I(V) curve is shown in Fig. 1.26. Further experiments to optimize this device and to study its stability will be done over the next contract.

1.7 Summary of Chapter I.

To summarize, we have studied the following during this contract:

1. Growth of more stable, high quality a-Si:H material using high temperature ECR discharge.

2. Control over microstructure of the film, and the ability to change it smoothly from amorphous to polycrystalline by controlling the etching properties of the plasma.

3. Understanding of the influence of compensation on the stability of the material.

4. A study of the plasma properties of the ECR discharge, including measurements of ion energies and densities.

5. A study of the initial stages of instability, with some evidence for the presence of two separate mechanisms of instability, one related to impurities, and the other to bond breaking and equilibration.

6. Fabrication of 8% efficiency (initial) devices at high temperatures using the ECR system. To do this, we had to overcome several difficult problems related to buffer layers and B diffusion, which we successfully did.

7. Fabrication of a low gap a-Si:H (1.67 eV) film using He diluted ECR discharge.

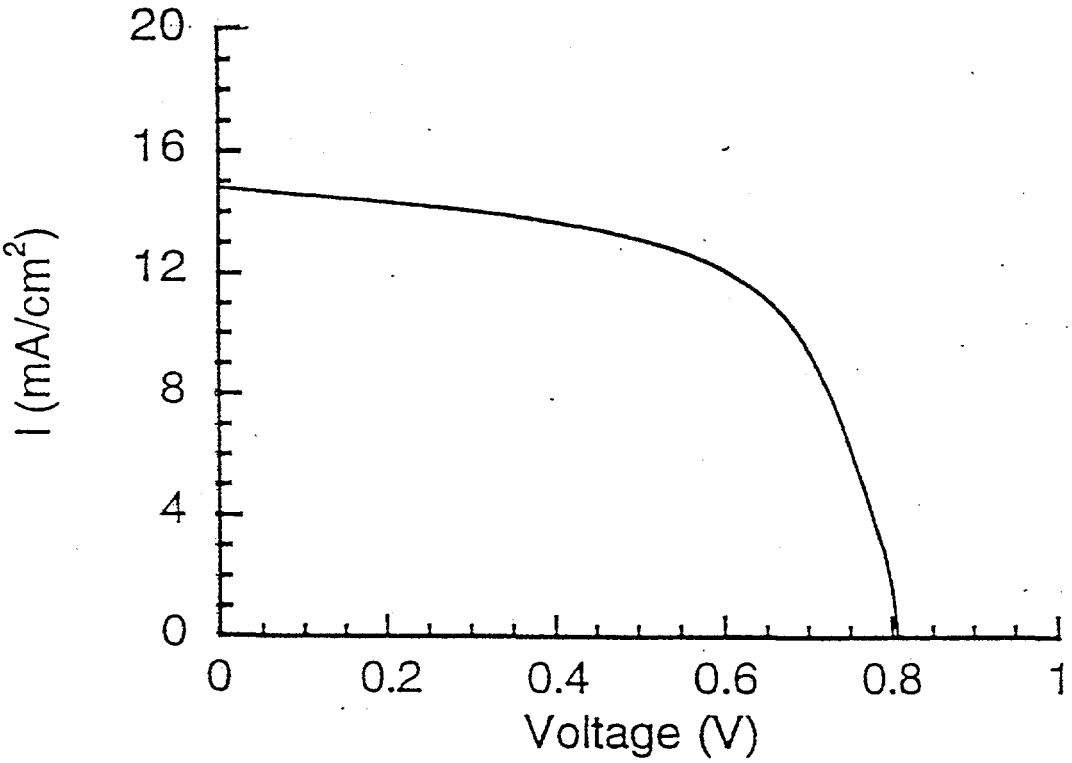

Fig. 1.26 I(V) Curve of best ECR-deposited a-Si:H solar cell

Chapter II
Design and Fabrication of Alternative Device Structures in a-Si:H

2.1 Objective

One of the objectives of this program was to design and fabricate alternative device structures in a-Si:H which may be potentially more stable than standard a-Si:H cells. In this chapter, we report on such structures.

2.2 Physics of Instability of Devices

It has been generally recognized that the instability of devices is directly related to the creation of defects, both at the *p-i* interface, and in the bulk of the *i* layer. The *increasing* defect density has two consequences.

1. It *increases* the number of defects contributing to recombination. As a result, the lifetime of both electrons and holes decreases. Consequently, there is a decrease in collection or quantum efficiency (QE) of photo-generated carriers, both near the *p-i* interface, and in the bulk of the *i* layer.

2. It *decreases* the electric field in the middle of the *i* layer [18,19], particularly under forward bias (near the maximum power point of the I-V curve). A schematic diagram of the decreased field, based on a simple model used by us [18], is shown in Figure 2.1.

The combination of reduced lifetime and reduced electric field is catastrophic for the device. In particular, the quantum efficiency is reduced dramatically under forward bias. In Figure 2.2, we show an illustrative decrease in QE under forward bias of 0.6 V before and after light-induced degradation [18]. Note that in this model, we do not account for a further loss in QE due to increased electron recombination at the *p-i* interface. The predicted decrease in QE, shown in Fig. 2.2, is the primary reason why the fill factor in the cell decreases after light-induced degradation. Quite clearly then, if we can reduce the loss in QE under forward bias after degradation, we can improve the stability of the cell.

The conventional way of achieving this aim is to use a very thin *i* layer. A thin *i* layer leads to a higher field in the mid-gap region, and hence, the cell is less susceptible to degradation. However, using a very thin cell has potential problems, among them a tendency to generate shunts under illumination [20]. Also, a very thin *i* layer leads to incomplete light collection, and puts unreasonable demands on the amount of light-trapping that practically can be achieved. Therefore, it would be useful if we could counteract at least a part of the degradation in performance of solar cells caused by the increasing defect density. In the previous chapter, we

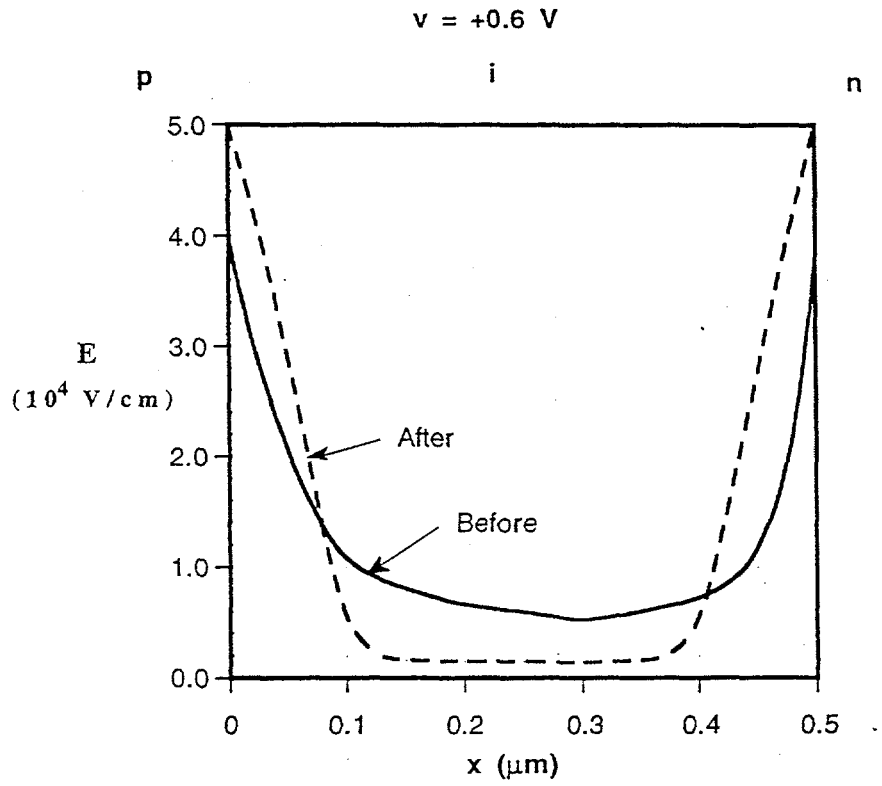

Fig. 2.1 Calculated electric field profile in the i layer of a device before and after light soaking

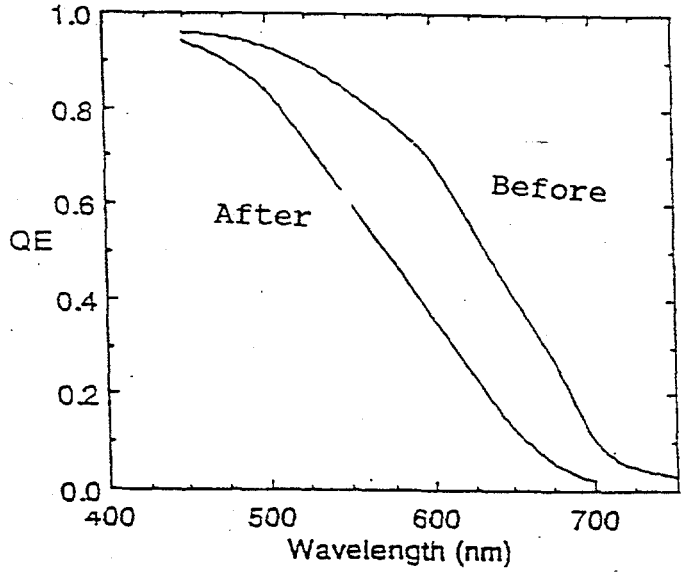

Fig. 2.2 Calculated Quantum Efficiencies in a device before and after light soaking

addressed how to do this by improving the basic material, using chemical means (H etching during growth). In this chapter, we show how to potentially increase the electric field in the device by using bandgap grading strategies.

2.3 Concept of Bandgap Grading and Design of Devices

In principle, a structure which would use a graded bandgap in the *i* layer by grading the valence band only, can achieve an extra electric field in the device (see Fig. 2.3). Since the electric field is only low in the middle portions of the device, the grading should be used in the middle only . Also, the effect of grading should be mainly felt on the valence band, and not on the conduction band. If upon grading both conduction and valence bands move, then the band diagram will look as shown in Fig. 2.4, and that would be unfortunate, since it will serve to retard the transport of electrons to the back *n* contact.

The question now is: How do we achieve this grading, and how much do we need? For a 400-nm-thick *i* layer, it is the middle 150 nm which needs the electric field. To provide a high electric field in this region (> 1E4 V/cm), we need a grading of 0.15 eV; all in the valence band if possible.

To address the question of how do we achieve this sort of bandgap change in a-Si:H, we recall that the bandgap of a-Si:H is not fixed. It varies from about 1.7 eV for a material made at higher temperatures (300-350°C) without H_2 dilution, to almost 1.85 eV for material made at lower temperatures with H_2 dilution [21]. In the previous chapter we have seen that we can even get 1.66 eV, using He electron-cyclotron-resonance (ECR) discharge. Thus, in principle at least, it appears that about 0.15 eV may be available for grading.

Unfortunately, not all this change in bandgap upon H_2 dilution ends up in the movement of the valence band, though the literature does suggest that most of it does [6]. A little reverse grading in the conduction band does not hurt the device, since the electrons have a much higher diffusion length than holes, their mobility-lifetime ($\mu\tau$) product being in the range of 5-10x10^{-7} cm^2/V, giving a field-free diffusion length before degradation of 1-2 μm. Given their much higher diffusion length, the electrons do not need quite the field assist that holes do, except near the *p-i* interface, where their diffusion length is much lower. The diffusion length of electrons is lower near the *p-i* interface, because the Fermi level is in the bottom half of the gap in that region. As a result, many empty states and positively charged defects are likely to be there. These defects can capture electrons rather easily . Of course, to provide such a field for electrons is precisely why we use a graded buffer layer, made from a-(Si,C):H with a varying ratio of Si:C between the *p* and the *i* layers [17] (see Fig. 2.5). We will have more to say about buffer layers later on in this chapter.

Based on the above analysis, a simple device that can easily be fabricated (at least in principle) to see if the grading strategy works is shown in Fig. 2.6. It consists of the following layers:

1. A *p* a-(Si,C):H layer.

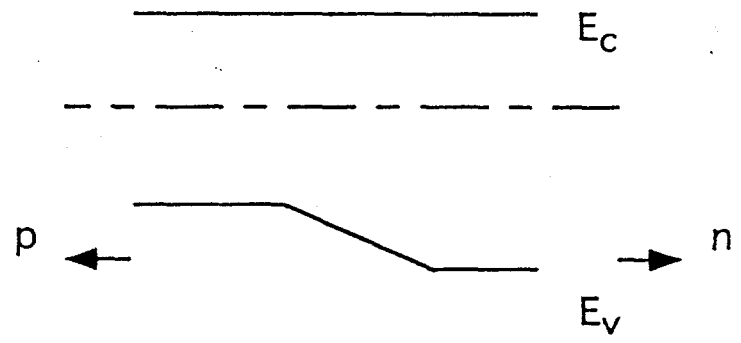

Fig. 2.3 Desired bandgap profile to create an additional electric field in the middle of the i layer to assist holes

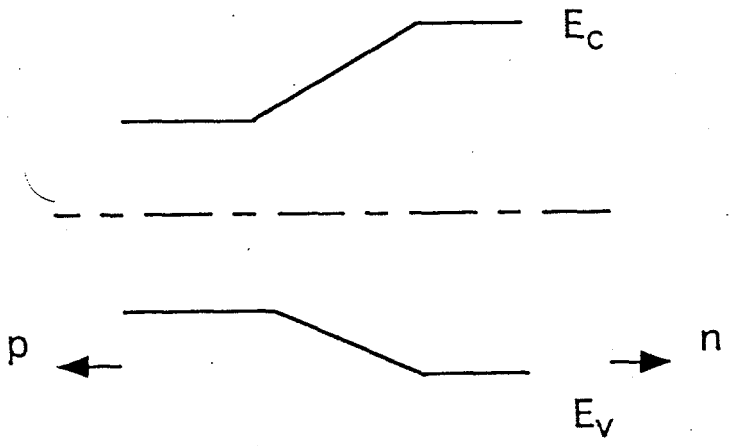

Fig. 2.4 Undesired bandgap grading, which impedes the transport of electrons

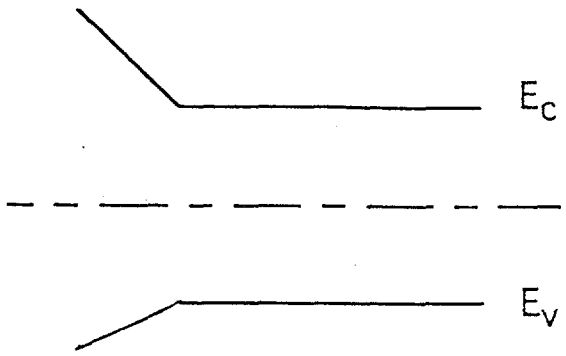

Fig. 2.5 Band diagram of buffer layer at p-i interface

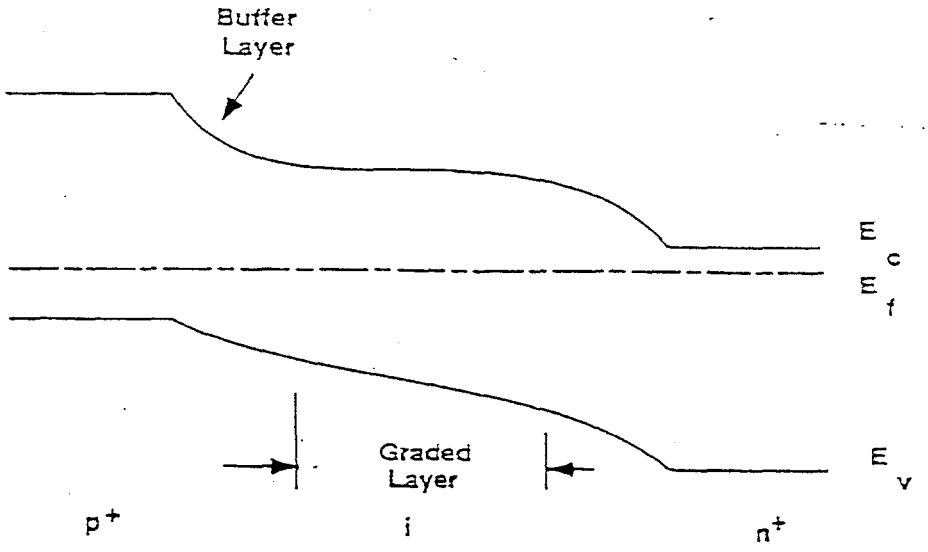

Fig. 2.6 Band diagram of graded gap cell used in this study

2. A graded-gap, thin, buffer layer, made by varying the ratio of methane to silane in the gas phase.

3. A lower gap (about 1.72 eV) *i* layer, starting with a higher temperature (350°C) deposition from silane, extending for about 100 nm.

4. A graded gap *i* layer, extending for about 120 nm, made by lowering the deposition temperature to about 250°C, and increasing the hydrogen-to-silane ratio from 0% hydrogen to 80% hydrogen. The final bandgap is in the 1.80 eV range, providing only about 0.08 eV of grading, as opposed to 0.15 eV called for in the design. But it is enough to demonstrate the concept.

5. A constant gap a-Si:H layer of about 1.80 eV, made at about 250°C, about 100 nm thick.

6. A final *n* layer.

The cell can be made either in the substrate or the superstrate mode. We have chosen to use superstrate structures deposited on tin oxide substrates provided by Solarex Corp. The back metal contact was Al, evaporated thermally. The entire device was made using RF triode glow-discharge deposition [27].

2.4 Problems with Devices

We face several unique problems when trying to make a device with such a graded gap design.

2.4.1 Reduction of tin oxide at high temperatures

This is the same problem discussed in Chapter 1 and the solution is similar, namely start the deposition of the *p* layer at a lower temperature (200°C). Since the glow discharge plasma is not as intense as the ECR plasma, we can use hydrogen as the diluent gas while making the *p* layer, unlike the case for the ECR system, where the use of hydrogen led to unpredictable and non-reproducible results.

2.4.2 Diffusion across the p-i interface

This problem is also similar to the problem faced in the ECR system. The solution is similar, namely the use of a buffer layer with a higher C/Si ratio at the *p* interface than would be the case for a cell made at lower temperatures. Once again, one has to be careful about the use of C, since it leads to a step in the valence band edge if not done properly, leading to strange looking I(V) curves, with inflection points. See Chapter 1 for details.

2.4.3 Problems with tunneling across tin oxide/p layers

Traditionally, it has been assumed that a suitable tunnel junction exists between the heavily *n*-doped tin oxide substrate layer and the adjacent *p* a-(Si,C):H layer. However, the limited

conductivity of the high-gap *p* a-(Si,C):H layer (which is typically used to make the best devices) can lead to series resistance problems at that interface. In particular, as one goes to non-textured tin oxide substrates or to zinc oxide substrates, the resistive loss problem becomes worse. In the worst case, a double diode exists in the device, as illustrated in the I(V) characteristics shown in Fig. 2.7. This phenomenon can be understood by plotting the band diagram of the *p*-SnO_2 interface (see Fig. 2.8). We have used the appropriate work functions or electron affinities described in the literature [28] for drawing this diagram. It is immediately obvious from this diagram that the limited conductivity of the high gap *p* a-(Si,C):H layer leads to a Schottky barrier at the interface whose depletion width extends some substantial amount into the *p* layer. As a result, the tunneling of holes from the *p* layer into the tin oxide is impeded, leading to a non-ohmic contact to the *p* layer.

To overcome this problem, we have devised a new structure for the *p* layer, where the bandgap of the *p* layer is kept smaller at the tin oxide interface, and then graded up by changing the C:Si ratio as the layer grows (See Fig. 2.9). The *p* layer next to the tin oxide, being of a narrower gap, has a higher conductivity, and hence, the depletion width is shorter, leading to efficient tunneling of holes from the *p* layer into tin oxide. We use such layers for all our devices now, whether on textured or non-textured substrates, and both for tin oxide and zinc oxide substrates. Since we started using such layers, all the double-diode problems have disappeared. It is our understanding that this new device structure, which we have described at NREL team meetings, has now been adopted by many of the university and industrial groups for solving their diode problems.

2.5 Device Results

The device results for our graded-gap cell are shown in Fig. 2.10. There, we show the I(V) curve for a device made with the grading scheme discussed above in Sec. 2.3. The device efficiency is in the 8+% range, with a very good fill factor (70%), indicating a good device. This device result is in spite of a part of the device being made at higher temperatures. The back metallization for the device was Al, and the device area was 0.08 cm^2.

In contrast, if we do not use a graded gap, but make the device at higher temperatures, the results are as shown in Fig. 2.11. Quite clearly, the device of Fig. 2.11 has a lower fill factor and lower efficiency than the device of Fig. 2.10. These results are confirmed by plotting the ratio of the quantum efficiencies for the two devices under reverse and zero bias [17] in Fig. 2.12. It will be recalled from our previous work [17] that the QE ratio measurement is a very sensitive measurement to see where recombination is taking place in the device. In particular, a high ratio for 400-450 nm light denotes problems with electron recombination near the *p-i* interface, and a high ratio in the red regions of the spectrum denotes problems with hole collection for light incident from the *p* layer. The much lower ratio for the appropriately graded structure, shown in Fig. 2.13, compared to the ratio for the ungraded device shown in Fig. 2.14, is a clear indication that the grading scheme has worked to improve the collection of holes in the device, even though the experimentally achieved grading was much lower than the design value.

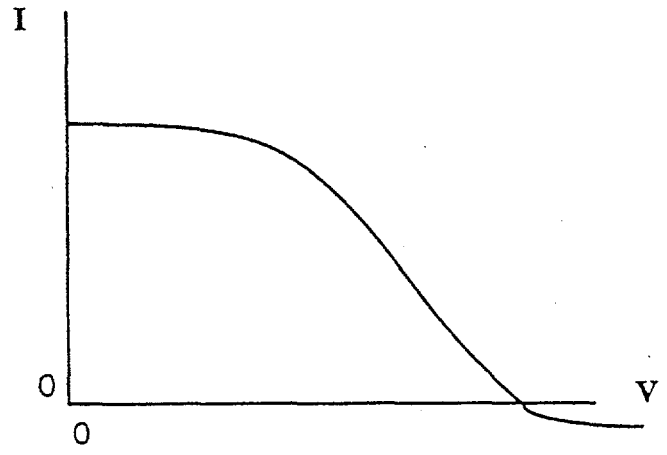

Fig. 2.7 A classical double-diode type I(V) characteristic

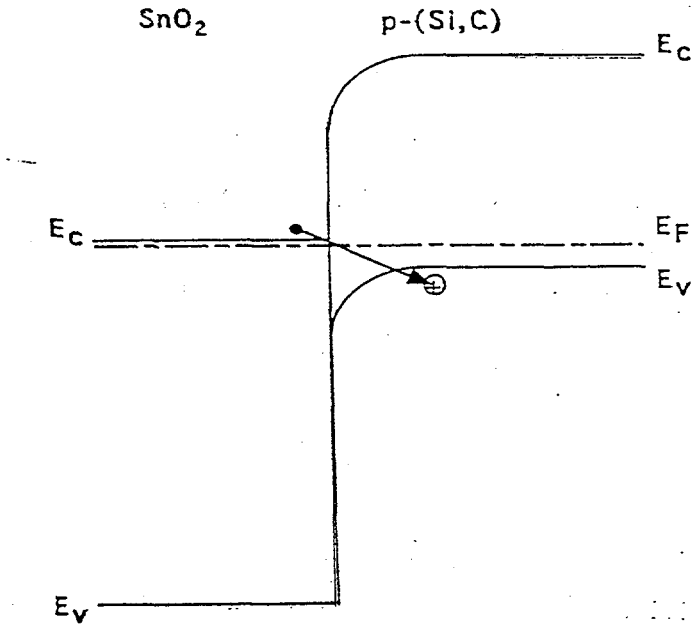

Fig. 2.8 Band diagram of p-(Si,C):H/n SnO_2 interface. showing potential tunneling problems which can lead to non-ohmic characteristics

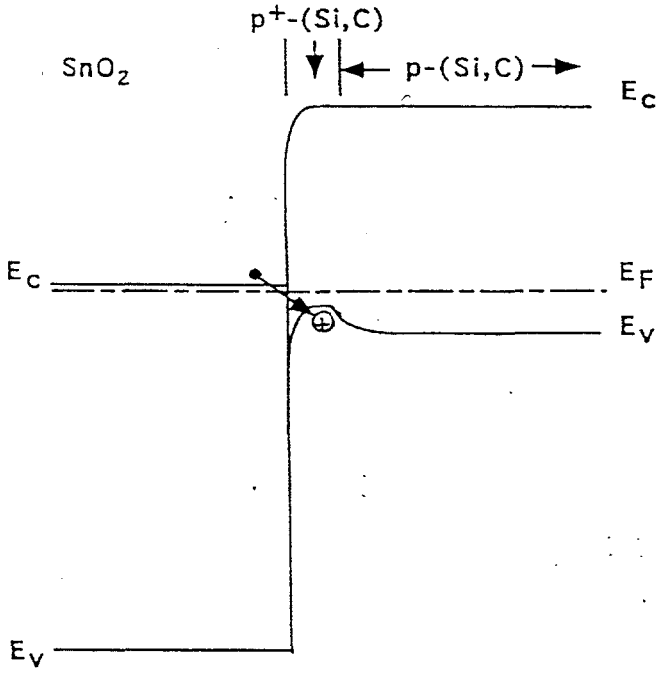

Fig. 2.9 Band diagram of new device structure, interposing a narrower gap p layer next to the tin oxide, which eliminates double diodes

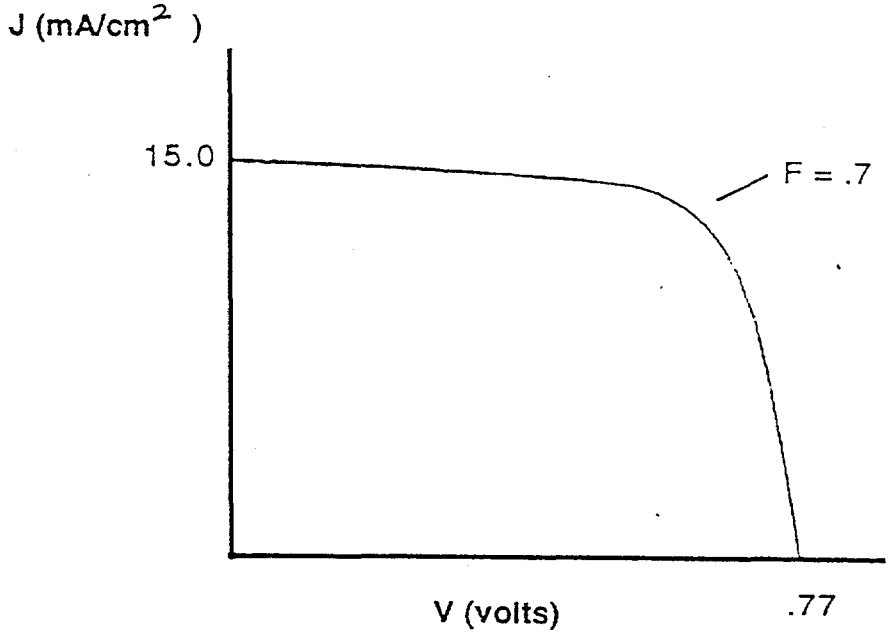

Fig. 2.10 I(V) curve of a graded gap a-Si:H solar cell

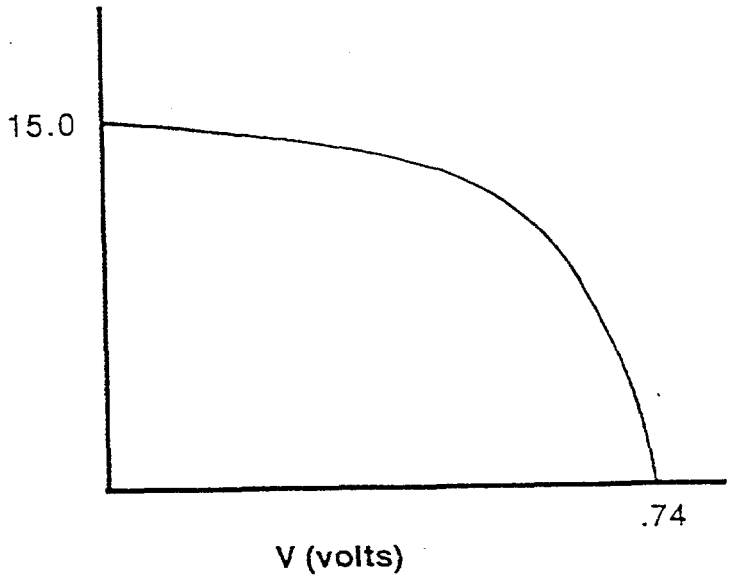

Fig. 2.11 I(V) curve of an ungraded, higher temperature cell

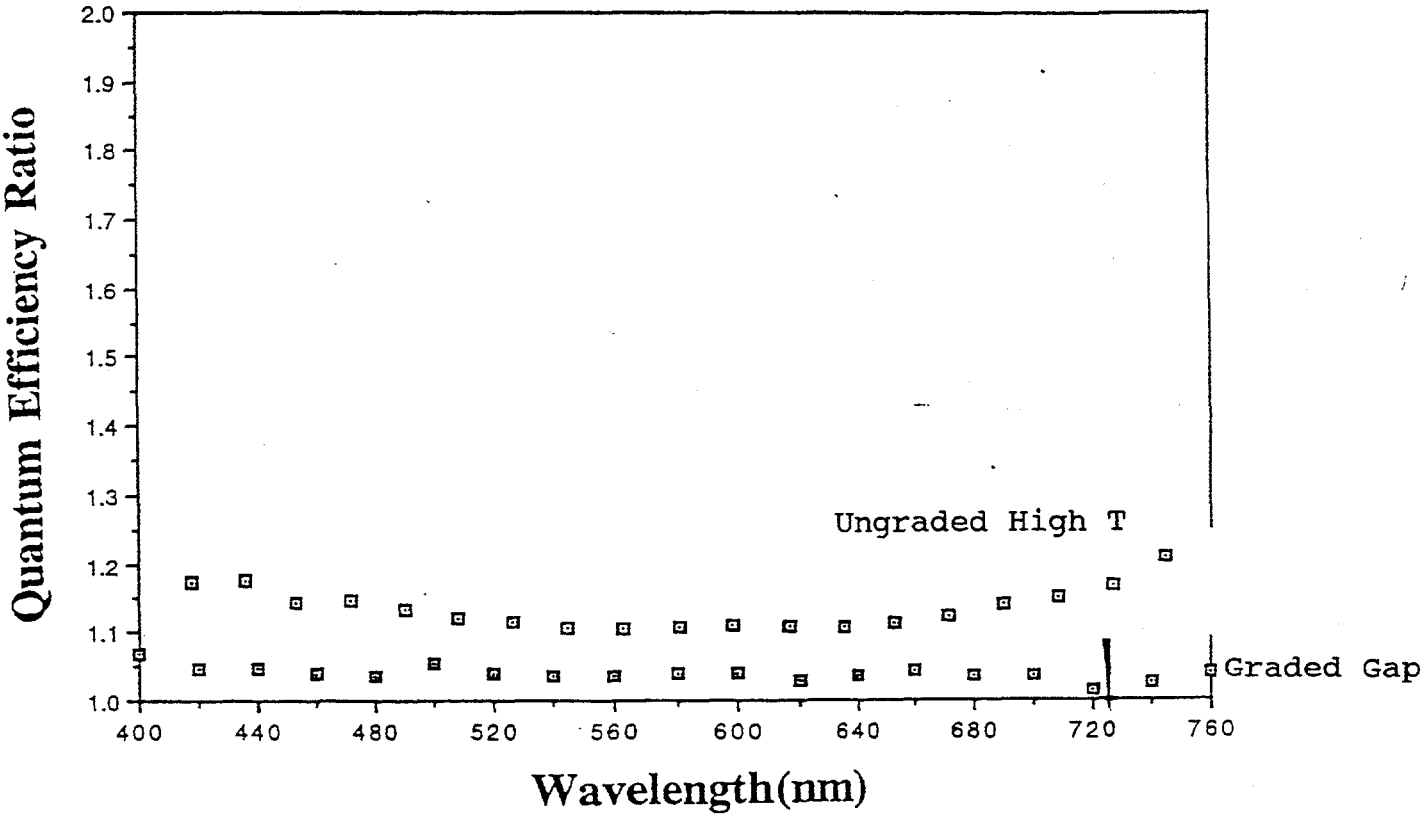

Fig.2.12 Comparison of QE ratio(-1V/0V) for graded and ungraded cells made at the same temperature

This preliminary device result was very encouraging, and we decided to study its stability. To do that, we measured two cells, one graded and one a standard glow discharge cell deposited at 250°C. Each of the cells had the same *i* layer thickness (about 350 nm), each was in the 8-9% efficiency range and each had high fill factor (70% range initially). The high fill factors are an indication of the good material quality in each cell. We subjected these cells to intense light soaking under 7 x sun illumination from a xenon arc lamp. The change in fill factor, which is the parameter that changes the most under light soaking, is plotted in Fig. 2.13 as a function of light soaking time under intense illumination for both these cells. It is quite obvious from the figure that the cell with the graded bandgap is significantly more stable than a standard glow discharge cell.

This preliminary result gives us hope that by incorporating many of the schemes for controlling bandgap and stability, described in Chapter 1, we can design and fabricate a cell which is more stable, both because its design is better, and because the material is better. That is what we plan to do over the next contract periods. While achieving the appropriate band grading in new materials is not going to be trivial, it is worth pursuing because of the enormous potential for improvements in stability.

Note also that we have not discussed how to improve the stability of the *p-i* interface in this section. That topic will also be a subject of research over the next contract period.

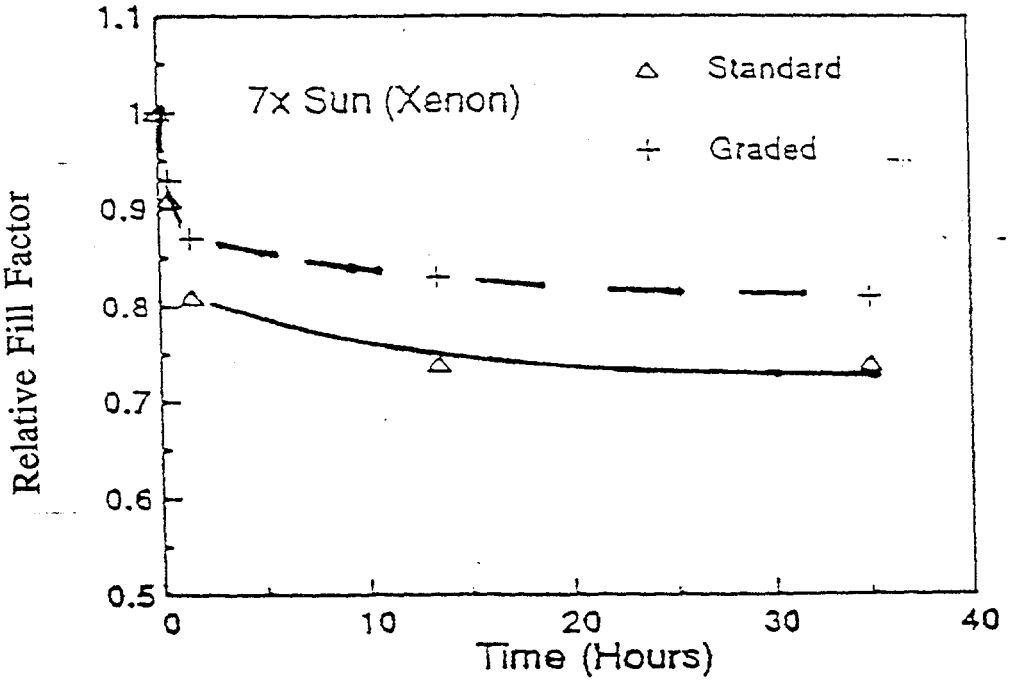

Fig. 2.13 Comparison of degradation in fill factor of two a-Si:H solar cells with similar i layer thicknesses, and similar efficiencies(8%). The graded cell is much more stable.

Chapter III
Research on a-(Si,Ge):H Films and Devices Deposited using Triode Glow Discharge

3.1 Objective

The objective of this research is to develop growth techniques and device grading strategies for reproducibly fabricating higher performance devices of low bandgap materials.

3.2 Problems with Material Growth

The growth of high-quality a-(Si,Ge):H films presents the experimentalist with several difficulties. Among these are:

1. The bond energy of germane is much lower than the bond energy of silane. As a result, during a plasma-growth process, the decomposition rate of germane is much higher than that of silane. Consequently, the Ge/Si ratio in the solid phase (in the film) is much higher than in the gas phase. The high decomposition rate of germane, in principle, can also lead to severe problems related to gas-phase homogenization, i.e., reactions between decomposition products of germane produce higher order germanes, e.g., Ge_2H_6. These radicals can then be decomposed to form GeH_2 and other polymers, which can lead to problems with film growth. It is generally accepted that the best a-Si:H films result when growth is from silyl (SiH_3) radicals, because these radicals offer a simple, step-by-step method for the growth of tetrahedrally coordinated films (see Ch.I). It is logical to assume that a similar conclusion may be applicable to the growth of a-(Si,Ge):H films, namely that the best film may be grown from silyl and germyl radicals, and not from higher order polymers or from secondary products such as GeH_2. Therefore, the high fractionation of germane by the plasma is a cause for concern. To reduce the reactions between the various germane decomposition products, one can use several strategies. Among these are: (a) use of low pressures, so as to avoid gas phase collisions between radicals produced by germane, and (b) use of a high dilution rate with He or H, so as to avoid collisions between germane radicals.

   We decided to use a combination of both these strategies, so as to promote the growth of reproducible films of this material, while staying with germane and silane as the primary feedstocks. The reasons for choosing silane and germane as the primary gases was that these gases area readily available in ultra-high purity (from e.g. Voltaix Inc.).

2. The very different bond strengths between Ge and H and Si and H mean that, unless one is careful, one may end up with dihydride-type bonding in the material, especially if the growth is done at low temperatures (200°-250°C). In order to preserve the Ge-H bond, one may inadvertently use growth conditions that lead to SiH_2-type bonding. This is

particularly true if one goes over into the physical vapor deposition type growth, as opposed to chemical vapor deposition type mode [24]. This is likely to be the case when the growth rate is too high. It is therefore not surprising that the literature shows a tremendous scatter in the properties of these films. As an example, in Fig. 3.1, we plot the data on dark- and photo-conductivities as a function of Tauc gap of the material taken from a review paper [25].

In Fig. 3.2, we show the data on Urbach energies quoted by Cohen et al. [26] on a-(Si,Ge):H films deposited using photo-CVD or glow-discharge, that also show a wide scatter. Quite clearly, there is a problem with the reproducible deposition of good silicon-germanium alloy materials in this system.

3.3 Geometry of the Reactor

We chose a geometry and gas conditions which we hope avoids both these problems. The basic geometry of the reactor is shown in Fig. 3.3. It is a RF triode reactor, with the bottom electrode being the powered electrode. There is a grounded screen grid between the powered electrode and the substrate. In this geometry, the plasma is primarily confined between the bottom electrode and the screen, an effect which is visually obvious when one changes the polarity of the substrate. The substrate can be biased either positively or negatively with respect to the grid. Changing the substrate polarity changes the amount of light visible near the substrate, increasing it for positive polarity (electron bombardment) and decreasing it for negative polarity (ion bombardment). This ability to change the bombardment conditions of the substrate is an important advantage of this geometry. It will be recalled Dalal et al. [22] had used such geometries to produce high efficiency (10+%) cells in a-Si:H back in 1985, and also had produced decent quality a-(Si,Ge):H films with little dihydride bonding when the film was subjected to ion bombardment [27]. The combination of ion bombardment and the use of highly diluted gases has allowed us to make high-quality films reproducibly in this reactor.

3.4 Typical Growth Conditions

As a diluent gas, we used H_2. To accurately control the amount of Ge incorporation, we used a 10% germane/hydrogen mixture, with Si being provided by using 100% silane. Table 3.1 lists the growth conditions for a series of samples we produced. All the samples were produced at low pressures (around 20 mT). The slight changes in pressure are entirely due to increased gas flows and the limited pumping capacity of the turbo pump. In Table 3.2, we show the corresponding growth rates and electronic properties of the films.

Note the exceptionally good control over growth rates, where we tried to maintain a low growth rate (about 0.5 Å/s) over the entire range of films studied so as to achieve a CVD- rather than PVD-type growth. Slight increases in plasma power led to slight increases in growth rate, and small increases in H dilution led to small decreases in growth rates, as expected. The typical power densities are 0.1 W/cm^2, with the RF electrode area being about 200 cm^2.

Please note from Table 3.2 that the activation energies are approximately half the bandgap,

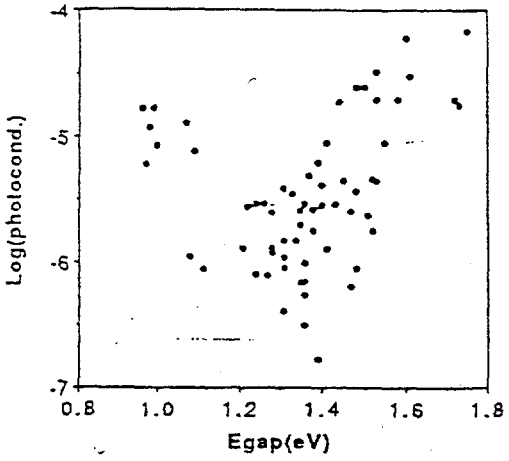

Fig.3.1 Photo and dark conductivities from previous work on a-(Si,Ge):H alloys (Ref: Fortmann[25]).

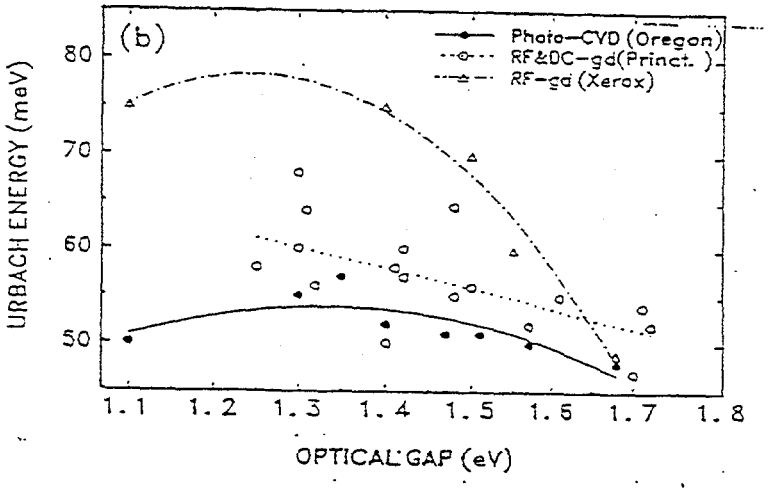

Fig.3.2 Urbach energy of valence band tails vs. Tauc gap in a-(Si,Ge):H alloys. (Ref: Cohen[26])

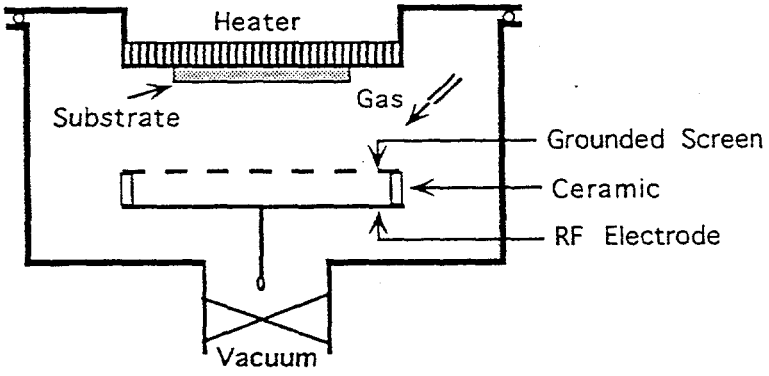

Fig. 3.3 Schematic diagram of RF triode reactor used in this work

Table 3.1 Deposition conditions of a-(Si,Ge):H films used for optical and electrical characterization

						Gas Flow Rates		
						100%	10%	100%
Sample #	Pressure (mTorr)	Temp (°C)	Time (min.)	Power (watts)	Vsub (volts)	SiH_4 (sccm)	GeH_4 (sccm)	H_2 (sccm)
1/300	20.9	350	180	25	0	4	0	40
1/303	19.0	300	180	22	-30	8	8	50
1/304	19.6	300	210	22	-30	10	6	52
1/305	19.9	300	210	22	-30	8	12	50
1/306	19.8	350	205	22	-30	8	12	50
1/307	22.0	350	210	22	-30	6	8	60
1/308	19.4	350	270	22	-30	10	6	52
1/309	22.0	300	310	22	-30	6	8	60
1/310	17.2	350	270	25	-30	8	8	50
1/311	20.1	350	270	26	-30	8	12	50
1/312	22.1	350	300	23	-30	6	8	60

Table 3.2 Electronic Properties of a-(Si,Ge):H films

Sample #	Thickness (μm)	Tauc gap (eV)	Act. energy (eV)	σ_d (S/cm)	σ_{ph} (S/cm)	Photosens. (σ_d/σ_{ph})	Growth rate (Å/s)
1/300	0.63	1.78	0.82	8.7e-05	2.0e-10	4.4e+05	0.58
1/303	0.61	1.59	--	7.4e-06	1.7e-10	4.4e+04	0.56
1/304	0.68	1.62	0.8	1.9e-05	6.1e-11	3.1e+05	0.54
1/305	0.68	1.47	0.5	1.4e-05	2.2e-09	6.4e+04	0.54
1/306	0.66	1.46	0.69	4.5e-06	6.0e-10	7.5e+03	0.54
1/307	0.55	1.52	0.75	7.3e-06	1.8e-10	4.1e+04	0.43
1/308	0.84	1.63	--	1.5e-05	5.0e-11	3.0e+05	0.52
1/309	0.8	1.54	0.74	5.5e-06	1.7e-10	3.2e+04	0.43
1/310	0.8	1.56	--	6.3e-06	9.4e-11	6.7e+04	0.63
1/311	0.88	1.47	--	3.2e-06	4.1e-10	7.8e+03	0.54
1/312	0.77	1.55	--	6.8e-06	1.8e-10	3.9e+04	0.43

indicating the absence of any major concentration of donor or acceptor states in the material. Undoubtedly, there is oxygen (a donor) in the material. In our best a-Si:H, using SIMS, we find it to be at the $5x10^{18}$ cm^{-3} level. However, the O concentration is not shifting the Fermi level significantly towards the conduction band.

3.5 Electronic Properties of Films

The dark- and photoconductivity results are plotted in Fig. 3.4 as functions of the Tauc gap. Upon comparing these with the results shown in Fig. 3.1, it is obvious that we have succeeded in getting a very good control over our film properties. It is also obvious that while the photo-conductivity of the material does decrease as the Tauc gap decreases (Ge content increases), it does not precipitously decrease; rather the decrease is gradual and systematic. We will have more to say about this quantity a little later in this section.

Another property that we measured was the subgap absorption of the film. This was measured using a two-beam photo-conductivity technique developed by Wronski and co-workers [9]. The results for a typical a-(Si,Ge):H film are shown in Fig. 3.5. From the figure, one can estimate the valence band Urbach energy of for this film as being in the range of 49 meV. The subgap absorption coefficient α at the shoulder (the mid-gap absorption) for this film is about 1.0 cm^{-1}, indicating a high quality film. α measured at the shoulder of the plot for the different films is plotted as a function of Tauc gap in Fig. 3.6. Once again, in accord with the results shown in Fig. 3.4, the subgap α, which is a measure of mid-gap defect densities, does not increase precipitously as we increase the Ge content of the film; rather, the increase is gradual and systematic.

It is instructive to study the product of photoconductivity and subgap α at the shoulder, and plot this product as a function of the Tauc gap (Ge content). Since the subgap α is a measure of the midgap defect density, and presumably an increase in defect density will lead to a decrease in *electron* $\mu\tau$ product (and hence in photoconductivity), the product of these quantities, when plotted vs. Tauc gap, will tell us if the midgap defects are the controlling factors in the photoconductivity. This plot is shown in Fig. 3.7. From that figure, it appears that indeed, $\alpha\mu\tau$ product is constant as a function of Tauc gap, strongly suggesting that the midgap defects are controlling photoconductivity. We will have more to say about the influence of midgap α on *hole* $\mu\tau$ product later on in this chapter (where we find a similar result). Note that our results agree with the conclusion of Cohen and co-workers [26], who found a similar result when they plotted the product of $\mu\tau$ and defect density derived from capacitance spectroscopy on Schottky devices.

3.6 Measurement of Ge Content in Films

We used energy disperse x-ray diffraction (EDS) to measure the Si/Ge ratio in the films. For these measurements, films similar to the ones shown in Table 3.1 were deposited on tin oxide coated substrates, so as to simulate the device deposition conditions. Table 3.3 shows the deposition parameters of these films. The corresponding EDS spectra for three of the films are shown in Fig. 3.8. Comparing the data in Table 3.3 and in Figure 3.8, we can see that indeed,

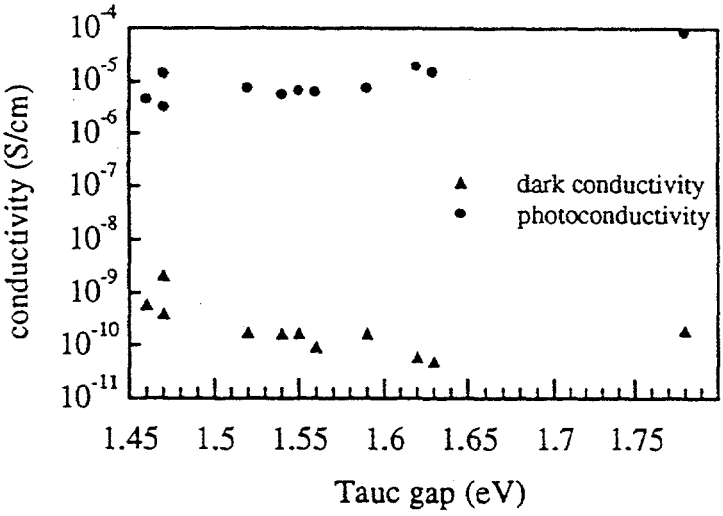

Fig. 3.4 Photo and dark conductivities of a-(Si,Ge):H films as a function of Tauc gap. The scatter of Fig. 3.1 is eliminated by using careful RF triode deposition

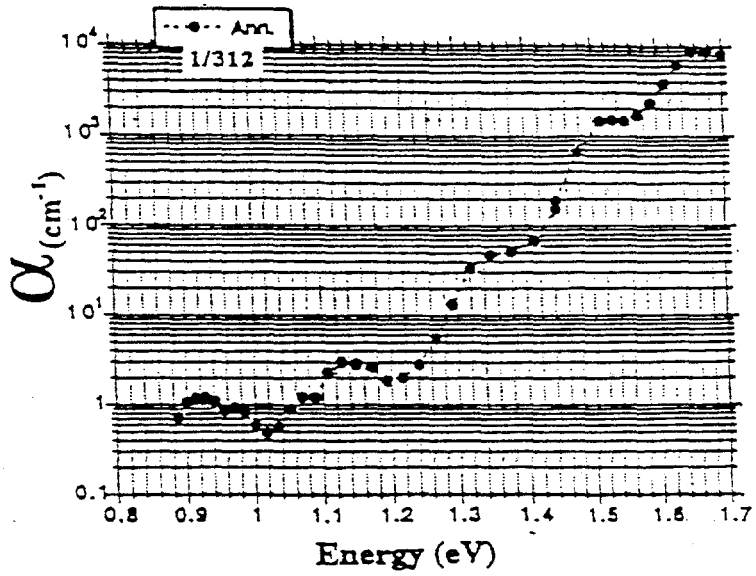

Fig. 3.5 Subgap absorption constant α as a function of photon energy for a typical a-(Si,Ge):H film

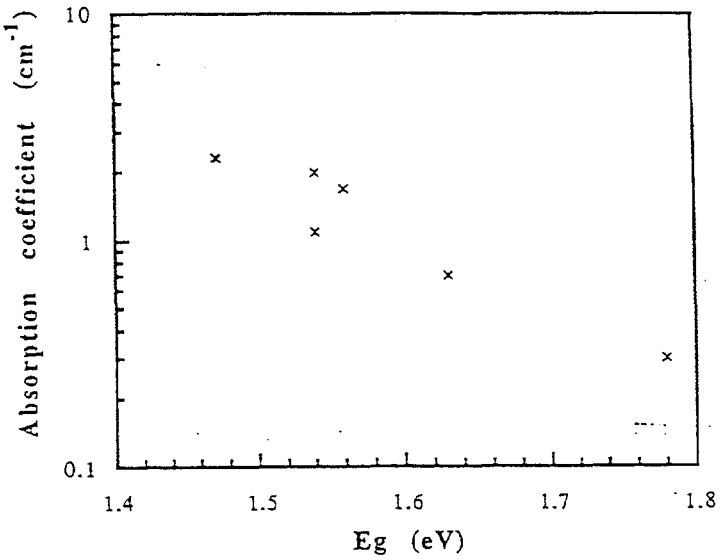

Fig. 3.6 Subgap Absorption coefficient α vs. Tauc gap for a-(Si,Ge):H films

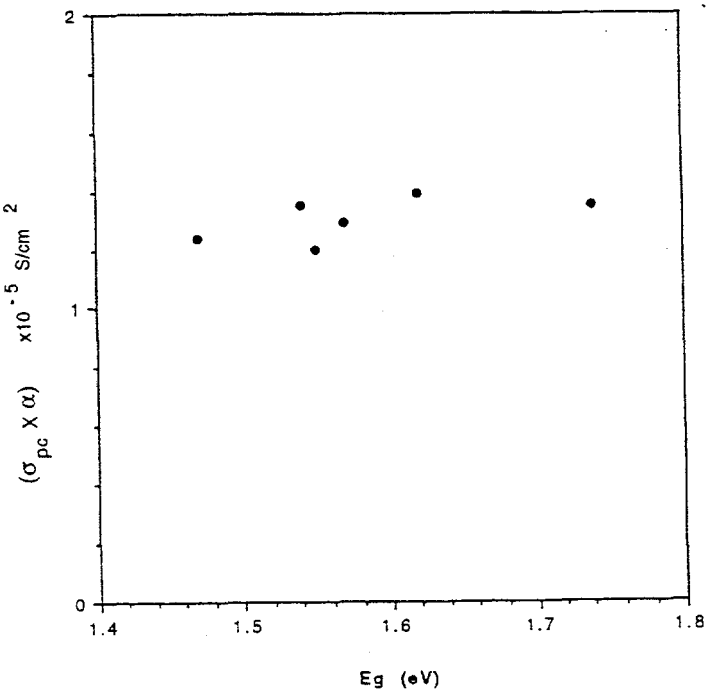

Fig. 3.7 Product (photoconductivity x α) vs. Tauc gap

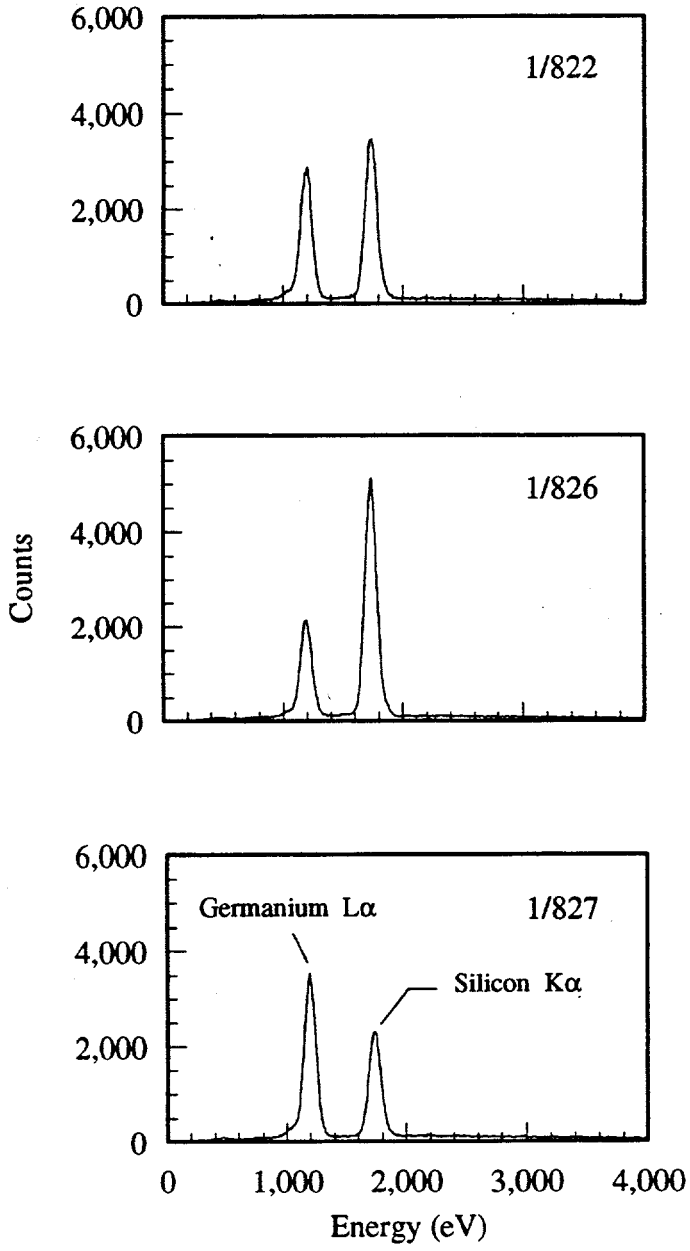

Fig. 3.8 Energy dispersive x-ray spectra of the a-(Si,Ge):H samples

Table 3.3 Deposition parameters of a-(Si,Ge):H films for EDS analysis

						Gas Flow Rates		
						100%	10%	100%
Sample #	Pressure (mTorr)	Temp (°C)	Time (min.)	Power (watts)	Vsub (volts)	SiH_4 (sccm)	GeH_4 (sccm)	H_2 (sccm)
1/821	18.0	300	180	22	-40	2	10	40
1/822	18.0	300	180	23	-40	2	10	40
1/826	18.2	300	180	21	-40	4	8	40
1/827	20.9	300	180	22	-40	2	16	40
1/828	18.2	250	180	22	-40	2	10	40
1/829	18.0	350	180	23	-40	2	10	40

Table 3.4 Alloy percentages and EDS peak count rates

Sample #	Location	Silicon atomic %	Germanium atomc %	Silicon Kα (counts/sec)	Germanium Lα (counts/sec)
1/821	center	62.8	37.2	157	147
	edge	64.8	35.2	265	227
1/822	center	66.1	33.9	299	241
	edge	65.8	34.2	295	242
1/826	center	78.9	21.1	438	177
	edge	79.6	20.4	448	173
1/827	center	51.4	48.6	194	297
	edge	51.6	48.4	200	305
1/828	center	65.5	34.5	299	248
	edge	65.7	34.3	287	238
1/829	center	66.0	34.0	306	250
	edge	66.3	33.7	317	255

as we increase the relative flow rate of germane, the relative intensity of the Ge peak measured in the film increases. An estimate of the concentration of Si and Ge in the film is made using the peak intensity, the x-ray signal from pure a-Si:H and a-Ge:H samples that we used for calibration, and the computer software supplied by the maker of the instrument. Using the calibration standards, the computer automatically calculates the Si/Ge ratio in the film. Corrections for factors such as atomic mass, absorption and x-ray fluorescence (ZAF corrections) are automatically made by the computer.

The values of Si and Ge determined by EDS for the films shown in Table 3.3 are listed in Table 3.4. By comparing the data in Tables 3.3 and 3.4, we can plot a linear relationship between the ratio of germane/silane flowing in to the reactor, and the Ge/Si ratio in the film. This is shown in Fig. 3.9. A linear ratio is very useful for making devices with different bandgaps, and for controlling the grading of bandgaps in devices.

Please note from Fig. 3.9 that a larger percentage of germane flowing into the reactor is incorporated into the film as Ge compared to the incorporation of Si from silane. This, of course, is a consequence of the larger fractionation rate of germane by the plasma compared to the fractionation rate of silane.

In Fig. 3.10, we plot the Tauc gap of the films as a function of Ge content determined by EDS.

3.7 Measurement of Urbach Energies of Films

It was pointed out earlier that we can measure Urbach energies from a measurement of subgap photoconductivity. In Fig. 3.11, we plot the Urbach energies measured in the films as a function of Tauc gap in the film. Note that the Urbach energy slowly, but systematically, increases as we increase the Ge concentration. This is a very significant result. It contradicts the assertion by several groups [28] that the Urbach energy of the valence band is not a function of Tauc gap or Ge content, but is consistent with the data of MacKenzie et al. [29] and von Roedern et al. [30]. While the increase in Urbach energies is small compared to some previous results , it is not insignificant. An increase from 45 meV for a-Si:H to about 52-54 meV for 1.46 eV material is not insignificant. In a-Si:H, an increase of this magnitude in valence band Urbach energy would be a cause of considerable concern. The best device-quality a-Si:H always has a low Urbach energy value, about 45 meV. We will show in a later section what happens to the performance of a-Si:H devices when the Urbach energy of the *i* layer increases from 45 to 50 meV.

Fundamental physical considerations, based upon localization of wave functions, reinforce this concern. The reason for having non-zero Urbach energies (or band-tails) is that the bond lengths and bond angles in amorphous materials are not fixed; rather they have a distribution. This distribution in bond lengths and angles leads to variations in the atomic positions, and hence, to bandtails. These very same variations also lead to changes in localized wave functions. The more extreme the variation in atomic position, the more severe the localization of the wave function around that atom [31]. The more severe the localization, the greater the number of localized (mid-gap) defects [31]. Of course, this relationship between the Urbach energy of

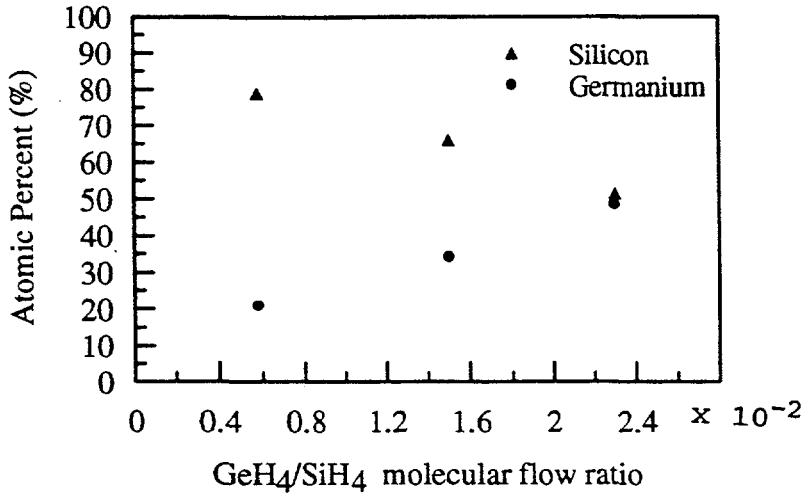

Fig. 3.9 The relationship between the incorporation of silicon and germanium into the amorphous network and the germane to silane molecular flow ratio into the reactor chamber

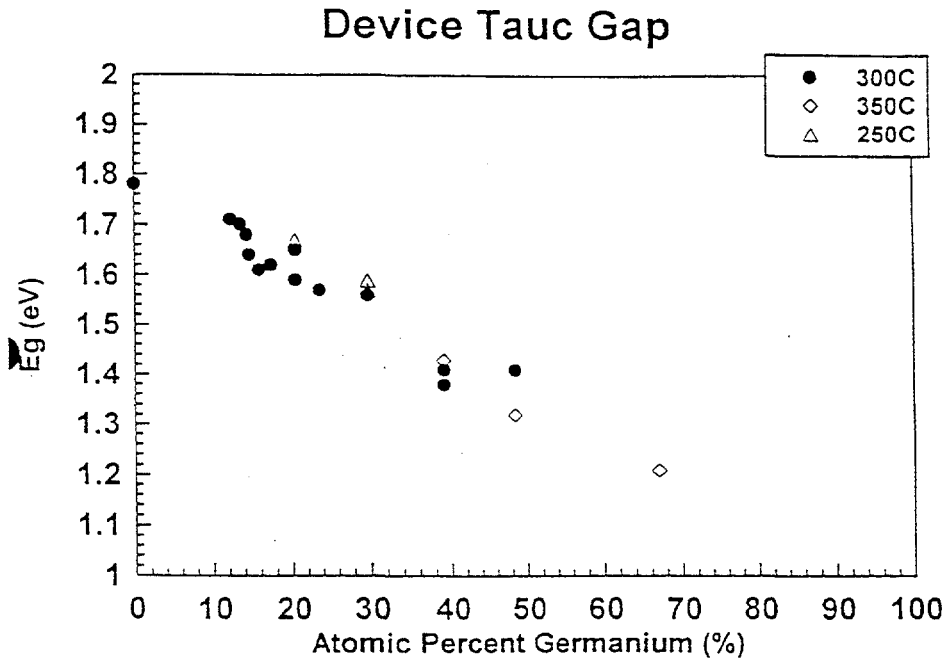

Fig.3.10 Tauc gap vs. Atomic Percent Ge measured in the film

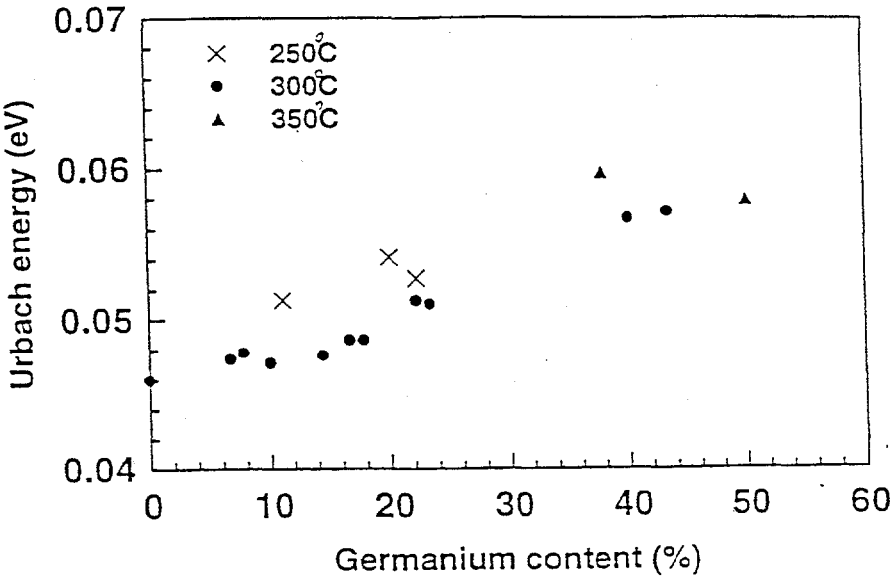

Fig. 3.11 Urbach energy of valence band tail states measured in films vs. Ge content of the film

valence band tails, and the defect density, is well known to the cognoscenti in a-Si:H.

Later on, we shall see how the Urbach energy measured in devices compares with the Urbach energies measured using sub-gap photoconductivity. We will show that in devices, a similar relationship holds between the Tauc gap (Ge content) and Urbach energies. Unfortunately, we have not been able to measure the Urbach energies of conduction band tails. This is something we plan to do over the next contract period, by making appropriate samples for measurement by the Syracuse University group, using their transient drift mobility techniques.

3.8 Measurement of Microstructure

We have measured the microstructure of the material using TEM. For this purpose, the films were grown on carbon-coated copper grids, 3 mm in diameter, which are then loaded into the TEM. Substrate temperatures were varied between 250°C and 350°C for this series, and the substrates were either biased to -30 V or were at 0 V.

In Fig. 3.12, we show the TEM photograph of an a-(Si,Ge):H film, deposited at low temperature (250°C) and no bias. There is a clearly discernable microstructure in this material. Next, in Fig. 3.13, we show the micrograph of a film deposited at the same temperature, using the same power, pressure, germane/silane ratio, etc. as for the film whose micrograph was shown in Fig. 3.12, except that now we use a negative substrate bias on the film during growth. Comparing Figs. 3.12 and 3.13, we see that the homogeneity of the film with the negative bias voltage is significantly better than that of the film without bias voltage. When we increased the deposition temperature to the 300°C range, with a bias voltage, even the small structure seen in Fig. 3.13 disappeared. The photograph showed just a smooth film with no discernable structure. Similarly, no structure was seen in a-Si:H film, even at 250°C deposition temperature.

From these results, we conclude that higher temperatures (300°C) and a negative bias voltage improve the structure of the film. We have thus shown that the flexibility of our reactor is indeed useful in improving material properties. For devices, all the results we report will be for conditions where the temperatures were high (300° to 350°C range), and the substrates were biased negatively to -30 V. The few devices we made at lower temperatures did not work very well and had worse electronic properties, as we will describe in a later section.

3.9 Device Fabrication

We fabricated superstrate devices from materials deposited as described in Section 3.4 above. The basic structure of the device is shown in Fig. 3.14. It consists of a *p-i-n* cell deposited on tin oxide coated glass substrates. These substrates were provided to us by Solarex Corp., and we thank them for their generosity and help.

Two types of devices were made. First, a single-gap *i* layer device with a constant bandgap *i* layer (except for a *p-i* buffer layer) was made. The band diagram of this device is shown in Fig. 3.15. It consists of a *p* a-(Si,C):H:B layer, followed by a graded bandgap, thin buffer layer (i_1) where the bandgap was graded continuously from the high gap of *p* layer to the low gap of

Fig. 3.12 TEM micrograph of a-(Si,Ge):H deposited at 250 C, no bias.

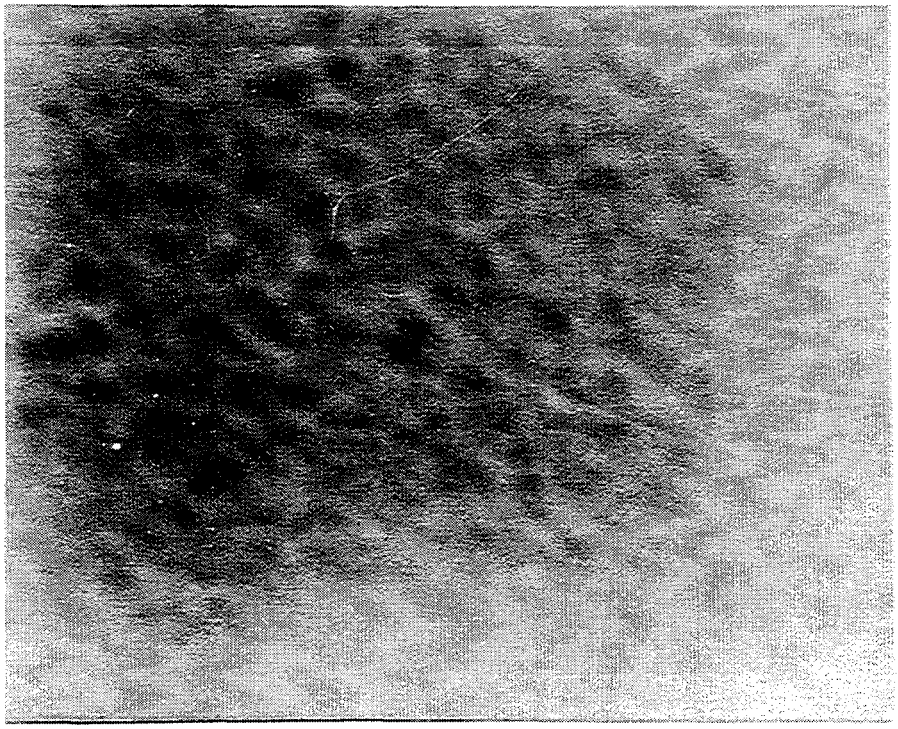

Fig. 3.13 TEM micrograph of a-(Si,Ge):H deposited at 250 C with negative bias voltage

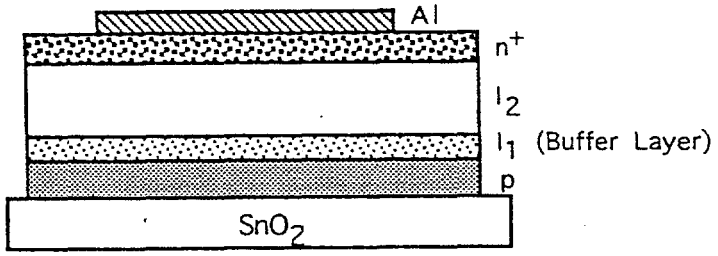

Device Structure

Fig. 3.14 Schematic diagram of the p-i-n devices studied to measure material properties indevices

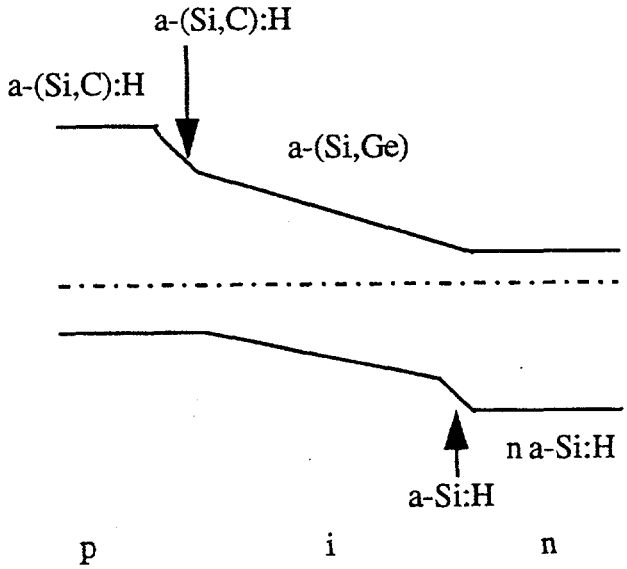

Fig. 3.15 Band diagram of p-i-n single-gap devices

i_2 layer. Finally, an a-Si:H:P $n+$ layer was deposited, followed by an Al contact, to finish the cell. This is what we call a one-bandgap cell. A series of such cells were made to measure material properties in the device.

An important result we discovered was that the buffer layer was critical in determining the performance of the cell. In common with the results for a-Si:H cells described in an earlier chapter, an abrupt as opposed to a graded) change in buffer layers led to problems with fill factors. In particular, a bad buffer layer led to inflection points in the I(V) curves, as seen in Fig. 3.16, presumably due to mismatches in the valence band between the i_1 layer and the p layer. Please see the discussion regarding proper design of buffer layers in Chapters I and II. We found that it was absolutely essential that the buffer layer be graded all the way from the p layer bandgap to the i_2 layer bandgap. This we achieved by changing the ratios of methane, silane, and germane during the fabrication of the buffer layer. Initially, near the p layer, a high ratio of methane to silane was used. Next, an a-Si:H layer without any methane or germane was deposited. Finally, the germane to silane ratio was increased during the final stages of the buffer layer. All of this took place over an approximately 2.5-minute deposition time.

Once we had solved the buffer layer problem, we proceeded to make a series of single-gap a-(Si,Ge):H cells with varying Si/Ge content in the i layer. A typical I(V) curve is shown in Fig. 3.17 for a device with 20% Ge and an i layer thickness of 400 nm.

3.10 Measurement of Material Properties in Devices

As mentioned earlier, the primary reason for making these single-gap devices was to systematically measure the properties of the material in the device. In particular, we were interested in measurements of Urbach energy for valence band tail states, deep level defects, and hole $\mu\tau$ product. The techniques used for these measurements were:

3.10.1 Urbach energy of valence band tails

It was recently shown by Dalal et al. [32] that a measurement of the sub-gap quantum efficiency (QE) of the device at zero or reverse bias provides an accurate indication of the Urbach energy of the i layer in the material. Basically, this phenomenon arises from the fact that QE primarily measures the collection of holes generated in the bulk of the i layer by the monochromatic beam (except for when the wavelength of light is very short; then, QE is measuring the collection of electrons generated near the p-i interface). In the sub-gap region of energies, the photon beam is initially exciting electrons from the valence band tail states into the conduction band (see Fig. 3.18). These holes are in thermal communication with the valence band, and hence can be easily collected by the junction field. *Therefore, a plot of QE vs. photon energy in the tail region directly gives us a plot of absorption coefficient vs. photon energy.* The inverse slope of the natural logarithm of QE vs. photon energy gives us the Urbach energy. However, when photon energies become smaller, the absorption is from mid-gap states to the conduction band, and then, the holes are no longer in thermal communication with the valence band and need a significant field assist. *Thus, mid-gap states cannot be calculated accurately from a measurement of subgap α, but the Urbach energy can be.* Please see ref. 32 for details.

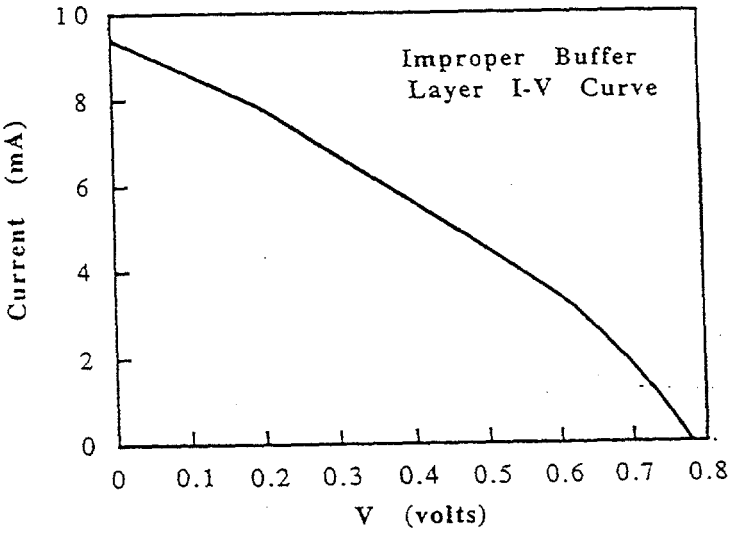

Fig. 3.16 I(V) curve showing inflexion when the buffer layer is wrong

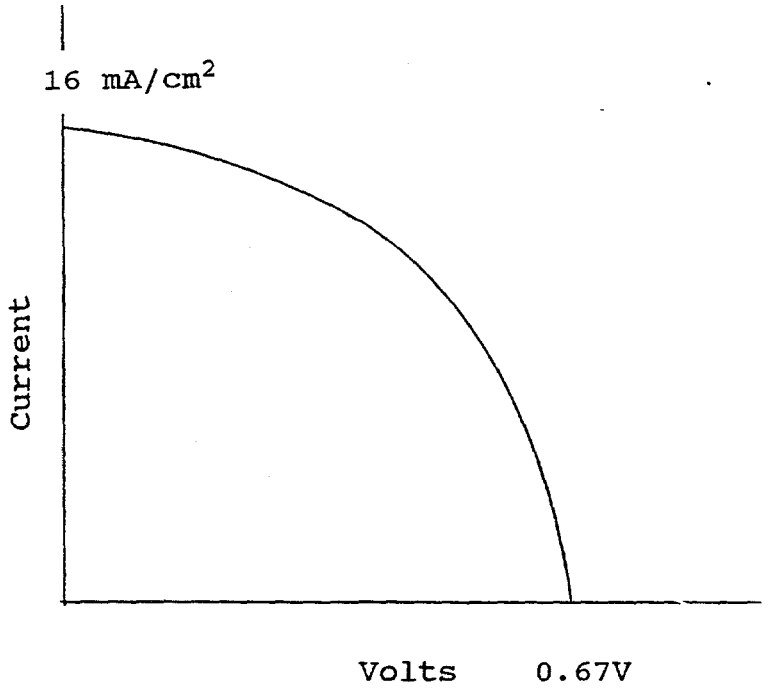

Fig. 3.17 Normal I(V) curve with appropriate buffer layer for a single gap, ungraded a-(Si,Ge):H pin cell

For this measurement to be accurate, it is necessary that we make a series of devices all identical except for changes in the bandgap of the *i* layer. That is exactly what we have done. In Fig. 3.19, we show a series of subgap QE plots for our single-gap devices. Quite clearly, the subgap QE curves are shifting to lower energies as Ge content increases (to the left in the figure). We then measured the slopes of these log(QE) vs. photon energy curves, and deduced the Urbach energies, and plotted them as functions of Tauc gap. These data are shown in Fig. 3.20. Once again, as in the case for films, the data indicate that Urbach energies do increase as the Ge content increases (Tauc gap decreases). The increases are not as large as previously believed, but nor are they zero. In particular, for devices near 1.4 eV, the Urbach energies appear to be in the range of 56 meV, and for 1.45 eV, in the range of 53-54 meV. For comparison, we also plot the data obtained from films prepared at 300°C in the same diagram. The Urbach energies are very comparable whether measured in devices or in films. Note again that the lower temperature material does not appear to be as good as the higher temperature material.

For comparison, in Fig. 3.21, we show the log(QE) vs. photon energy plots for two a-Si:H devices, one a very good a-Si:H device, with a 67% fill factor, and the other a poor one with a much lower fill factor. The Urbach energy for the good device is in the 45 meV range, whereas for the bad a-Si:H device it is 50-52 meV. From Fig. 3.21 and 3.22, and many other similar measurements that we have made, we conclude that it is very useful to make careful measurements of properties like Urbach energy in devices, since they play an important role in determining device properties. A film with a high Urbach energy will invariably lead to a poorer device, not surprising given that the Urbach energy is a measure of disorder in the material. We have also shown, by comparing Urbach energies in films and devices in a-(Si,Ge):H, that it is useful to measure these properties (and defect densities) in films, because they do correlate with devices.

This will become even more clear when we show the data on hole $\mu\tau$ products later. Thus, we have verified that, at present, there does appear to be a problem in a-(Si,Ge):H alloys, namely that Urbach energies (a measure of disorder) are higher than in the best a-Si:H, leading to higher defect densities in the material, and attendant device problems (see below). The problem becomes particularly severe as one goes to high Ge concentrations (35-40%). The Urbach energy does not seem to increase much at first as we add Ge, but beyond about 20%, begins to increase. It is possible that this is a structural problem, namely that we have not discovered how to make the best microstructure in 35-40% alloy, which is approximately where we need to be for multijunction applications. Clearly, this is where we will have to concentrate over the next contract period.

3.10.2 Hole $\mu\tau$ Product

The $\mu\tau$ product of holes is a very important parameter for devices. It is the quantity which primarily determines the fill factor of the cell. This assertion arises from the fact that over most of the cell, the holes are the minority carriers (the carrier with the lower $\mu\tau$ product) [17]. Only near the *p-i* interface do the electrons become the minority carriers. Therefore, in order to have a high collection efficiency for most wavelengths of light absorbed in the cell, the hole range, $\mu\tau$F, where F is the electric field, must be large compared to the thickness of the *i* layer. A

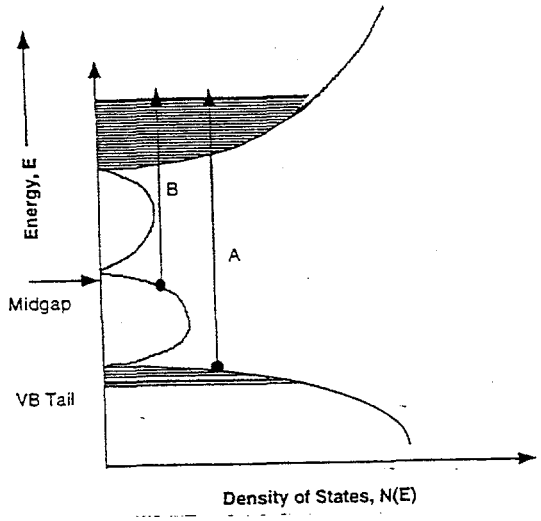

Fig. 3.18 Excitation of electrons and holes by subgap photons. Transition A leads to a mobile hole, and can be detected by QE measurements on devices

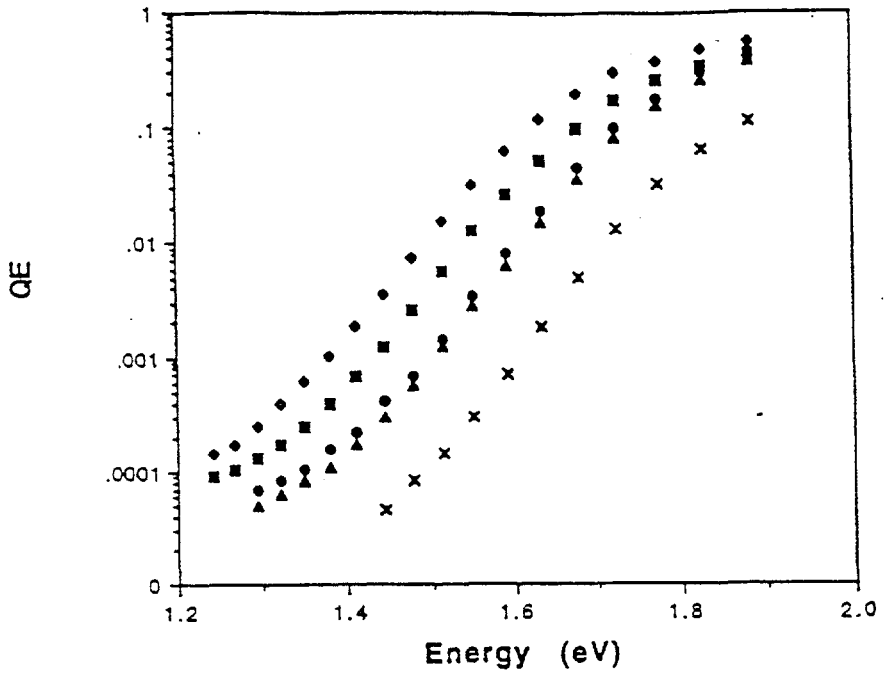

Fig. 3.19 Log QE vs. photon energy curves for a-(Si,Ge):H p-i-n devices with different Ge contents. The straight line portions give a measure of Urbach energy of valence band tails in the i layer.

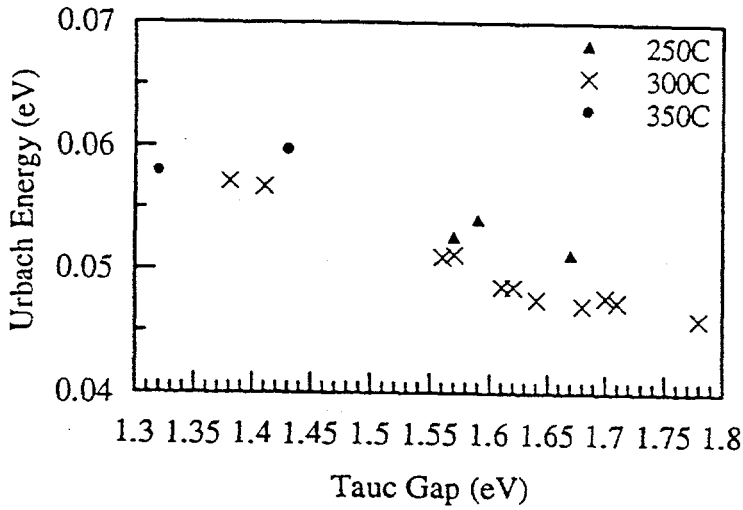

Fig. 3.20 Urbach energy vs. Tauc gap for a-(Si,Ge):H i layers measured in devices

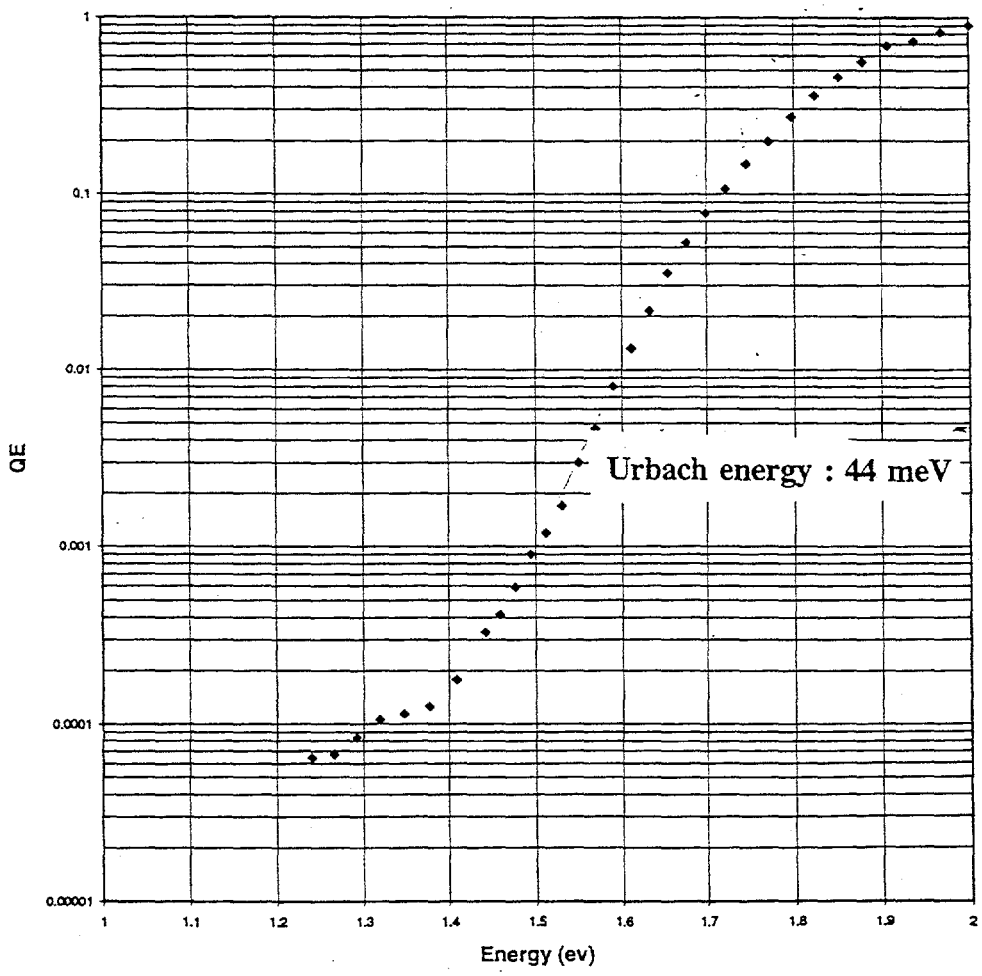

Fig. 3.21 Log QE vs. photon energy curve for a good a-Si:H device with high fill factor

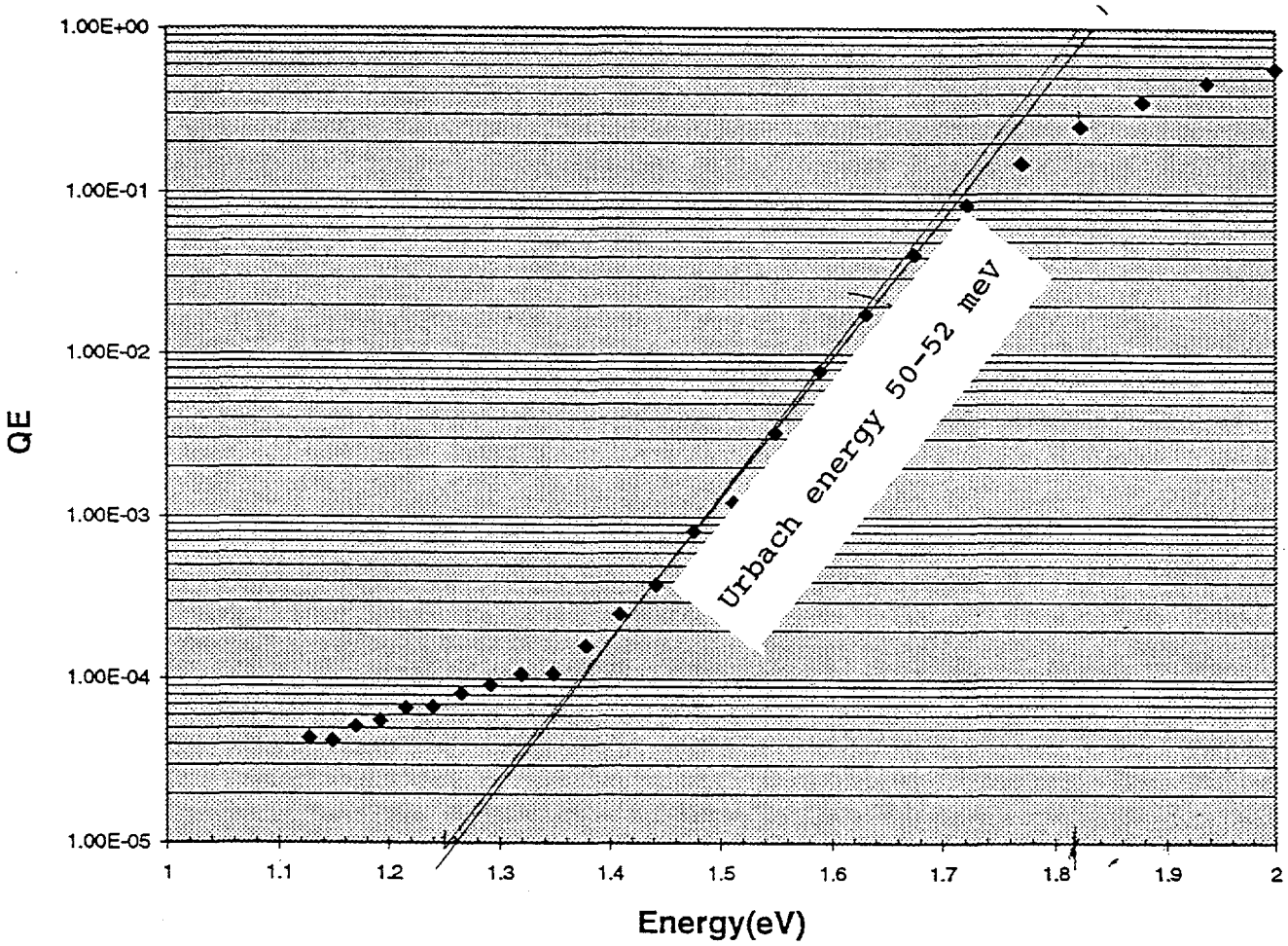

Fig. 3.22 Log QE vs. photon energy curve for an a-Si:H device with a poor fill factor, showing a high Urbach energy

ratio of 10:1 or 20:1 is desirable. In a-Si:H solar cells, this condition is easily met, since thehole $\mu\tau$ product is about 4-6 x $10^{-8}cm^2/V$, and the electric field is about 1-2 x 10^4 V/cm. Thus, the range is about 5-10 μm, much larger than the thickness of the *i* layer (about 0.4 μm). However, in a-(Si,Ge):H, the higher midgap defect density compared to a-Si:H severely reduces both the electric field in the middle of the *i* layer, and the hole $\mu\tau$ product. Therefore, collection efficiency is likely to suffer, particularly near the maximum power point of operation of the diode, when the diode is under forward bias, and the internal field is reduced significantly. These considerations are illustrated in Fig. 3.23, where we schematically show the electric field profiles in the device under zero and forward bias.

Surprisingly, this very important quantity has never been measured in a-(Si,Ge):H devices before. There have been some measurements of hole trapping lifetimes [26] and hence hole trapping $\mu\tau$, but it is not clear that this quantity is the same as device hole $\mu\tau$ product, since one is a transient phenomenon and the other is a steady-state phenomenon.

The basic principle of the measurement technique is quite simple. We measure the quantum efficiency of the device for many wavelengths, as a function of applied voltage. A typical set of measured curves for an a-(Si,Ge):H cell is shown in Fig. 3.24(points are experimental data). Under reverse bias, the QE increases, and under forward bias, it decreases. Since this increase or decrease is due to the increase or decrease in the field in the device, one should be able to model the field profile and obtain the hole $\mu\tau$ product from the curves. For a given device, one should be able to fit all the QE curves (for different wavelengths) using the same value of $\mu\tau$ product, except for the shortest wavelengths, where *p-i* interface recombination becomes important and the model is not valid. But certainly, for long wavelengths, such as 600-800 nm, the model should be valid and give a value for $\mu\tau$.

At this time, we need to know how to model the field. Earlier work [33] assumed a uniform field, an approximation that is acceptable for thin a-Si:H. However, this is not the case for a-(Si,Ge):H, since the high defect density makes the field anything but uniform. Therefore, we chose to model the field using the defect density profile used by Hack and Shur many years ago [19]. The only adjustable parameter we used for modeling the field was the mid-gap defect density g_o, expressed in $\#/cm^3\text{-}eV^3$. Once this parameter is selected, the field is known, and then, using different values of $\mu\tau$, we can model the QE vs. voltage curves, and fit them to the experimental profiles.

Note that our model specifically includes the non-uniform field profile, and hence, a non-uniform range over the thickness of the cell. The collection efficiency is calculated using a field assisted diffusion length, as defined by Smith [34]. This diffusion length is a function of the location of the absorbed photon, and one has to use a double integration over distance to derive the collection efficiency for any given wavelength.

The fits of experimental data and model results are carried out in Fig. 3.24, for a constant field assumption. Quite clearly, no fit is possible with a constant field assumption. On the other hand, when a varying field is used, as suggested by Hack and Shur [19], the fit is much better,

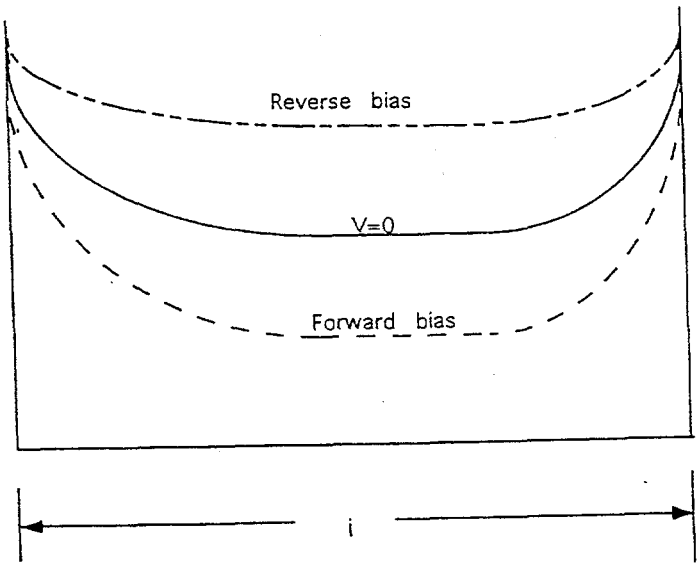

Fig. 3.23 E field profiles in the i layer of the device under forward, zero and reverse voltage bias

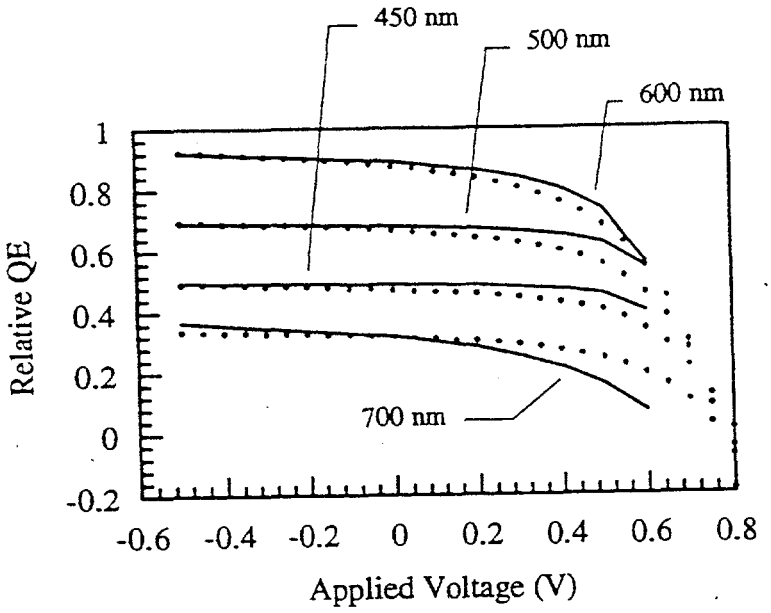

Fig. 3.24 Experimental data (points) showing the behavior of QE at different wavelengths as a function of applied voltage. The solid fit is to constant field approximation, an obviously poor fit.

as shown in Fig. 3.25. Note that it is not possible to fit the data for strong high forward biases (beyond the maximum power point) using such simple models, since forward injection changes the field profiles.

Using such fits, we have calculated the values of hole $\mu\tau$ products as a function of Tauc gap or Ge content. The results are shown in Fig. 3.26. Once again, in common with electron $\mu\tau$ products (photoconductivity) shown earlier, the hole $\mu\tau$ product is seen to decrease significantly as the bandgap decreases, a likely consequence of the simultaneous increase in defect densities. Note that this is to our knowledge the first time that such a careful measurement of this important quantity has been made in a device.

To see if the hole $\mu\tau$ product correlates with the increase in defect densities of films shown in Fig. 3.6 , we plot the $\alpha\mu\tau$ product vs. Ge content in Fig. 3.27. α is taken from Fig. 3.6, and hole $\mu\tau$ from Fig. 3.27. From Fig. 3.27, it is seen that there does seem to be an inverse correlation between hole $\mu\tau$ product and defect density. This result is similar to the case for the product of α x photoconductivity (which represents electron $\mu\tau$ product) shown in Fig. 3.7. *Therefore, we conclude that the electron and hole $\mu\tau$ products both correlate inversely with the defect density in the material.* This is a very important conclusion, because it says that *other factors, such as mobility, are not as important as the lifetime*, since, to a first approximation, it is the lifetime that depends inversely on the defect density.

Another way of plotting the result for hole $\mu\tau$ product is to plot it against the Urbach energies determined in the same samples where the $\mu\tau$ was measured. This plot is shown in Fig. 3.28. This figure clearly shows that the increase in Urbach energies contributes to a decrease in hole $\mu\tau$ product. The curve is almost an inverse exponential relationship (a straight line on a $\ln(\mu\tau)$ vs. Urbach energy plot). This says that the *defect density is increasing exponentially with Urbach energy.*

In summary, we have shown that by careful measurements of material and device properties, one can obtain significant information regarding the defects and electronic properties of the material. We have been able to obtain good agreement between the properties measured in the films and those measured in devices. Over the next contract, we will try to further improve the material.

3.11 Device Design and Analysis

An important part of our project has been to study design of a-(Si,Ge):H devices. In particular, we have concentrated on the design of graded-gap devices. Ever since the first work of Dalal et al. almost 9 years ago [35], there has been controversy in the literature about the proper grading scheme to use for optimizing a-(Si,Ge):H devices. For best results, one would want a grading scheme that benefits both electrons and holes. That is, one would want to change the bandgap by changing both conduction and valence bands appropriately, namely that the conduction band should move towards the Fermi level and valence band away from the Fermi level as we increase the bandgap. This ideal design is shown in Fig. 3.29. If one can achieve

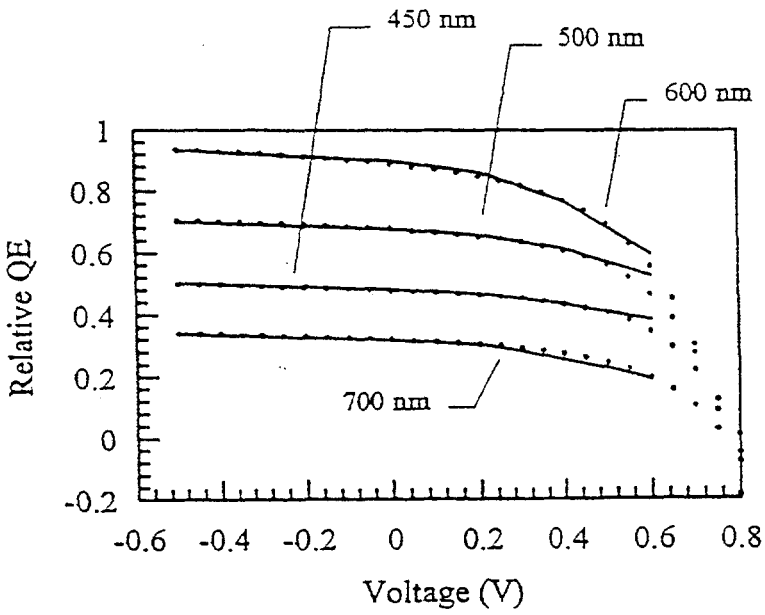

Fig. 3.25 Fit of experimental points to analytical curves using non-uniform field as per Hack and Shur model

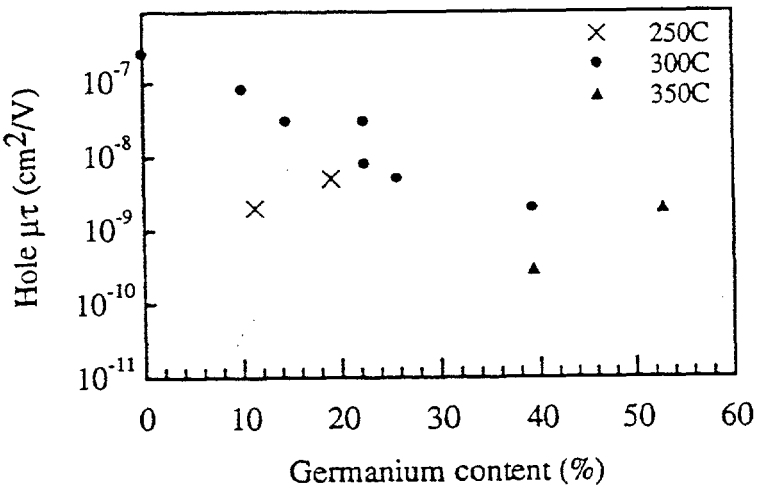

Fig. 3.26 Plot of hole $\mu\tau$ product, determined by fitting of Fig. 3.25, as a function of Ge content of the i layer for devices prepared at 3 different temperatures

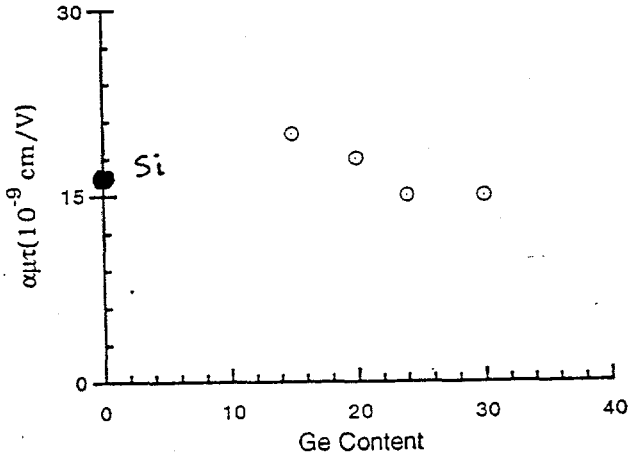

Fig. 3.27 Plot of $\alpha\mu\tau$ product of holes determined in devices vs. Ge content

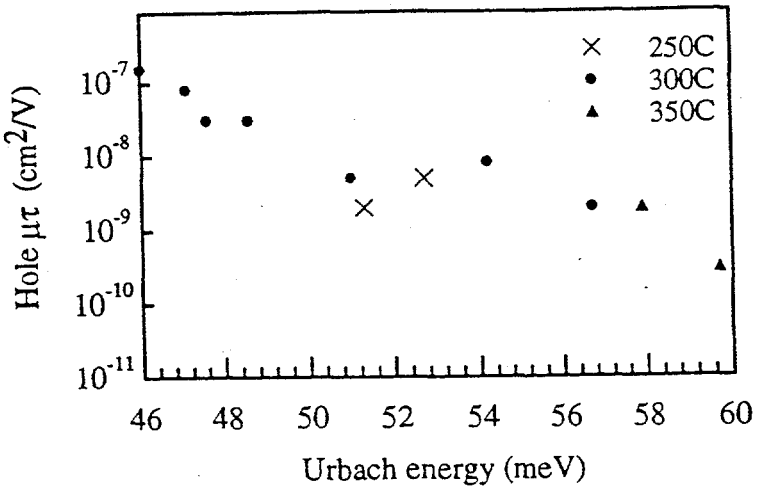

Fig. 3.28 Plot of hole $\mu\tau$ product vs. Urbach energy for devices prepared at 3 different temperatures

such a grading by changes in alloy compositions, including changes in H concentrations, that would be ideal. Unfortunately, that is not usually the case. Usually, when we change the bandgap by changing the alloy composition (e.g. Si/Ge ratio), both conduction and valence bands move closer to the Fermi level. Therefore, if one were to implement grading strategies to assist holes, as shown in Fig. 3.30, it would inevitably end up hurting the electrons. Guha et al. [36] used such a grading scheme, with a narrow buffer layer between the *p* and the *i* layers, to improve their cells. The band diagram of their grading scheme, including the buffer layer, is shown in Fig. 3.30.

There are several potential problems with the grading strategy used by Guha et al. [18]. In particular, their scheme wastes grading-created field by distributing this field over the entire *i* layer.

But the front and the back of the *i* layer are already high field regions; they do not need this grading assist. In contrast, the middle regions of the cell do. Under forward bias (operating point) the middle of the cell is depleted of field, and that is where one should provide the extra field. Therefore, the grading profile should be as shown in Fig. 3.31, where the grading is in the middle parts of the cell. The exact design of the cell depends upon the defect density in the cell (which of course is a function of position, since bandgap is a function of position), and also depends upon back reflection, thickness of the *i* layer, etc. We are currently developing such a detailed model, taking account of non-constant bandgaps and material properties such as $\mu\tau$ products, and hope to finish it over the next contract period. The preliminary results do show that the bandgap grading shown in Fig. 3.31 is valid.

3.12 Experiments on Graded Gap Cells

To make sure that the conduction and valence bands are moving as expected, we have made three different types of cells in a-(Si,Ge):H. The first was an ungraded, single-gap cell as discussed in the earlier section of measurements. The second was the forward graded cell with the type of grading shown in Fig. 3.31. In this cell, the narrow gap material was nearest the *p* interface, and the material nearest the *n* layer was standard a-Si:H. The third cell was a reverse graded cell, where the wide gap material (a-Si:H) was nearest the *p* interface, and the narrow gap material was nearest the back *n* contact. Near the back contact, over a very narrow region (20 nm or so), the bandgap was graded back to a-Si:H to avoid a spike at the *i/n* interface which might impede electron transport.

The I(V) curves for the three cells are shown in Fig. 3.32. The best curve is the one for a forward graded cell, and the worst the one for a reverse graded cell. We also measured detailed quantum efficiency spectra on these cells. In particular, the ratio of quantum efficiencies under reverse and zero bias tells a lot about the transport mechanism in these cells. These ratios are plotted in Fig. 3.33 for the reverse and forward graded cells. Note that for the forward graded cell, the ratio is near unity across the entire wavelength spectrum, but for the reverse graded cells, the ratio monotonically increases as the wavelength increases. This is almost a classical illustration of the beneficial or harmful effects of grading on hole transport. With forward grading, the internal field due to grading is strong enough at zero bias that the holes do not need

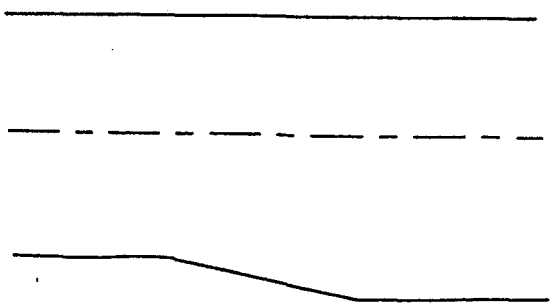

Fig. 3.29 Ideal graded gap cell design

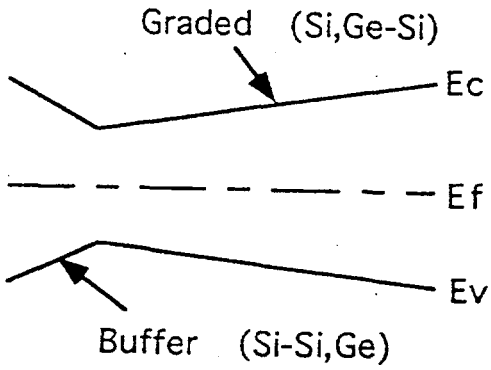

Fig.3.30 Band diagram of i-layer Grading strategy used by Guha et al.

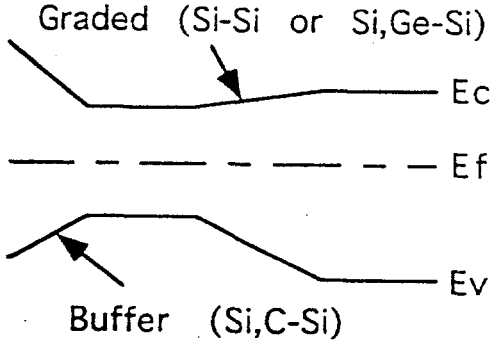

Fig.3.31 Band diagram of i-layer grading used in this study

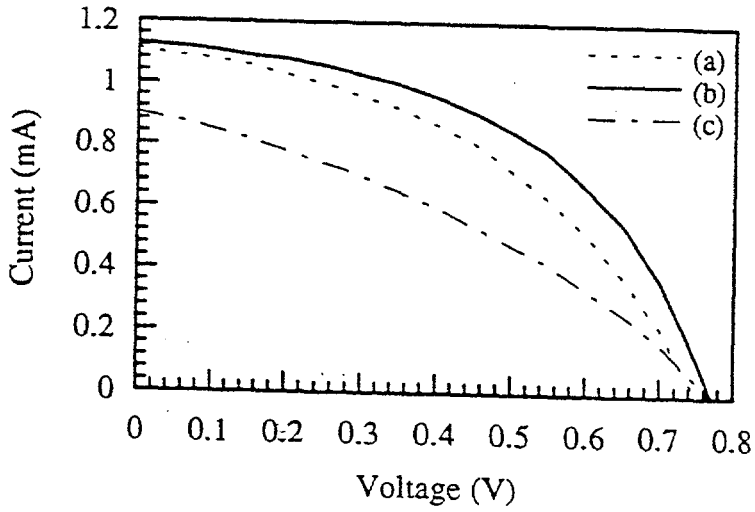

Fig. 3.32 Current-voltage relationship for the reverse graded (c), constant bandgap (a), and forward graded (b) devices

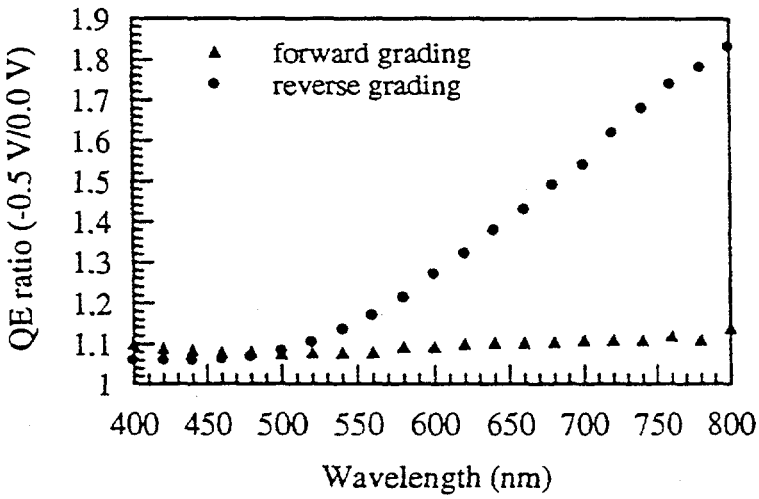

Fig. 3.33 Quantum efficiency ratios for the forward and reverse graded test devices

the additional field provided by reverse bias to improve their transport. For the reverse case, the field in the middle of the cell is low, since the grading-induced field opposes the hole transport, and the holes need the extra field provided by reverse bias to help in their collection. Note the smooth increase in QE ratio with wavelength; this simply says that the holes which are generated the furthest away from the *p* layer need the greatest amount of field assist.

It is instructive to study the influence of changing the forward grading. In particular, we can shift the bandgap profile as shown in Fig. 3.34. Here, we have shifted the lowest-gap region towards the middle of the cell by introducing a thin, constant gap region within the graded buffer layer. Basically, we have made the buffer layer thicker by putting in a thin (a few ten nm) a-Si:H layer in the middle. There is a dramatic change in the cell behavior when we do this. The corresponding I(V) curves are shown in Fig. 3.35. The curve for the cell with the thicker *p-i* interface layer (one with a thin a-Si:H layer within the buffer layer) has a higher voltage, but much lower fill factor. This is exactly what we would expect to happen. The reason is that this grading profile basically creates a second "diode' in series with the primary *p-i-n* junction (see the band diagram shown in Fig. 3.36). The electrons and holes generated within this narrow grading-induced diode are separated by the grading field, and create a photo-voltage which is in the same direction as the primary photo-voltage due to *p-i-n* junction. However, the discontinuity in valence bands between the a-(Si,Ge):H and a-Si:H creates havoc with transport of holes traversing from the back of the primary cell to the front; hence a lower fill factor. Once again, this figure emphasizes the critical design which must be used for the buffer layer in *p-i-n* solar cells, particularly when the i layer itself is being graded in bandgap. Those groups which do not use a proper grading for the buffer layer, a grading which goes all the way from a high gap a-(Si,C):H to a low gap a-(Si,Ge):H over a narrow region of the *i* layer, are doing themselves a great disservice. They may blame their poor fill factors on the material, whereas, in reality, the poor fill factors may be due to improper graded buffer layers.

This is an appropriate time to address the question of the back interface. Note that with the forward grading in our scheme, the *i-n* electric field is automatically driving holes away from the back interface. Since the back layer is doped a-Si:H, the back of this cell is exactly like the back of an a-Si:H cell. Now it would be nice if we could provide extra field assist for holes by further moving down the valence band of a-Si:H, e.g. by increasing H content. But we do not know how to do that just yet. It is something we are going to look at for our graded gap a-Si:H cells. See Ch. II. When we discover how to do this, of course, we will also implement it in the a-(Si,Ge):H cell.

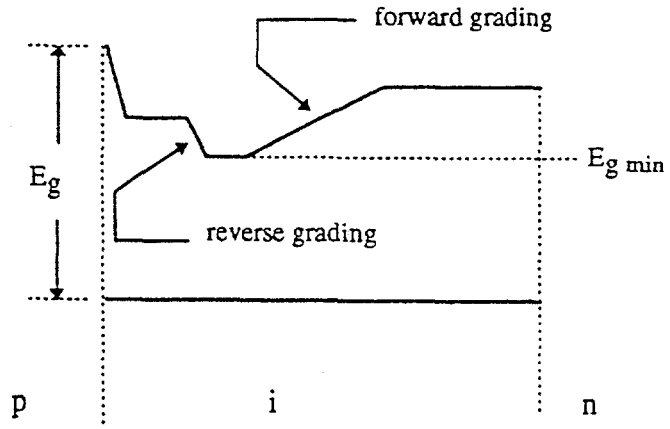

Fig. 3.34 Schematic diagram of structure with added a-Si:H layer in the buffer layer

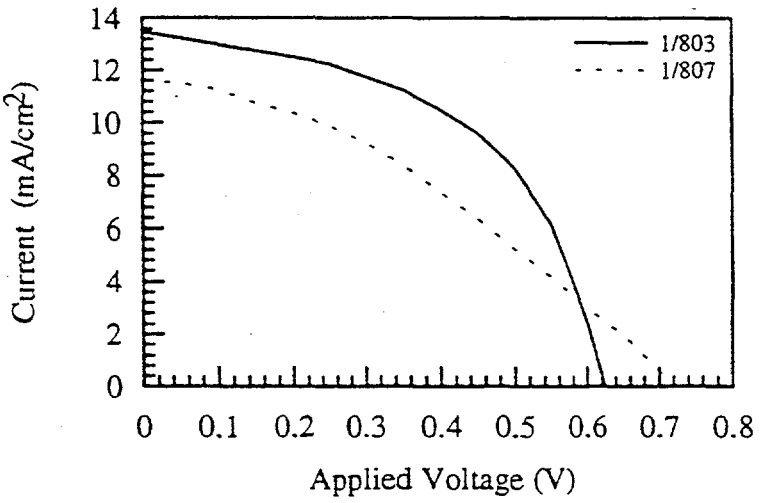

Fig. 3.35 Current-voltage characteristics indicating of a proper grading scheme (1/803), and an improper grading scheme (1/807)

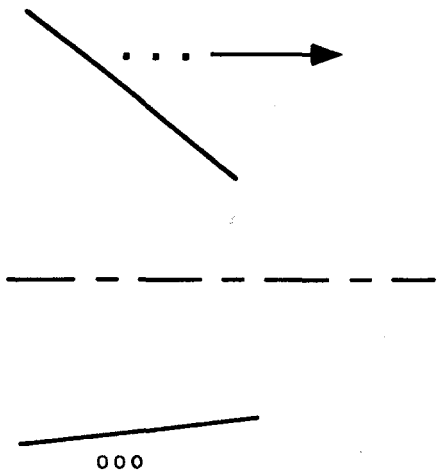

Fig. 3.36

Electron-hole separation achivered by differences in grading between conduction and valence bands

3.13 Summary of a-(Si,Ge):H Research

In summary, we have made the following progress over this first three-year contract period.

1. We have succeeded in growing highly reproducible films and devices of a-(Si,Ge):H using a controlled RF triode geometry. We have shown that the application of a negative bias voltage to the substrate is important for growing the best films, presumably because of improved ion bombardment.

2. We have carefully measured the electronic properties of the material, and have shown that the Urbach energy of valence band tails does increase, by small but significant amounts, as the Ge content increases. The increase is small for low Ge content, but beyond about 20%, the Urbach energy increases rapidly. Corresponding to this increase in Urbach energy, there is an increase in subgap absorption coefficient α.

3. We have succeeded in measuring both electron and hole properties across the range of our alloys, by making careful measurements of quantum efficiency in devices, using specially and carefully prepared devices. Using such techniques, we have verified that the hole $\mu\tau$ product deduced from devices, and the electron $\mu\tau$ product measured in materials, both decrease as the midgap defect density increases with Ge content. The products of subgap α and electron or hole mt products are almost constant across the $\mu\tau$ bandgap range studied, indicating that midgap defects control the $\mu\tau$ products in an almost perfect inverse relationship.

4. We have shown that our new bandgap grading scheme does appear to work well in the proof of concept diagnostic devices we have made. A reverse grading scheme does not work. The detailed QE analysis of the diagnostic devices clearly shows this to be the case.

5. We have shown that the design of the buffer layer is critical for achieving good a-(Si,Ge):H cells. A bad design of the buffer layer can mislead one into blaming the material for the poor properties, when in reality, it is the buffer layer grading which is creating some of the problems.

6. We have shown how quantum efficiency spectroscopy is a powerful technique for analyzing device performance, especially when combined with device modeling and band diagrams. While more detailed device physics of a-(Si,Ge):H cells is still being developed, and computer models are being used, our simple models have a great deal of predictive power, and are very useful in achieving a better understanding of the device and the material.

7. We have shown that there is a very good agreement between the material measurements performed on films and material measurements performed on devices, when both are made carefully. A good material does not mean one can make a good device, since the

design of the device, and factors such as diffusion across interfaces, are also critical in achieving good performance. But a bad material will never make a good device. Every time we use a highly defective material, the device invariably turns out to be poor performing. Therefore, making good materials is a necessary prerequisite for making good devices. Note that all the measurements to date have been in the annealed state. In the future, we plan to measure material parameters, both in films and in devices, in the light-soaked state.

References

1. J. A. Reimer, R. W. Vaughn and J. C. Knights, Phys. Rev. Lett., 44, 193 (1980)

2. S. J. Jones, Y. Chen and D. L. Williamson, Proc. of Amer. Inst. Phys., Vol. 268, 357 (1992)

3. J. C. Knights and R. A. Lujan, Appl. Phys. Lett. 35, 244 (1979)

4. W. Luft and Y. S. Tsuo, "Hydrogenated a-Si and Alloy Deposition Processes", (Dekker, NY, 1993) p. 148.

5. R. Arya et al., Proc. of 23rd. IEEE Photovolt. Spec. Conf., 790 (1993)

6. D. Adler, in "Semiconductors and Semimetals", Vol. 21A (1984)

7. V. L. Dalal, C. M. Fortmann and E. Eser, Proc. Amer. Inst. Phys. Conf., 73, 15 (1981)

8. C. C. Tsai and R. Nemanich, J. Non-Cryst. Solids, 35-36, 1203 (1980)

9. S. Lee, S. Kumar and C. Wronski, J. Non-Cryst. Soldis, 114, 316 (1989)

10. V. L. Dalal and C. Fuleihan, Proc. Mat'l. Res. Soc. 149, 601 (1989)

11. M. Stutzmann, W. Jackson and C. C. Tsai, Phys. Rev. B32, 23 (1985)

12. D. Redfield and R. Bube, Appl. Phys. Lett. 54, 1037 (1989)

13. V. L. Dalal et al, Appl. Phys. Lett. 64, 1862 (1994)

14. V. L. Dalal, R. Knox, N. Kandalaft, K. Han and B. Moradi, Proc. Am. Inst. Phys. Conf., 268, 388 (1992)

15. N. Johnson, C. Nebel, P. Santos, W. Jackson, R. Street, K. Stevens and J. Walker, Appl. Phys. Lett. 59, 1443 (1991)

16. H. Shirai, J. Hanna and I. Shimizu, Proc. Am. Inst. Phys., 234, 203 (1991)

17. V. L. Dalal, J. Booker, M. Leonard, A. Vaseashta and S. Hegedus, Proc. 18th. IEEE Photovolt. Conf., 847 (1985)

18. V. L. Dalal, B. Moradi and G. Baldwin, Proc. of Am. Inst. of Phys., 234, 298 (1991)

19. M. Hack and M. Shur, J. Appl. Phys., 58, 997 (1985)

20. M. Bennett et al., Proc. of 23rd. IEEE Photovolt. Conf., p. 865 (1993)

21. J. Yang, X. Xu and S. Guha, Proc. of MRS, 336, 687 (1994)

22. A. Vaseashta, V. L. Dalal, A. Greenwald, J. Booker and M. Leonard, Proc. of 18th. IEEE Photovolt. Conf., p.847 (1985)

23. J. M. Essick, R. T. Mather, M. Bennett and J. Newton, Proc. of MRS, 297, 705 (1993)

24. C. C. Tsai, J. C. Knights, G. Chang and B. Wacker, J. Appl. Phys., 59, 2998 (1986)

25. C. M. Fortmann, Proc. MRS, 192, 27 (1990)

26. J. D. Cohen, Final Report to NREL, NREL/TP-451-7163 (1994)

27. V. L. Dalal et al, Proc. 18th. IEEE Photovolt. Conf., 1500 (1985)

28. S. Guha, J. Payson, S. C. Agarwal and S. R. Ovshinsky, J. Non-Cryst. Solids, 97-98, 1455 (1987)

29. K. D. Mackenzie, J. R. Eggert, D. J. Leopold, Y. M. Li, S. Lin and W. Paul, Phys. Rev B31, 2198 (1985)

30. B. von Roerden, A. H. Mahan, T. McMahon and A. Madan, Proc. of MRS, 49, 167 (1985)

31. See, for example, N. Mott and E. Davies, " Electronic Processes in Non-Crystalline Solids," (Cambridge, 1982)

32. V. L. Dalal, R. Knox and B. Moradi, Solar Energy Materials and Solar Cells, 31, 349 (1993)

33. R. S. Crandall, J. Appl. Phys. 54, 7176 (1983)

34. R. A. Smith, "Semiconductors", (Cambridge, 1978)

35. V. L. Dalal, Final Report to SERI (1986)

36. S. Guha et al, Appl. Phys. Lett., 54, 2330 (1989)

Appendix A

THE ROLE OF CHARGED DEFECTS IN PHOTO-DEGRADATION OF HYDROGENATED AMORPHOUS SILICON

VIKRAM L. DALAL*, SANJEEV CHOPRA* AND RALPH KNOX+
* Dept. of Electrical and Computer Engineering and Microelectronics Research Center
+ Microelectronics Research Center
Iowa State University,Ames, Iowa 50011

ABSTRACT

We examine the role of charged defects in inducing degradation of electronic properties of a-Si:H upon exposure to light.We measure the kinetics of decay of photo-conductivity of a-Si:H films at different light intensities, and the corresponding changes in mid-gap optical absorption. We find that the initial,rapid decay of photo-conductivity can be modeled quite well by invoking Adler's model of conversion of charged defects to neutral dangling bonds(D^- to D^0 conversion). A consequence of this conversion is a decrease in sub-gap absorption upon photo-induced degradation. We see such a decrease in absorption. The magnitude of the decrease is quantitatively in the range expected from the observed decrease in photo-conductivity. Therefore, we conclude that charged defects coexist with neutral defects in a-Si:H, and they play a major role in early stages of photo-degradation.

INTRODUCTION

The degradation of electronic properties of amorphous Silicon (a-Si:H) upon exposure to light is a well known phenomenon [1,2] which is of considerable technological importance. Two distinct physical models have been put forward to explain this degradation phenomenon. The first model,generally known as the bond-breaking or bond-equilibration model[3,4] suggests that the decay is due to increases in mid-gap defect densities (D^0)created by breaking of weak bonds upon energetic transfer from electron-hole recombination.The increase in D^0 states leads to increased recombination and hence a decrease in electron and hole lifetimes and hence in properties such as photo-conductivity. Indeed, all previous experiments show that the degradation in electronic properties is accompanied by an increase in defect densities (D^0 states).[5]The second model, proposed by Adler[6]suggests that the degradation in electronic properties is due to conversion of charged defects (D^- and D^+)states to a structurally different D^0state upon light soaking.In this model, charged defects (D^- and D^+) coexist with neutral dangling bonds (D^0), the former with a negative correlation energy and the latter with a positive correlation energy. It is thought that the existence of localized charge fluctuations due to microscopic non-homogeneities in the material leads to the existence of these charged defects. [7,8]In this model, the capture of a photo-generated hole by a D^-state, or the capture of a photo-generated electron by a D^+state can lead to the formation of a structurally different, stable D^0state. The creation of this neutral D^0state can lead to the recombination of an electron-hole pair at that site, thereby leading to a decrease in photo-conductivity and electron and hole diffusion lengths.

This model was first quantified by Dalal[9], who showed that the initial rapid decay in photo-conductivity of a-Si:H films (and

the similar rapid decay in fill-factor of solar cells) can be explained by invoking Adler's model.Later work [10] showed that since a-Si:H was generally doped n-type by the presence of accidental donors such as O, the material should have significant concentrations of donor-induced D^-states. Therefore, an increase in O concentration of films led to an increase in the rate of decay of photo-conductivity.A similar result was observed for films doped with other residual donors, such as very small concentrations of P.[10]

EXPERIMENTAL DESIGN

A critical test of Adler's model would be to actually measure the densities of D^- and D^0 states before and after degradation. Such measurements are generally difficult to interprete because D^- and D^0 states lie close together in energy (U is small,20-50 meV).[11]However, a D^- to D^0conversion should result in a decrease in sub-gap absorption, since a D^-state has 2 electrons, and a D^0state has 1 electron.In this letter, we report the first observation of such a decrease in sub-gap absorption of light upon light-induced degradation, in contrast to all previous measurements, where only increased absorption was observed.

SAMPLE PREPARATION AND EXPERIMENTAL TECHNIQUE

The samples used in the study were prepared by a low-pressure, Electron-Cyclotron-Resonance technique, using Hydrogen or Helium as the exciting gas and Silane as the precursor gas. The details of the apparatus and the technique have been presented elsewhere.[12]The samples were typically 1-2 micrometers thick, and were deposited on 7059 glass substrates.The samples typically had dark conductivities in the range of 10^{-11} S/cm , and photo-conductivities under 100 mW/cm^2 AM1.5 illumination in the range of $2\text{-}5\times10^{-5}$S/cm.The Fermi levels were typically in the range of 0.85 eV below the conduction band edge. The samples were deposited at different temperatures, from 240-320 C. As expected, the samples deposited at lower temperatures had a higher H, and SiH_2content than samples deposited at higher temperatures. This point will become important in interpretation of our data.

Coplanar photo-conductivity was measured as a function of time at different light intensities. The measurement times extended from 1 second to 24 hours after the onset of illumination. This fact is important because it was earlier shown by Dalal and co-workers [9,10]that there were two distinct zones of degradation,an earlier rapid one, and a later, more gradual one. The earlier,rapid degradation was postulated to be due to trap-to-dangling bond conversion, and the gradual degradation was postulated to be due to bond-breaking. Before light soaking, the samples were annealed at175-185 C for 12 hours. Sub-bandgap absorption was measured by measuring sub-gap photo-conductivity,using a standard two-beam chopped photo-conductivity technique.[13]The photo-conductivity corresponding to the chopped light source was converted into absorption coefficient α by comparing the actual α to photo-conductivity derived α at energies in 1.7-1.8 eV range.

RESULTS

Figure 1 shows the initial decay of photo-conductivity for a sample deposited at higher temperature at two light intensities, 100 mW/cm^{2}and 50 mW/cm^2. According to Dalal's model, the two

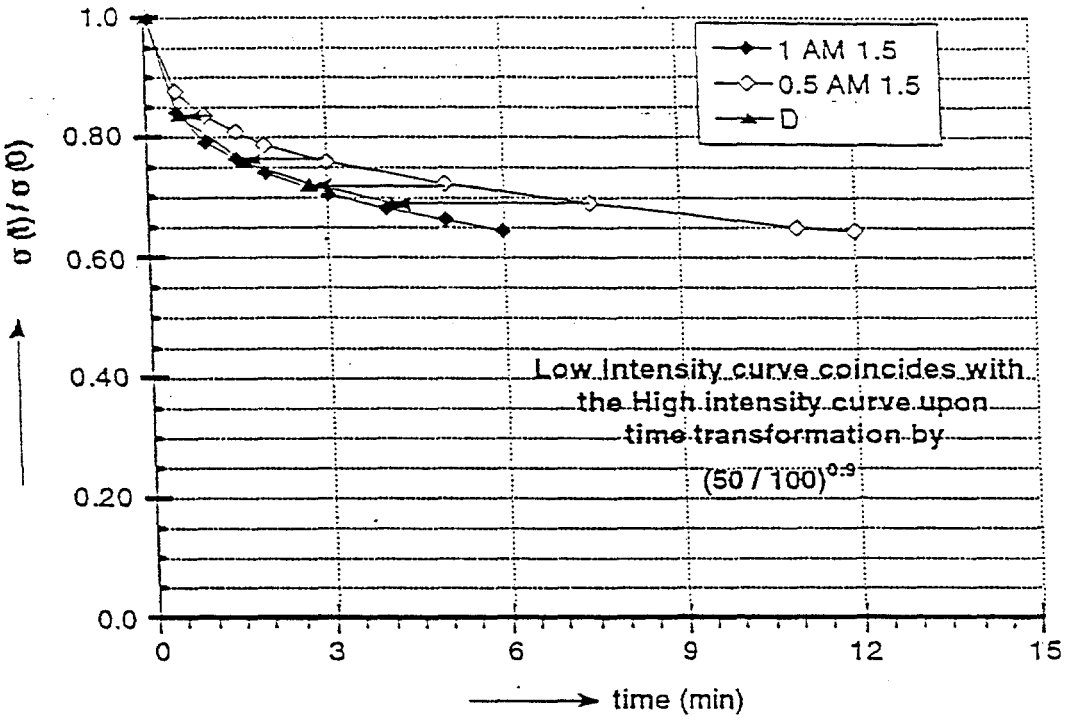

Photo-conductivity decay for sample 195 at two different light intensities

Figure 1

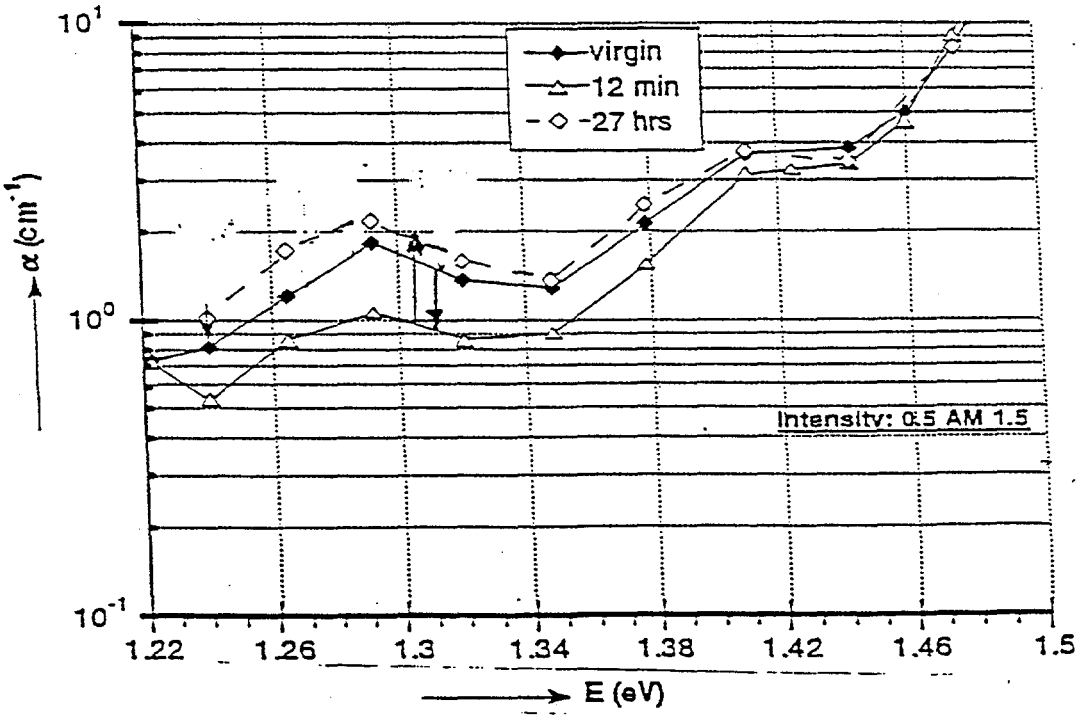

Figure 2

Sub-gap optical absorption spectra of sample 195

curves should be identical when the time scale for the low intensity sample is reduced by the ratio $(I_1/I_2)^{\gamma}$, where γ is the exponent in the relationship between photo-conductivity (σ_1)and light intensity (I),$\sigma_1 \_ I^{\gamma}$.In Fig. 1, we show that such a remapping makes the two curves almost identical within experimental errors.In Fig. 2 we show the sub-gap absorption of this film at different times after the onset of light-soaking. As seen from the figure, sub-gap absorption at first decreases, and then increases upon further light soaking. This is easily explained by the observation that both trap-to-dangling bond conversion, and bond breaking phenomena are occuring simultaneously, though on very different time scales. D^- to D^0 conversion is a more rapid process than bond-breaking, and hence, at very early times, sub-gap absorption decreases.However, the trap conversion can only proceed until all traps are converted to dangling bonds, and is thus self limiting.From this point on, the creation of additional dangling bonds can only lead to increased D^0states, and hence increased sub-gap absorption,as observed.

The above explanation is supported by the further observation that the rate of creation of D^0states by bond-breaking is strongly dependent upon the presence of weak Si-Si or Si-H_2bonds.[10] The higher the density of weak bonds, the higher the rate of creation of D^0 states by bond-breaking. Therefore, samples prepared at 240 C may not show a decrease in sub-gap α at all, even after relatively short degradation times (15-20 minutes), whereas the samples prepared at higher temperatures (320C) should show such a decrease. This is indeed what was observed experimentally. The measured samples fell into three groups. Most of the samples prepared at higher temperatures showed an initial decrease and a later increase in sub-gap absorption. The samples prepared at mid-temperatures showed little change in sub-gap absorption over the first 15-20 minutes, and then an increase, and the samples prepared at the lowest temperatures showed only an increase in sub-gap absorption.

To illustrate this point, we show, in Fig. 3, the decay of photo-conductivity over time for two films, one a high temperature film(320C), and the other a lower temperature film(250C). The higher temperature film decays much more slowly than the film prepared at lower temperature. In Fig.4,we show the corresponding changes in sub-gap absorption for the two films. From these two figures, we can conclude that the film deposited at higher temperatures shows a negative change in α, whereas the film deposited at lower temperature does not.

We can further check for the validity of the model by examining the magnitude of the photo-conductivity decay for short-time degradation, and correlating this decay with the increase in D^0 states due to trap conversion. Assuming that photo-conductivity is inversely proportional to the density of D^0, we can write down that $\sigma(t)/\sigma(0)=D_i/(N_i+D_i)$, where D_i is the initial density of D^0 states, and N_i, the initial density of negatively charged trapping states. From Fig. 1, at 12 minutes, the initial decay has almost saturated, and the ratio N_i/D_i works out to be 0.5. Next, we can

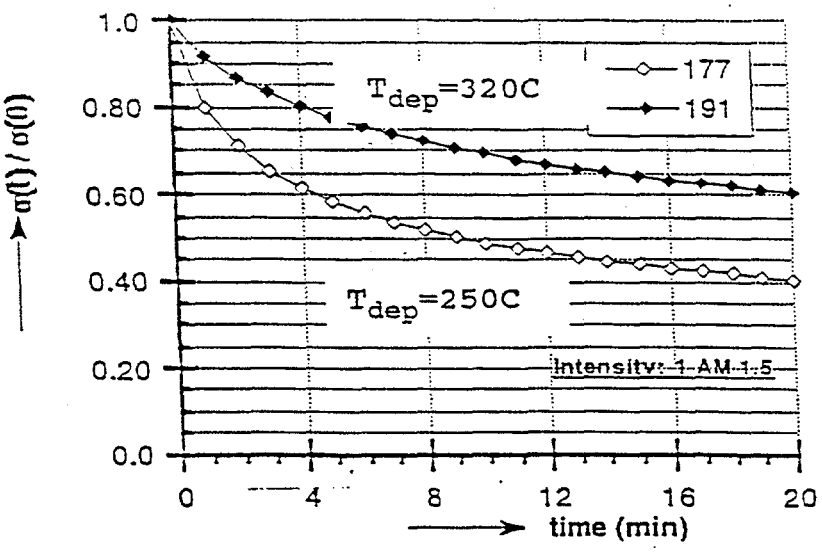

Figure 3. Photo-conductivity decay of samples 191 and 177

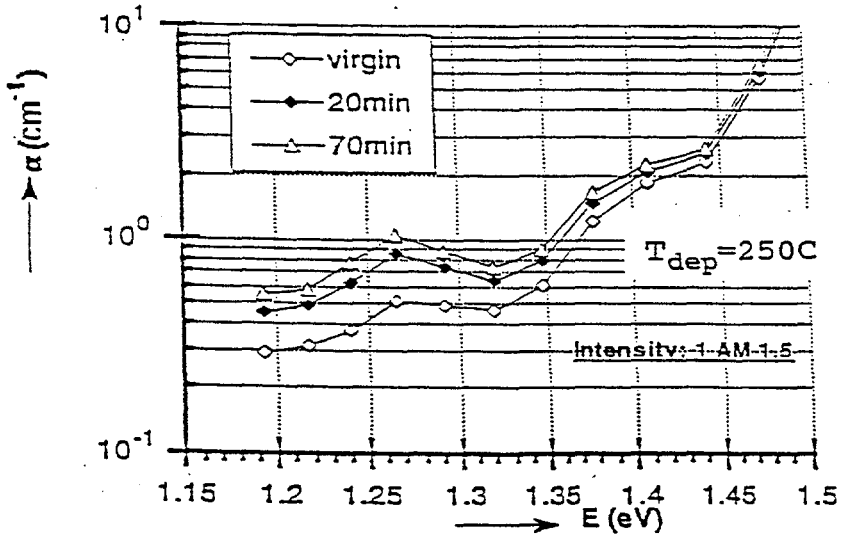

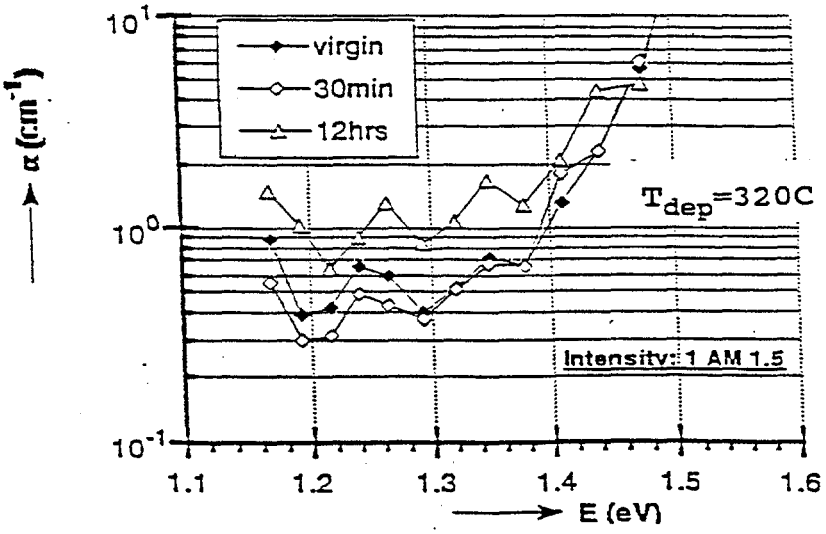

Figure 4 Sub-Band Gap Absorption Spectra of Sample 191

calculate the reduction in absorption due to N states changing into D states by simply counting the number of electrons in N and D states, and saying that absorption is proportional to the number of electrons. Then, at the same time of 12 minutes, we expect that absorption to be in the ratio $\alpha(t)/\alpha(0) = (N_i/2 + D_i)/(N_i + D_i)$. Putting in the value of 0.5 for N_i/D_i, gives us a calculated $\alpha(t)/\alpha(0)$ of 0.82, and the experimental value from Fig. 2 is 0.71, within the range, given the extreme simplicity of the model.

CONCLUSIONS

In summary, we have observed,for the first time, a decrease in sub-gap absorption upon light soaking, as predicted by Adler's model of trap-to-dangling bond conversion. The quantitiative data on the influence of light intensity on the kinetics of the decay, and the magnitude of the decrease in sub-gap α, agree with the previous work of Dalal which quantified Adler's model.Therefore, we conclude that trap-to-dangling bond conversion plays a role in degradation of the electronic preperties of a-Si:H upon light soaking. We further conclude that there are two separate and distinct mechanisms for degradation, namely trap-to-dangling bond conversion, and bond-breaking. Both phenomena are active simultaneously in a-Si:H, which implies that both charged defects,which are negatively correlated, and neutral defects, which are positively correlated, exist simultaneously in the material.

This work was partially supported by Solar Energy Research Institute,Electric Power Resedarch Institute and Electric Power Research Center at Iowa State University. We thank N. Kandalaft and Greg Baldwin for making some of the measurements.

REFERENCES

1. D. Staebler and C. Wronski, Appl. Phys. Lett. 31,292(1977)
2. C. Wronski and R. Daniels, Phys. Rev B-23, 794(1980)
3. M. Stutzmann, W. B. Jackson and C. C. Tsai, Phys. Rev. B-32, 23(1985)
4. D. redfield, Appl. Phys. Lett. 52, 492(1988)
5. C. R. Wronski and N. Maley,in " Amorphous Silicon Materials and Solar Cells", Proc. Amer. Inst. of Phys., vol 234,11(1992)
6. D. Adler, J. De Phys.(Paris), 42-C4, 3(1981)
7. H. M. Branz and M. Silver, Phys. Rev. B-42, 7420(1990)
8. H. M. Branz, R. Crandall and M. Silver, in " Amorphous Si Materials and Solar Cells", Proc. of AIP, vol. 234, 29(1992)
9. V. L. Dalal, in " Stability of a-Si Alloy Materials and Devices", Proc. of AIP, Vol. 157, 249(1987)
10. V. L. Dalal and C. Fuleihan, in " Amorphous Silicon Technology", Proc. of Mat'l. Res. Soc., 149,601(1989)
11. J. M. Essick and J. D. Cohen, in "Amorphous Siliocn Technology", Proc. of Matl. Res. Soc.,149, 149(1989)
12. V. L. Dalal, R. D. Knox, B. Moradi, A. Beckel and S. Van Zante, in "Amorphous Si Materials and Solar Cells", Proc. of AIP, vol. 234,234(1992)
13. S. Lee, S. Kumar and C. Wronski, J. Non-Cryst. Solids, 114,316(1989)

Growth of High Quality Amorphous Silicon Films With Significantly Improved Stability

Vikram L. Dalal*, E. X. Ping*, Mark Leonard+, Mohan Bhan+ and Sanjiv Kaushal*

+ Microelectronics Research Center
* Dept. of Electrical and Computer Engineering
Iowa State University
Ames, Iowa 50011

Abstract

We report on the results of a systematic series of experiments aimed at improving the stability of amorphous Silicon(a-Si:H) films. We find that very low levels(0.2 to 0.4 ppm) of compensation by Boron, when combined with growth conditions that favor a robust microstructure in the material, result in films with significantly improved stability and very low defect density even after prolonged high intensity light soaking. The films were grown using a reactive plasma beam technique using a remote plasma beam from an electron-cyclotron-resonance source. The improvement in stability is seen under both short-term(a few minutes) light soaking, and also under prolonged light soaking under high intensity (10xsun) illumination conditions. We conclude that the improvement in initial stability is a result of compensation of native donors(probably oxygen) in the material by Boron. The surprising reduction in long term instability and corresponding defect density upon compensation implies that the microstructure and structural changes around the native impurities may play a role in the long-term instability of the material.

Instability of amorphous Silicon upon light soaking is a major technological problem. The effect was first discovered by Staebler and Wronski in 1977[1], and since then, much work has been done to try to elucidate the reasons for the instability, and to try to reduce it.[2-7] Several models have been put forward to try to explain the instability, among them bond breaking[3], equilibration between metastable states[4] and influence of localized impurities or inhomogeneities[5-8].There is a lively debate about whether there is only one kind of Staebler-Wronski effect, or if different types of instabilities occur, even in device quality films. There is considerable evidence[8,9] that the initial degradation in material properties is due to the presence of impurities, while the longer term effect may be due to some other mechanism. Among the techniques being used to reduce instability are the use of UHV "superchamber" to reduce impurity contents of the film[10], making materials with low H content by depositing at high temperatures[11-13], or using chemical annealing[14] to change the microstructure during growth. In this paper, we show that introducing very small amounts of a compensating dopant (B) into the film during growth, when combined with low H incorporation conditions, significantly reduces the instability, both long term and short-term.

The films were deposited in an electron-cyclotron-resonance(ECR) plasma reactor under low-pressure conditions. We have shown previously that it is possible to deposit device-quality films in

such a reactor, even at high temperatures[13,15,16]. The basic geometry of the reactor and the plasma conditions have been described elsewhere.[13,16] The deposition system routinely pumped down to 3-4 x 10^{-8} T before growth and was plasma-cleaned before growth so as to reduce impurity content in the film and to lose the memory of the previous run. During the series of runs, no high levels of dopants were introduced in the system, in order to keep the system as pure as possible. A virtual load-lock was used to load the samples. The O content in the film, measured using SIMS, was typically below $5x10^{18}/cm^3$. A systematic series of films were deposited at temperatures of 325C, 350C, 375 C and 400 C using a remote-plasma ECR apparatus, with a high flux of atomic hydrogen from the ECR plasma decomposing the silane which is introduced near the substrate. We chose these conditions, because in our previous work,[13,15] we have shown that such conditions produce films which have low H content(6-8%), and are more stable than standard glow-discharge films. During deposition, some films were deposited using a very small, controlled amounts (0.1 to 0.3 vppm) of diborane, diluted in H_2 added to the silane. Care was taken to maintain identical plasma deposition conditions for both non-compensated and compensated films. Many identical film runs were made so as to eliminate any spurious one-time effects. All the films were approximately the same thickness(0.7 to 0.8 μm), and all were grown at approximately the same power and growth rate(about 0.5 A/sec).

The typical electronic properties of undoped films and films with varying amounts of diborane compensation, deposited at 325 C are shown in Table I. It is clear from the table that the undoped and B compensated films are of electronic quality- a conclusion we have proved in the past by making devices from these films.[15] The sub-gap absorption spectra of three of these films are shown in Fig.1. The spectra were measured using the standard two-beam photo-conductivity technique developed by Wronski et al.[17], and verified using CPM techniques. From Fig. 1, it is clear that the addition of appropriate amounts of diborane(0.2 vppm in our case) seems to produce films with significantly lower subgap α, where α is the absorption coefficient, but with further increases in diborane content, subgap α increases. A similar behavior was seen for the films deposited at higher temperatures. The Urbach energies for the films are all very comparable, in the range of 45-47 meV. However,the dark and photo-conductivities of the three films are very different, with addition of B at first decreasing the dark conductivity, and then increasing it, presumably because the film becomes p type.

The films were subjected to two types of light soaking. First, they were subjected to AM1.5 light soaking from an ELH lamp source for 5 minutes. In Fig. 2, we show the photo-conductivity(σ_L) decay behavior of four films, uncompensated and compensated with varying amounts of B. It is obvious from the figure that the rate of decay in photo-conductivity of the film decreases significantly as more

B is added during growth.

Next, the films were subjected to an intense, focussed beam from the ELH lamp, with the short wavelengths(<550 nm) eliminated by the use of an a-(Si,C) film which was used as a filter. This was done to achieve saturation in the entire film with reasonably uniformly absorbed light. The intensity was 10 x Sun. The samples were turned upside down periodically during the soaking so as to illuminate from both surfaces. Periodically during this light soaking, measurements were made of subgap α. The results on changes in subgap α at the shoulder as a function of light soaking time are shown in Fig. 3 for three of the films. The defect density in all the films seems to tend towards saturation after about 20 hours of intense light soaking. It is also seen from Fig. 3 that the film with the right amount of diborane compensation has the lowest subgap α, and hence defect density, a value lower than that of the nominally undoped film. Increasing the amount of B actually leads to an increase in saturated defect density.

In Fig. 4, we show the corresponding behavior of defect density for films deposited at 375 C. These films had a lower H content(about 5-6% compared to about 8% for films deposited at 325 C), and these films tend to saturate at very low defect densities, lower than the 325 C films, a result similar to our earlier work.[15] In particular, we would like to point out the extremely low values of subgap α obtained in the compensated film(< 1/cm) even after 30

hours of 10 x sun illumination. This implies a defect density of the order of $1x10^{16}/cm^3$ after degradation, a remarkably low value, lower than comparable glow-discharge films by about a factor of 5. Once again, the film with the right amount of B compensation saturates with the lowest defect density, a phenomenon we observed in all the films we studied.

We explain these results by suggesting that there are at least two different types of degradation mechanisms in a-Si:H. The initial degradation of the film is probably due to the conversion of charged defects(traps) into dangling bonds upon a monomolecular capture of a light generated carrier. The native impurities in the film, particularly O and N, act as donor states, giving rise to negatively charged states(T_3- states of Adler) at the same time.[5] Compensation reduces the number of native impurities which act as donors, perhaps by forming donor-acceptor pairs,and thus preventing the formation of a negatively charged state. Thus, compensation reduces the initial rate of decay in photo-conductivity. For more details on the trap-conversion model, we refer the reader to our earlier experimental and analytical work.[8,9]. The suggestion of compensation receives strong support from the dramatically reduced dark and photo-conductivity upon addition of B.(See Table I.)

We next turn to the behavior of subgap α of the different films upon degradation. Redfield[6] has suggested that the impurities in a-Si:H films may play a major role in degradation through changes

in localized bonding around the impurities. In particular, he had suggested that impurities can act as donor(or acceptor) states, and that they can bond either substitutionally, or in a 3-center bond with Si. The substitutional state, in his model, is the ground state,and the 3-center bond, the metastable state. The two states are in equilibrium, with about 0.2 eV energetic separation between them. Increasing the donor density increases the number of 3 center bonds,i.e. the number of metastable states(defects), and since the number of ground states has gone up, also increases the saturated defect density. We suggest that upon compensation, the impurity donors and acceptors may form donor-acceptor pairs, thereby reducing the number of both ground states and 3-center bonds associated with donors, and hence reducing both the initial and final defect densities. When too much Boron is added, then we again get an increase in acceptor-induced ground states and 3-center bonds, and hence, an increase in both initial and final defect densities.

It is also noteworthy that our results support the earlier contention of the group at Sanyo,[7,10] that Oxygen impurities have a major role in the Staebler-Wronski effect .

Note that in order to observe this phenomenon, it is necessary to have a material which is fairly homogeneous on a microscopic scale,i.e, the material must have few SiH_2 type defects, which are generally associated with a poor microstructure. Our ECR technique,

where a combination of H etching and high temperatures are used to control the microstructure and produce a material with low H content, allows us to do this.[13]

In conclusion, we have shown that compensation by Boron, when combined with conditions which lead to a robust microstructure in a-Si:H, and a low hydrogen concentration in the films, can produce high quality a-Si:H films which are much more stable than uncompensated, high H content films. The compensation reduces both the initial and the long-term Staebler-Wronski type degradation in the films. We speculate that possible microstructural changes associated with formation of donor-acceptor pairs in the material are responsible for this behavior. The technological implications of this work are that to achieve a high degree of stability in a-Si:H, it is necessary to have both a robust microstructure with little excessive Si-H bonding, and very low levels of impurities.

We thank the support of National renewable Energy laboratory(NREL) for this work. S. Kaushal was supported by a grant from Electric Power Research Center of Iowa State University,and E. Ping was supported by a grant from Electric Power Research Institute. We also thank Frank Jeffrey for many interesting discussions.

References

1. D. Staebler and C. Wronski, Appl. Phys. Lett., 31,292(1977)

2. See, for example," Amorphous Si Materials and Solar Cells", Ed. B. Stafford, Proc.of AIP, Vol. 234(1991)

3. M. Stutzmann, W. B. Jackson and C. C. Tsai, Phys. Rev. B32, 23(1985)

4. D. Redfield and R. Bube, Appl. Phys. Lett. 54,1037(1989)

5. D. Adler, J.de Phys. 42-C4,3(1981)

6. D. Redfield, Modern Phys. Lett.,B5,933(1991)

7. Y. Kuwano, S. Tsuda, N. Nakamura, M. Nishikuni, K. Yoshida, T. Takahama, M. Isomura and S. Nakano, Proc. AIP, Vol. 157,126(1987)

8. V. L. Dalal, Proc. of AIP, 157,249(1987)

9. V. L. Dalal and C. Fuleihan, Proc. Mat'l. Res. Soc., 149,601(1989)

10. S. Tsuda, Y. Kuwano, N. Nakamura, Japan J. Appl. Phys.,26,33(1987)

11. N. Johnson, C. Nebel, P. Santos, W. Jackson, R. Street, K. Stevens and J. Walker, Appl. Phys. Lett.59,1443(1991)

12. A. H. Mahan, J. Carapella,B.Nelson, R. Crandall and I. Balberg, J.Appl. Phys.69,6728(1991)

13. V. L. Dalal, R.Knox, N. Kandalaft and G. Baldwin, Proc. of 22nd. IEEE Photovolt. Spec. Conf.,1399(1991)

14. H. Shirai, J. Hanna and I. Shimizu, Proc. of AIP, 234,203(1991)

15. V. L. Dalal, M. Leonard and G. Baldwin, J. Non-Cryst. Solids(1993) To be published.

16. V. L. Dalal, R. Knox, N. Kandalaft, B. Moradi and K. Han,Proc.

of AIP, 268,388(1992)

17. S. Lee, S. Kumar and C. Wronski, J.Non-Cryst. Solids,114,316(1989)

Figure captions

Fig. 1. Absorption spectra of 3 a-Si:H films, undoped and with controlled ratios of diborane to silane in the gas phase, deposited using ECR conditions at 325 C. The ratios used are indicated in the figure in vppm. α is the absorption coefficient.

Fig. 2. The initial decay in photo-conductivity(σ_L) under AM1.5 illumination for the three films whose α(E) curves are shown in Fig.1.

Fig. 3. Changes in α at 1.2 eV as a function of light soaking time under 10 x Sun illumination from a filtered ELH lamp for undoped and compensated films whose α(E) curves were shown in Fig. 1.

Fig. 4. Changes in α at 1.2 eV for undoped and compensated film made at 375 C substrate temperature, plotted as a function of light soaking time under 10 x sun filtered ELH lamp illumination.

Table I

Properties of a-Si:H Films Deposited Using H-ECR Process(325 C)

	Undoped	Diborane compensation		
		0.1vppm	0.2 vppm	0.3 vppm
Tauc gap(eV)	1.74	1.74	1.74	1.74
Dark conductivity(S/cm)	$2.5x10^{-10}$	$1.2x10^{-10}$	$3.5x10^{-11}$	$1.2x10^{-10}$
Photo conductivity(S/cm)	$1x10^{-4}$	$2.8x10^{-5}$	$1.8x10^{-5}$	$3.x\ 10^{-5}$

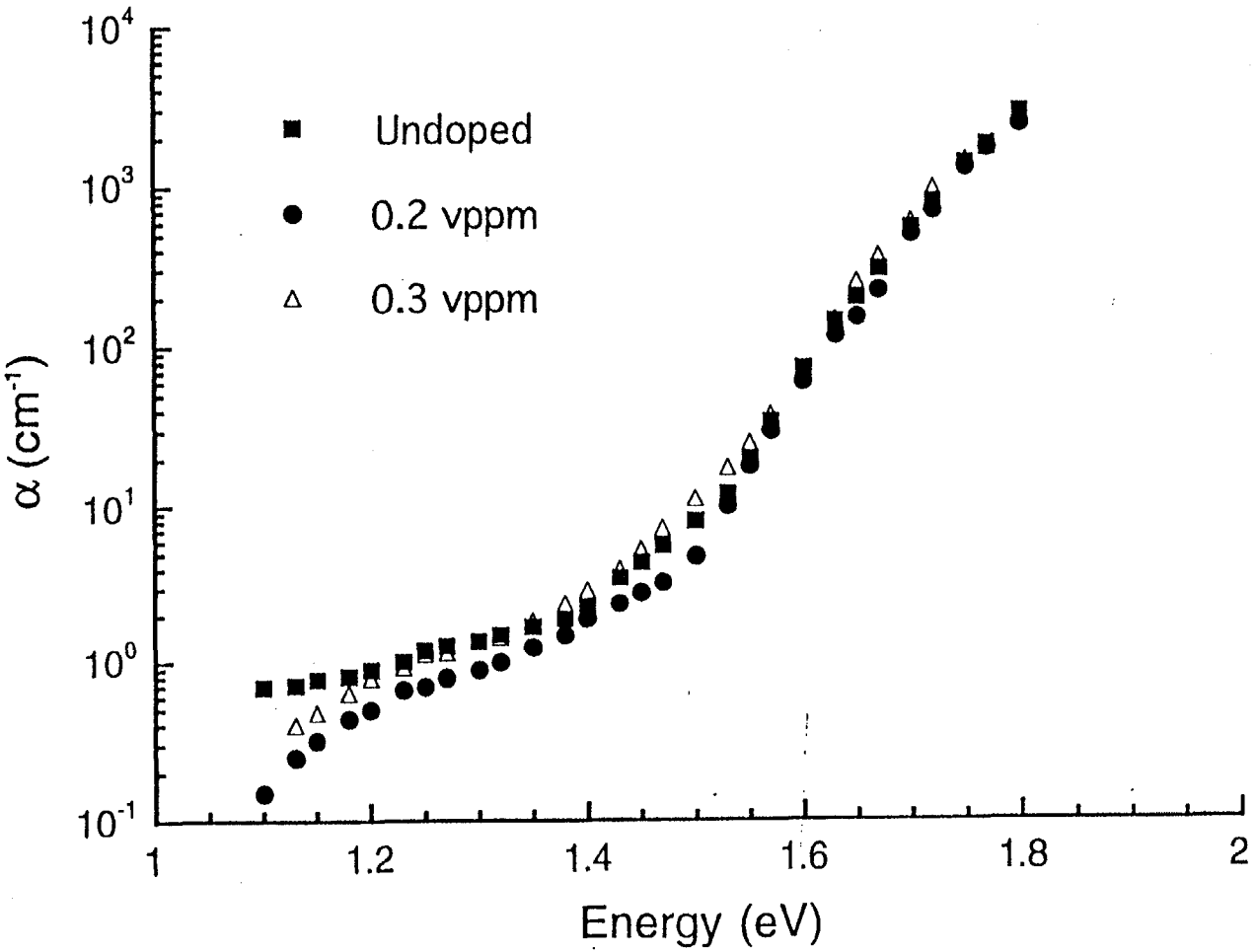
Undoped
0.2 vppm
0.3 vppm
α (cm-1)
10^4
10^3
10^2
10^1
10^0
10^-1
1
1.2
1.4
1.6
1.8
2
Energy (eV)

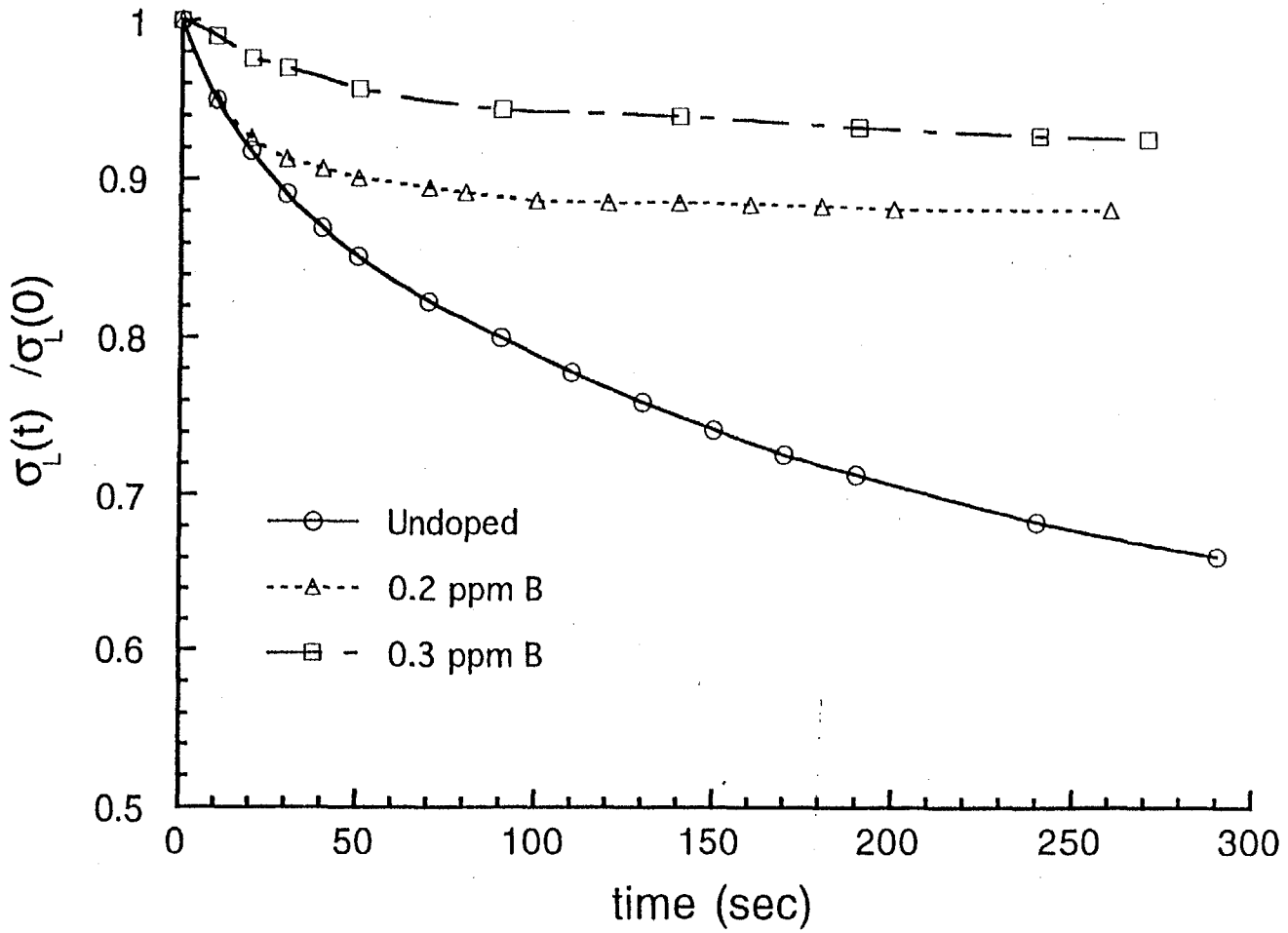
1
0.9
0.8
0.7
0.6
0.5
$\sigma_L(t)\ /\sigma_L(0)$
0
50
100
150
200
250
300
time (sec)
Undoped
0.2 ppm B
0.3 ppm B

Fig. 2

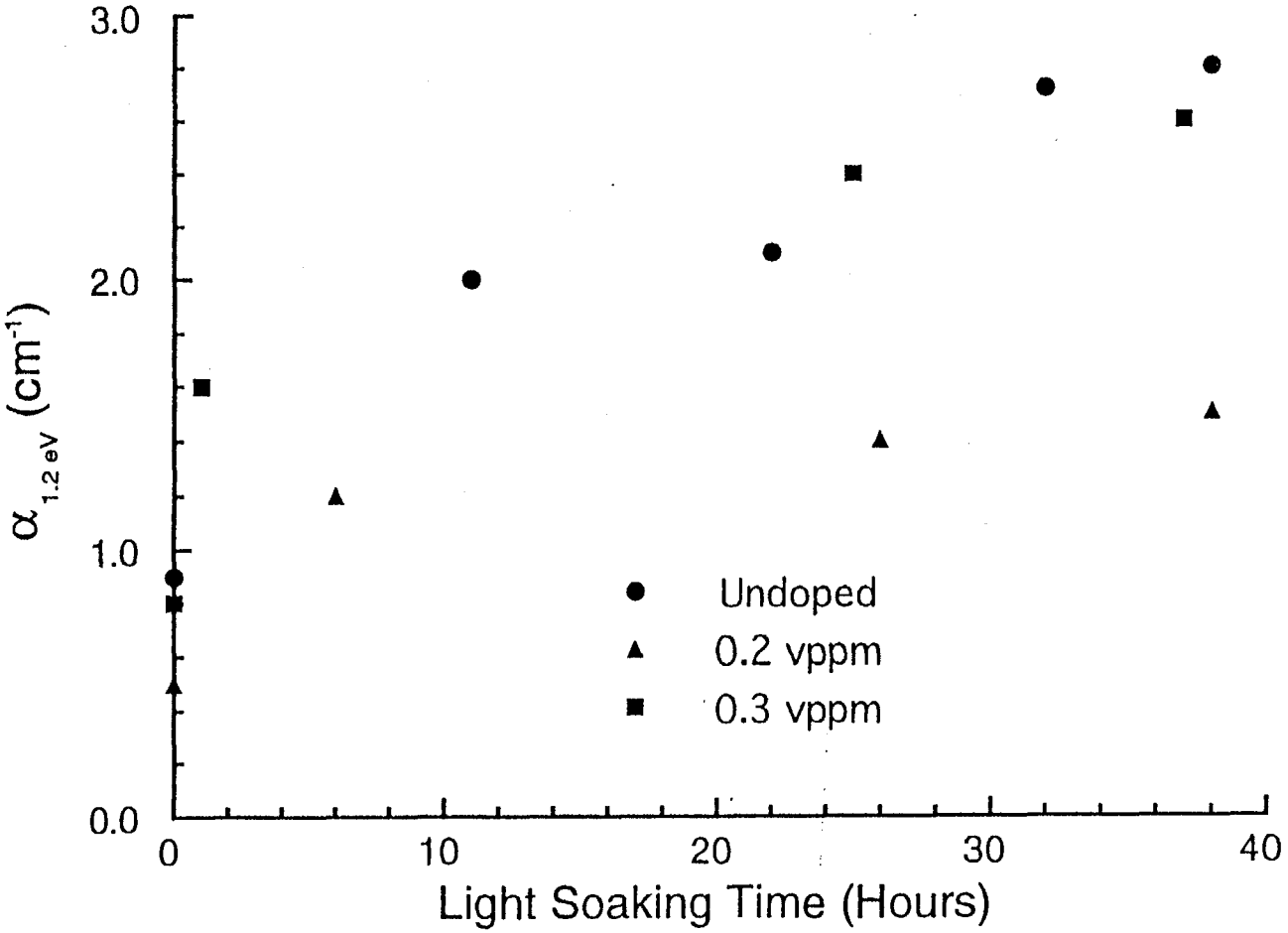
3.0
2.0
1.0
0.0
$\alpha_{1.2\,eV}$ (cm^{-1})
0
10
20
30
40
Light Soaking Time (Hours)
Undoped
0.2 vppm
0.3 vppm

Fig. 3

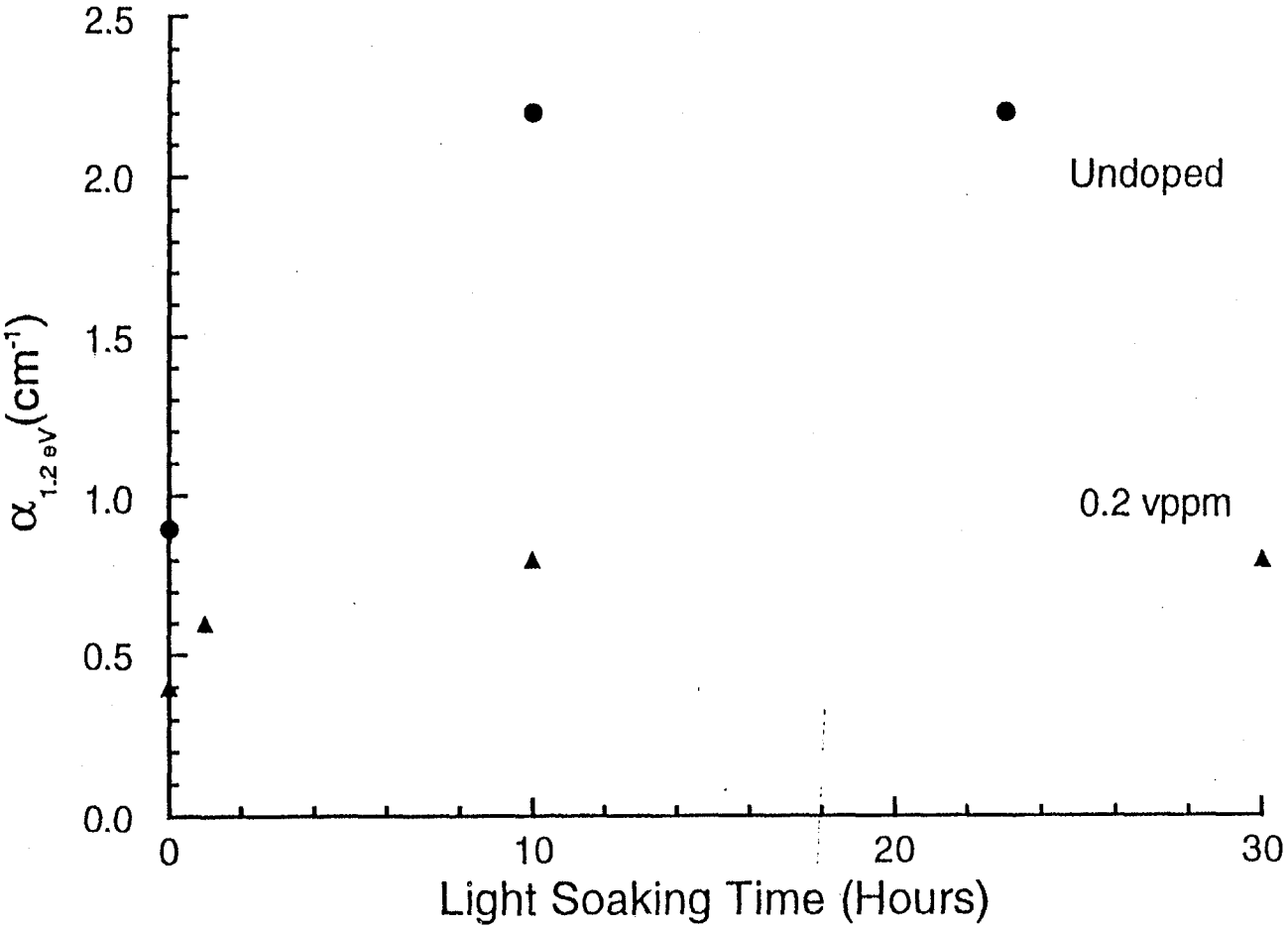
2.5
2.0
1.5
1.0
0.5
0.0
$\alpha_{1.2\,eV}(cm^{-1})$
Undoped
0.2 vppm
0
10
20
30
Light Soaking Time (Hours)

Fig. 4

REPORT DOCUMENTATION PAGE

Form Approved
OMB NO. 0704-0188

Public reporting burden for this collection of information is estimated to average 1 hour per response, including the time for reviewing instructions, searching existing data sources, gathering and maintaining the data needed, and completing and reviewing the collection of information. Send comments regarding this burden estimate or any other aspect of this collection of information, including suggestions for reducing this burden, to Washington Headquarters Services, Directorate for Information Operations and Reports, 1215 Jefferson Davis Highway, Suite 1204, Arlington, VA 22202-4302, and to the Office of Management and Budget, Paperwork Reduction Project (0704-0188), Washington, DC 20503.

1. AGENCY USE ONLY (Leave blank)	2. REPORT DATE	3. REPORT TYPE AND DATES COVERED
	April 1995	Subcontract Report, 10 March 1991 - 30 August 1994

4. TITLE AND SUBTITLE

Comprehensive Research on the Stability and Electronic Properties of a-Si:H and a-SiGe:H Alloys and Devices

5. FUNDING NUMBERS

C: XG-1-10063-8

TA: PV531101

6. AUTHOR(S)

V. Dalal

7. PERFORMING ORGANIZATION NAME(S) AND ADDRESS(ES)

Iowa State University
Ames, Iowa

8. PERFORMING ORGANIZATION REPORT NUMBER

9. SPONSORING/MONITORING AGENCY NAME(S) AND ADDRESS(ES)

National Renewable Energy Laboratory
1617 Cole Blvd.
Golden, CO 80401-3393

10. SPONSORING/MONITORING AGENCY REPORT NUMBER

TP-411-7695

DE95004088

11. SUPPLEMENTARY NOTES

NREL Technical Monitor: W. Luft

12a. DISTRIBUTION/AVAILABILITY STATEMENT

12b. DISTRIBUTION CODE

UC-1260

13. ABSTRACT *(Maximum 200 words)*

This report describes work on the growth of a-Si:H and a-(Si,Ge):H materials and devices using well-controlled growth techniques. The a-Si:H materials were grown at higher temperatures (300°–375°C) using electron-cyclotron-resonance (ECR) plasma techniques with a remote H beam. These films have excellent electronic quality and show significant improvements in stability compared with glow-discharge-produced a-Si:H materials. Several problems were encountered during the fabrication of devices in these materials, and we were able to overcome them by a systematic work on buffer layers in these cells. We also studied alternative designs for improving the stability of a-Si:H cells and produced graded-gap a-Si:H cells using glow-discharge that are more stable than comparable standard, ungraded glow discharge devices. Finally, systematic work was done to produce good-quality a-(Si,Ge):H films, using triode radio frequency (RF) glow-discharge with ion bombardment during growth. Diagnostic devices were made using these films, and the properties of the material, such as Urbach energies and hole mobility-lifetime products, were measured in these devices. We found a systematic increase in the Urbach energies, and a corresponding decrease in the hole and electron $\mu\tau$ products, as the Ge content of the alloys increases.

14. SUBJECT TERMS

photovoltaics ; solar cells ; amorphous silicon ; germanium ; alloys ; silicon germanium alloys

15. NUMBER OF PAGES
108

16. PRICE CODE

17. SECURITY CLASSIFICATION OF REPORT	18. SECURITY CLASSIFICATION OF THIS PAGE	19. SECURITY CLASSIFICATION OF ABSTRACT	20. LIMITATION OF ABSTRACT
Unclassified	Unclassified	Unclassified	UL